Transactions, **SMiRT-26**
Berlin/Potsdam, Germany, July 10-15, 2022
Special Session

DEVELOPMENT AND EXPECTATION OF SEISMIC ISOLATION OF NUCLEAR POWER PLANT STRUCTURE

Hou Nannan[1], Dong Jianling* [1,2]

[1]Institute of Nuclear and New Energy Technology, Tsinghua University, Beijing, China (hnn18@mails.tsinghua.edu.cn)
[2]Collaborative Innovation Center of Advanced Nuclear Energy Technology, Tsinghua University, Beijing, China

ABSTRACT

Seismic isolation has been widely applied in the architecture field including normal buildings and bridges worldwide, but it is still immature in the field of nuclear power plants especially nuclear structure. Since the environment and functions of nuclear power plants are more complex than normal architecture and nuclear power plants require much higher safety and reliability than other projects, seismic isolation of nuclear power plants needs particular designs. The base isolation can not only bear the vertical load of the structure, but also reduce the response of seismic on the upper structure due to the low lateral stiffness of isolation devices so as to improve the safety of the nuclear structure in the earthquake. In addition, base isolation can make the seismic isolation design of the main structure and equipment of nuclear power plants achieve standardization unrestricted by the magnitude of design ground motion. This paper summarizes the development of the seismic isolation of nuclear power plant structure up to now, especially since 2018, and the research and implementation in China, and also describes the challenges and adverse effect of base isolation applied in the field of nuclear power plants. Finally, this paper gives the expectation for the future research on the basis above.

Keywords: seismic isolation, three-dimension isolation, nuclear power plant

INTRODUCTION

Nuclear energy has the advantages of high efficiency, safety, stability and little impact on the environment. The Fukushima incident warns us that the safety of nuclear power plants under earthquakes must be considered. The following measures can be taken to reduce earthquake hazards: 1) reasonable site selection; 2) seismic fortification requirements and standard of nuclear power plant; 3) isolation technology.

Base isolation technology can make the seismic design of nuclear power plants not stick to the level of design ground motion and implement standardized operation, so as to improve the overall reliability and safety of nuclear power plant. At present, base isolation technology can be adopted for nuclear island with the SSE design seismic standard of more than 0.3g, so that the actual seismic acceleration of the nuclear island can be controlled within 0.3g. This paper summarizes the research results of seismic isolation in the field of nuclear power plants and tries to give the development direction in the future.

BASE ISOLATION

Applications in Nuclear Power Plants Worldwide

∗ Corresponding author. Tel.: 8610-62785907; E-mail addresses: dongjl@mail.tsinghua.edu.cn.

Base isolation is widely used in the United States, Japan, France and other countries. The application of isolation technology in nuclear power plants can be divided into three types: whole building (foundation) isolation, floor isolation and equipment isolation.

Two liquid metal reactors in the United States have adopted isolation technology, namely PRISM and sodium cooled fast reactor SAFR. PRISM adopts 20 high damping synthetic rubber bearings for horizontal isolation of reactor vessel, which have sufficient stiffness under low strain and can resist wind and small earthquake. The test results show that the peak spectral acceleration is reduced from 16.5g to 0.25g by seismic isolation, and the horizontal spectral peak above 2Hz is eliminated. SAFR adopts 100 high damping thick rubber bearings for isolation in both horizontal and vertical directions. The test results show that the horizontal and vertical isolation frequencies are lower than 1Hz and 4Hz respectively, which effectively avoids the natural frequencies of most equipment.

France applied the base isolation to Koeberg nuclear power plant in South Africa and Cruas nuclear power plant in France in 1977 and 1984 respectively. The former adopts laminated rubber bearings and sliding friction plates, and the latter adopts only laminated rubber bearings. The synthetic neoprene seismic isolation bearings used in Cruas was aging with the increase of service life, which affects the performance under earthquake; The isolators with bimetallic interface used in Koeberg was prohibited because of poor mechanical properties. ITER under construction in France has designed a seismic isolation scheme for Tokamak device, which uses a square laminated elastic isolator made of 6 layers of elastomer and embedded steel plate and has formulated a new specification. The Heysham nuclear power plant and Torness nuclear power plant were built in the UK in 1983 and 1988 respectively, in which base isolation was also adopted in factory buildings. Italy launched a research and development (R&D) program in 1988 to support the development of isolation guidelines and qualification procedures for isolation systems.

In the 1980s, Japan studied and tested the feasibility of base isolation of nuclear island. Influenced by the beyond design basis accident of Koshwazaki Kariwa nuclear power plant under M6.8 earthquake in 2007 Niigata, the Japan Electric Industry Association announced to start the development of the next generation light water reactor and carried out a new round of experimental research on nuclear island base isolation in 2008. The project entitled "safety enhancement of light water reactor" supported by the Japanese government considers two kinds of reactor: pressurized water reactor and boiling water reactor. The sodium cooled fast reactor JSFR, one of the six fourth generation reactor types proposed by the International Forum, adopts base isolation.

The fourth generation reactor KALIMER designed by South Korea also adopts the base isolation. And a new type of three-dimensional base isolation bearing is developed for a transportable self-supporting reactor STAR-LM. Yoo B et al. tested the performance of the laminated rubber bearing used in KALIMER and provided real test data for the practical application of isolation design. Hong Pyo Lee et al. studied and established the scale model of APR 1400 reactor nuclear structure in Korea, and carried out the analysis and experiment of dynamic load response on the structure by using the sliding isolation structure EQS support (EradiQuake system).

Research of Seismic Isolation in China

At present, Tianwan nuclear power plant and ALSTOM Taishan nuclear power plant have adopted spring isolators in conventional island. And AP1000 steam turbines of Sanmen and Haiyang and the megawatt half speed nuclear power steam turbine units designed and produced by Shanghai steam turbine plant including Siemens and Alstom models of CPR1000 Nuclear Power Plant have also adopted spring isolators. Yangjiang units 1, 2 and 3 and Fangchenggang unit 1 have been successfully put into operation, and the units are still in good operation. The megawatt half speed nuclear power steam turbine units designed and produced by Dongfang Electric, especially the ARABELLE steam turbine generator units, are all spring supported.

In terms of nuclear islands, there has not yet been mature achievements published and applied in China. Shenzhen CGN Engineering Design Co., Ltd. has cooperated with France to implement the seismic isolation design research of CPR1000. And Shanghai Institute of Nuclear Engineering began to plan the

seismic isolation design of AP1000 in 2008 to increase the actual seismic design capacity from 0.3g to 0.6g on the premise that the original standard design of the imported AP1000 units remains unchanged. Shanghai Institute of Nuclear Engineering first proposed the isolation scheme of using the base isolation bearings in nuclear island and configuring the locking device released according to a certain threshold value. About 282 sets of supporting isolation devices are fully distributed under the bottom plate of the nuclear island of the whole AP1000, directly taking 0.9g as the working condition beyond the design basis, so as to keep the nuclear island within the original seismic margin of 0.5g.

STANDARD

Many countries including Japan, the United States and France have made relevant specifications for seismic isolation design of nuclear power plants, among which the specifications of Japan and the United States have developed for a long time and are mature.

Codes for Seismic Isolation of Nuclear Power Plants in Japan

Since Japan is a country with many earthquakes, the seismic isolation related policies are more comprehensive. In 2000, Japan Electric Power Association issued the world's first seismic isolation design code for nuclear power plant structures, “Technical Guide for Seismic Isolation Structure Design Of Nuclear Power Plants” (JEAG 4614-2000), and Japan Nuclear Safety Agency issued guidelines for seismic isolation structure review rules (JNES-SS-1001) in 2009.

JEAG 4614-2000 describes the following aspects: 1) classifying the nuclear facilities using seismic isolation; 2) Isolation design and evaluation method; 3) Load combination and necessary safety margin; 4) Performance requirements of isolation bearing and energy dissipation device; 5) Design requirements of auxiliary system (such as machinery, pipeline, etc.); 6) Quality control and maintenance requirements of isolation bearing.

JNES-SS-1001 is generally based on deterministic method. Although seismic probabilistic risk assessment method is required when considering residual risk, safety margin design method is used in the design of isolation system.

Codes for Seismic Isolation of Nuclear Power Plants in the United States

The United States issued “Seismic Design Criteria for Structures, Systems and Components in Nuclear Facilities” (ASCE 43-05) in 2005, which provides a set of design standards more stringent than ordinary buildings to ensure that nuclear facilities can maintain the expected performance under earthquake. However, the specification does not contain relevant contents of seismic isolation. “Seismic Analysis of Safety-Related Nuclear Structures” (ASCE SEI 4-16) adds a chapter on the design, analysis and testing of seismic isolation structures of nuclear power plants on the basis of ASCE-05.

Codes for Seismic Isolation of Nuclear Power Plants in China

The code for seismic design of nuclear power plants (GB 50267-1997) in China does not contain isolation related contents. But the standard for seismic isolation design of buildings (GB/T 51408-2021) was issued in April 2021, where Chapter 9 specifies the seismic isolation design standard of nuclear power plant buildings which is applicable to nuclear power plant buildings that use isolation bearings to achieve base isolation. The contents include: general provisions such as fortification objectives and site selection, seismic isolation design, floor response spectrum, requirements of isolation bearings, inspection rules of rubber isolation bearings, seismic monitoring and alarm, etc.

NEW TYPE SEISMIC ISOLATION

Common isolators include laminated rubber isolation bearings and sliding bearings such as friction pendulum, both of which can realize horizontal isolation but can't work well in vertical direction. In addition, they will increase the horizontal displacement response while reducing the horizontal acceleration response, which might cause the fracture of the connecting pipelines between the isolation parts and the non-isolation parts. Besides, the base isolation system may amplify some seismic wave responses under long-period ground motion, so it is very necessary to improve and innovate the traditional isolation system.

Three-dimensional seismic isolation

3-D seismic isolation can be achieved by one isolator acting in three directions, such as rubber bearings with low vertical stiffness, coil springs with separate dampers, or by two isolation systems in series.

Yoo B et al. applied the 3-D isolation structure shown in Figure 1 to STAR-LM reactor. The dynamic analysis shows that compared with the non-isolated structure, the 2-D and 3-D isolation system can reduce the acceleration response in the horizontal direction, and the 3-D isolation system can also reduce the floor acceleration by 2.4 times in the vertical direction.

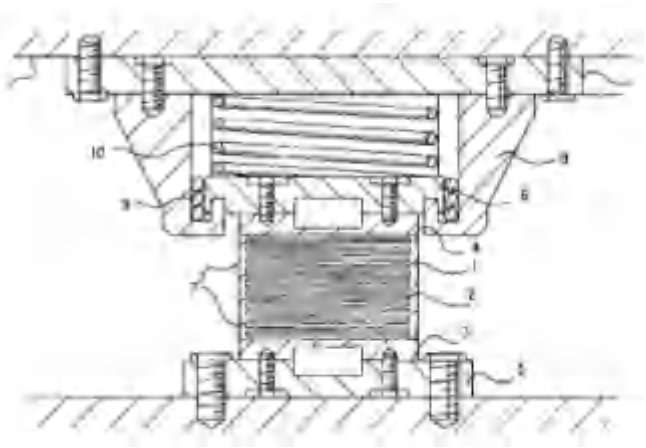

Figure 1. Schematic Drawing of 3-D Seismic Isolation Device.

In 2000, Japan carried out a large-scale research on the application of 3-D isolation technology to fast breeder reactor (FBR), and proposed three kinds of isolation devices: 1) rolling sealed air spring; 2) Steel wire reinforced air spring; 3) Hydraulic 3-D isolation device. The calculation and experimental results show that the isolation structure has significant anti shaking performance and vertical and horizontal isolation performance. Through the shaking table test of rolling sealed air spring and hydraulic swing suppression system, it is confirmed that the 3-D isolation device can be applied to nuclear power plant. Kageyama Mitsuru and others developed a 3-D isolation system composed of 3-D air spring, viscous damper and anti-sway device. Experiments show that the system is feasible in practical engineering. The 3-D isolation device is evaluated from performance, system reliability, easy maintenance and economy. It is concluded that the performance of the rolling sealed air spring shown in Figure 2 is better than the other two isolation devices, especially in terms of suitable performance for nuclear power plant.

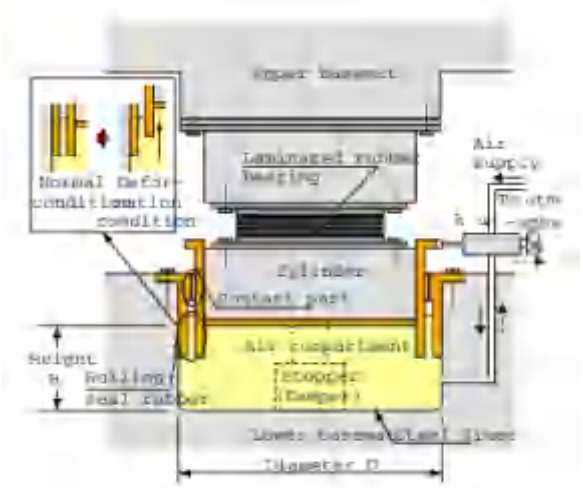

Figure 2. The 3-D base isolation device with rolling sealed air spring.

For laminated rubber bearings, increasing the thickness of single-layer rubber layer can reduce the vertical stiffness of the bearings. And if the total thickness remains unchanged, the horizon shear stiffness will be similar to that of ordinary rubber bearing. So, it is also a feasible way to realize 3-D isolation. However, the increase of the thickness of the rubber layer will reduce the first shape coefficient of the bearing, so the mechanical properties of the thick rubber bearing needs to be further studied. The SAFR reactor in the United States adopts 100 thick rubber isolation bearings with shape coefficient between 3 and 6. Kenji Kanazawa and others designed thick rubber bearings to avoid increasing the difficulty of vulcanization processing due to the thickening of the rubber layer.

Wang Tao and others designed a 3-D isolation system composed of thick rubber isolation bearings and oil dampers. The shaking table test of 1/15 scale model shows that it has the same isolation effect as the traditional isolation system in the horizontal direction. Although the response in the vertical direction is amplified, it can be used for vertical isolation of important equipment and pipelines in nuclear power plants.

In addition to the overall 3-D isolators mentioned above, vertical isolation can also be adopted for main equipment on the basis of overall horizontal isolation. The advantage is that the offset between the gravity center of superstructure and the position of the supporting structure can be very small, so the equipment will not have excessive swing response, and the characteristics of each isolation system will be simpler than the former.

S. Kitamura et al. designed a model that the reactor vessel and main components are suspended on a large public deck supported by an isolation device composed of large conical disk springs on the basis of overall horizontal isolation, as shown in Figure 3. The vertical isolation effect of the system is verified by the vibration test of the model.

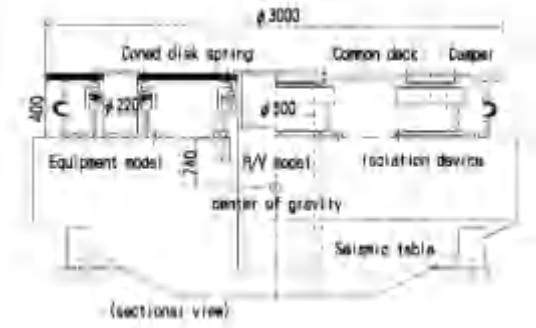

Figure 3. Vertical isolation system model.

Several new isolation devices

The research shows that the isolators may have large deformation under low frequency and high energy earthquake. Tuned mass damper composed of spring, mass and damper has been widely used in buildings, machinery, transportation and other fields. Zhou Fulin and others studied the application of TMD technology in heavy structures and verified its effectiveness in seismic isolation, and found that the lower the isolation layer is, the more obvious the damping effect is. Iuliis designed a new structure combining friction pendulum and TMD based on an ordinary building model. The dynamic analysis shows that it has good isolation effect. Mikayel also designed a base isolation structure combined with TMD and determined the best parameters. Hou Gangling compared the isolation effect of TMD and ordinary base isolation based on the containment model of AP1000 nuclear power plant. The results show that the base isolation can make TMD part have better effect and TMD can reduce the influence of the change of BIS bearings' stiffness and damping ratio. The BIS-TMD system has good isolation effect and high stability.

Because of the heavy self-weight, high cost and complex installation process of traditional laminated rubber bearings, Kelly used fiber reinforced materials to replace the steel plate in the laminated rubber bearings. The results show that its performance is similar to that of steel, which greatly reduces the self-weight of the bearings and makes the process simpler.

For sliding isolation bearings, some researchers introduced shape memory alloy (SMA) into sliding isolation system to improve their performance. Large size SMA spring can not only generate large displacement, but also carry heavy load, and has good reset and damping performance. Cardone et al. designed and manufactured two SMA sliding isolation devices and carried out shaking table test. The results show that the structure can be reliably used for isolation. Ozbulut et al. designed an isolation system composed of a sliding bearing and SMA and made time history analysis and optimization design of bridge structures. However, the application of SMA in the field of nuclear power plants has not been published.

Due to the rapid development of material science, various new materials, such as piezoelectric materials and shape memory materials, make the prospect of seismic isolation devices broader. For example, the polymer material composed of natural rubber and special filler developed in China has large damping and low cost.

PROBLEMS AND FUTURE DEVELOPMENT DIRECTION

Comparing the response results of isolated model with that of non-isolated model, it is concluded that the seismic response can be greatly reduced by isolation. But at present, the isolation technology also has the following problems:

(1) Either rubber bearing or sliding bearing will increase the displacement of the structure in the horizontal direction, which may rupture the connecting pipelines;

(2) The friction pendulum bearing is composed of multiple curved metal parts, which is difficult to manufacture, and when the superstructure slides to the height of concave curved surface, the vertical vibration of the structure will increase. Rubber bearing relies on polyurethane spring to provide reset ability, which may fail in harsh environment;

(3) If the isolation bearing is located in the radioactive area, it is required that the bearing has good radiation protection and heat resistance, and it is difficult to check the performance;

(4) The isolation system using only rubber bearings can only achieve horizontal isolation and the vertical response actually increases under the combined action of horizontal and vertical ground motion;

(5) Due to the complex internal structure of nuclear power plants, the isolation devices may cause stress concentration and damage to some equipment and pipelines. However, there is few research on the seismic performance of local equipment and pipelines;

(6) As the sliding support needs to be provided with a stopper, it may cause the superstructure to collide with the stopper and cause damage.

The future research on seismic isolation of nuclear power plants can be carried out from the following aspects:

(1) In view of the Fukushima incident, it is also worth studying how to deal with the tsunami caused by the earthquake and the impact of frequent typhoons in coastal areas on the isolated nuclear power plants;

(2) 3-D isolation must be realized. Especially for the whole structure with 3-D isolation, the bearing stiffness is small, so how to ensure its stability and safety needs further research;

(3) Based on the research on the isolation performance of the overall structure, it is necessary to study the isolation performance of local structures such as internal equipment and pipelines;

(4) Whether the isolation devices and materials can work continuously under the action of multiple main earthquakes and aftershocks to ensure the safety of the nuclear power plant is worthy of further study.

(5) New isolation materials could be studied and applied.

CONCLUSION

At this stage, the research on anti-seismic technology of nuclear power plants has been relatively mature, but anti-seismic technology cannot completely solve the harm caused by earthquake to nuclear power plants. Seismic isolation is undoubtedly an important development direction in seismic safety. However, due to the particularity and complex structure of nuclear power plants, there are few practical application examples of seismic isolation technology in nuclear power plants and many problems are still to be solved. Therefore, the research on nuclear power plant isolation technology is of great significance.

REFERENCES

Wen J, Si G, Sun Z, Li H. Proposal on Research and Design of Base Seismic Isolation for Nuclear Power Plant Buildings in China [J]. Nuclear Safety, 2010(04):50-55.

Xia Z. Seismic Input of NPP & Topic of Seismic-Isolated Research for AP1000 Nuclear Island [J]. Engineering Sciences, 15(4):1-112.

Xie L, Zhai C. A prospective study on applicability of base isolation in nuclear power plants[J]. Journal of Earthquake Engineering and Engineering Vibration, 2012, 32(1):1-10.

Frederick F. Tajirian, James M. Kelly, Ian D. Aiken. Seismic Isolation for Advanced Nuclear Power Stations. 1990, 6(2):371-401.

Martelli Alessandro, Masoni Paolo, Forni Massimo, Indirli Maurizio, Spadoni Bruno, Pasquale Giacomo di, Lucarelli Vittorio, Sano Tito, Bonacina Giuseppe, Castoldi Aldo. ENEA activities on seismic isolation of nuclear and non-nuclear structures[J]. North-Holland,1991,127(3)

Y.Sawada, et al., Seismic Isolation Test Program, Proc.of the 10th SMiRT.1989

Li H. The Discussion on the Accident of the Japan's Kashiwazaki Kariwa Nuclear Power Plant in Earthquake[J]. Nuclear Safety,2008(01):11-19.

Lin X, Wei L, Chen M, Tao R, Liao S. Development and Application of Isolation Technology in Nuclear Power Plant [J]. Shandong Industrial Technology, 2018(17):163-164.

Yamamoto Z, et al. Development of Isolation Technology for Next Generation Light Water Reactor Nuclear Power Plant (Part 1) Development Plan of Isolation Technology [z]. 2006.

Inoue K, Fushimi M, Moro S, et al. Development of three-dimensional seismic isolation system for next generation nuclear power plant [C]//Proceedings of the 13TH World Conference on Earthquake Engineering. Vancouver: International Association for Earthquake Engineering, 2004.

Morishita M, Inoue K, Fujita T. Development of three-dimensional seismic isolation systems for fast reactor application[J]. 2004.

Shimada T, Kashiwazaki A, Fujiwaka T, et al. 103 Study on Three Dimensional Seismic Isolation System for Next Generation Nuclear Power Plant: Hydraulic Three-Dimensional Base Isolation System[J]. 2004.

Zhuang Chuli , Zhang Yongshan , Wang Dayang, et al. State of the Art of Nuclear Power Plant Using Base Isolation [J]. South china journal of seismology, 2014, 34(2):25-33.

Yoo B, Kulak R F. Application of seismic isolation to the STAR-LM reactor [C]//Proceedings of the 10TH International Conference on Nuclear Engineering Arlington Virginia USA: The American Society of Mechanical Engineers, 2002.

Bong Yoo,Jae-Han Lee,Gyeong-Hoi Koo,Hyeong-Yeon Lee,Jong-Bum Kim. Seismic base isolation technologies for Korea advanced liquid metal reactor[J]. Nuclear Engineering and Design,2000,199(1).

Hong-Pyo Lee,Sunyong Kim,Myung-Sug Cho,Yong-Soo Ji. Application of sliding seismic isolator to building structures considering cost, performance and inspection: a case study[J]. Structure and Infrastructure Engineering,2015,11(7).

José M. Jara,Manuel Jara,Hugo Hernández,Bertha A. Olmos. Use of sliding multirotational devices of an irregular bridge in a zone of high seismicity[J]. KSCE Journal of Civil Engineering,2013,17(1).

Hong-Pyo-Lee, Myung-Sug Cho, Yeon-Soo Moon, Woo-Jin Han, Yong-Soo Ji. A Study on Isolation Performance of Eradi Quake System using Shaking Table Test and Analysis [C]. 15th SMiRT. Seoul, Korea, 2017.

Wang Xuemin. A summary of the basic structure of the conventional island turbine [J].Shanxi Architecture, 2018,44(27):53-55.

Xia Z, Wang M, Wang X. Base Isolation Device Nuclear Power Plant with Locking Function, CN201546235U[P].

Xia Z, Li S, Wang X , et al. General Consideration for Seismic Input of NPP Seismic Design and Seismic-isolated Research for AP1000 Nuclear Island [J]. Southern Energy Construction, 2017.

Japan Electric Association. JEAG 4614-2000, design and technical guideline of seismic isolation structure for nuclear power plant[S]. Japan: Japan Electric Association, 2000.

Japan Nuclear Energy Safety Organization. JNES SS-1001, regulatory guideline for reviewing, seismic isolation structures (2009 Edition) [S], Japan: Japan Nuclear Energy Safety Organization,2009.

Zhou Zhiguang. The Status and Development of Design Codes for Seismic Isolated Nuclear Power Plants [J]. Structure Engineers, 2013,29(05):180-187.

American Society of Civil Engineers(ASCE), ASCE 43-05 Seismic design criteria for structures, systems, and components in nuclear facilities [S]. ASCE, 2005.

American Society of Civil Engineers(ASCE), ASCE 4-16 Seismic Analysis of Safety-Related Nuclear Structures [S]. ASCE, 2017.

ANDREW, S, WHITTAKER, et al. SEISMIC ISOLATION OF NUCLEAR POWER PLANTS[J]. Nuclear Engineering & Technology, 2014.

Sayed M A, Go S, Cho S G, et al. Seismic responses of base-isolated nuclear power plant structures considering spatially varying ground motions[J]. Structural Engineering and Mechanics, 2015, 54(1):169-188.

Shimada Takahiro，Fujiwaka Tatsuya, Moro Satoshi. Study on three-dimensional seismic isolation system for next generation nuclear power plant: hydraulic three-dimensional base isolation system [C]// Asme/jsme Pressure Vessels & Piping Conference. 2004.

Shimada, T, Suhara, et al. Three dimensional seismic isolation system for next-generation nuclear power plant with rolling seal type air spring and hydraulic rocking suppression system[J]. PRES VES P, 2005.

Kageyama M, Hino Y, Moro S. Study on Three-Dimensional Seismic Isolation System for Next Generation Nuclear Power Plant: Independent Cable Reinforced Rolling-Seal Air Spring[C]// Asme/jsme Pressure Vessels & Piping Conference. 2004.

YABANA S, MATSUDA A. Mechanical properties of laminated rubber bearings for three-dimensional seismic isolation[C]//12th World Conference on Earthquake Engineering, Auckland, New Zealand, Paper.2000(2452).

Wang Tao, Li Jichao, Wang Fei. Experimental Study on Thick Rubber Bearings of Three-Dimensional Isolation of Nuclear Power Plants [J]. Nuclear Power Engineering, 2015,36(05):37-40.

Tajirian F F, Aiken D I, et al. Elastomeric bearings for three-dimensional seismic isolation [C]. 1990. ASME PVP. Nashville, Tennessee.

Kenji Kanazawa, Kazuta Hirta, Akihiro Matsuda. Shaking Table Test of Three-Dimensional Base Isolation System Using Laminated Thick Rubber Bearings [C]. 15th SMiRT. Seoul, Korea, 1999.

Wang Tao, Wang Fei, Ding Lutong. Theoretical and experimental study on three-dimensional base-isolated nuclear power plant [J]. China Civil Engineering Journal,2012,45(S1):238-242.

Wang Tao. Seismic performance of three-dimensional base-isolated nuclear power plant [C]. Professional Committee of Reactor Structural Mechanics, Chinese Society of Mechanics. Proceedings of the 17th National Conference on Reactor Structural Mechanics. 2012:55-60.

Li Hailong, Chu Qibao, Xu Yu, Yang Hongyi, Wen Jin. Research and Apply of Nuclear Power Plant Seismic Isolation in Japan [J]. Development Innovation of Machinery Electrical Products, 2013,26(03):13-14+20.

Lin J, Wang Y. Optimal Analysis of Tuned Mass Dampers [J]. Earthquake Engineering and Engineering Vibration,1996(01):116-121.

Zhou F, Zhang Y, Tan P. Theoretical Study on Story Isolation System [J].China Civil Engineering Journal,2009,42(08):1-8.

Hou Gangling, Zhao Can, Wang Xiaodong, Sun Hai, Zheng Gang, Chen Yaodong, Shen Feng. Shield Building with Inter-Story Isolation for AP1000 Nuclear Power Units and Its Seismic Performance Study [J]. Nuclear Power Engineering,2018,39(06):86-91.v

Iuliis D M , Petti L, Palazzo B. Combined Control strategy base isolation and tuned mass dampers: an effectiveness analysis of its application to nonlinear benchmark base isolated structure[C]//14th World Conference on Earthquake Engineering, Beijing, China, 2008

Taniguchi T, Kiureghian A D, Melkumyan M. Effect Of Tuned Mass Damper On Displacement Demand Of Base-isolated Structures[J]. Engineering Structures, 2008, 30(12):3478-3488.

Hou Gangling, Wang Bingyuan, Li Meng, Song Tianshu, Pan Rong. BIS-TMD shield building for AP 1 000 nuclear power plants and its seismic performance studies [J]. Earthquake Engineering and Engineering Dynamics,2018,38(04):132-142.

Yang Q, Li C, Xu H, Liu W. Seismic Response Analysis of Isolated Nuclear Power Plant Based on Negative Stiffness Damping [J]. Atomic Energy Science and Technology,2019,53(04):718-727.

Graesser E J , Cozzarelli F A . Shape memory Alloys as New Materials for Aseismic Isolation[J]. Journal of Engineering Mechanics, 1991, 117(11):2590-2608.

Eunsoo, Choi, Do-Hyung, et al. Shape memory alloy bending bars as seismic restrainers for bridges in seismic areas[J]. International Journal of Steel Structures, 2009.

DONATELLO, CARDONE, MAURO, et al. THE BEHAVIOUR OF SMA ISOLATION SYSTEMS BASED ON A FULL-SCALE RELEASE TEST[J]. Journal of Earthquake Engineering, 2008.

Donatello, Cardone, Peyman, et al. Shaking Table Tests of the Smart Restorable Sliding Base Isolation System (SRSBIS)[J]. Journal of Earthquake Engineering, 2011.

Ozbulut O E , Hurlebaus S . Optimal design of superelastic-friction base isolators for seismic protection of highway bridges against near-field earthquakes[J]. Earthquake Engineering & Structural Dynamics, 2011, 40(3).

Zhuang Peng, et al. Hysteretic Performance of a SMA Spring-friction Bearing [J]. Journal of Vibration and Shock,2016,35(09):94-100+116.

GB 50267-1997, Code for seismic design of nuclear power plants [S].

Zhou Fulin, Tan Ping, Liu Dewen. The earthquake threat and countermeasures to the safety of nuclear power plants [J]. Journal of Chinese Engineering Science,2013,15(04):36-40.

U.S. NRC. RG 1.208: A performance-based approach to define the site-specific earthquake ground motion[S]. U. S. NRC, 2007.

U. S. NRC. NUREG/CR- 6241(1994):Technical guidelines for seismic design of nuclear power plants [S].Translation of JEAG 4601-1987.

U.S. NRC. RG1.60 Rev 1: Design response spectra for seismic design of nuclear power plants[S] .U. S. NRC, 1973.

Wang Yan. Seismic Isolation and Its Application in Nuclear Power Station [J]. Journal of Hebei Institute of Architectural Engineering, 2004(01):38-41.

Hou Gang-ling, Chen Shuhua, Li Dongmei. Analysis of Structural Seismic Response of Nuclear Power Plant Concrete Containment Vessel with Isolating Devices [J]. Nuclear Power Engineering, 2011,32(S1):76-79.

Li Dongmei. A Dissertation for the Degree of M.Eng Seismic Analysis of a Reinforced Concrete Containment vessel on Isolating Devices [D]. Harbin Engineering University,2007.

Zhao Chunfeng, Chen Jianyun. Influence of Base Isolation System on Seismic Resistance of Nuclear Power Plant Containment [J].Explosion and Shock Waves,2014,34(05):615-621.

Zhuang Peng, Xue Suduo, Han Miao. Experimental study of hysteretic performance of SMA spring-friction bearing [J]. Earthquake Engineering and Engineering Dynamics,2016,36(04):163-169.

YAN Weiming, DAI Yingnan, CHEN Shicai. Shaking Table Test of a Base-isolated Nuclear Power Plant [J]. Journal of Beijing University of Technology,2018,44(12):1513-1520.

Kasalanati A , Constantinou M C . Experimental Study of Bridge Elastomeric and Other Isolation and Energy Dissipation Systems with Emphasis on Uplift Prevention and High Velocity Near-Source Seismic Excitation[J]. Technical Report Mceer, 1999(99-0004).

Shang Shouping, Cui Xianglong. New progress and problems in research and application of base isolation [J]. Journal of Guangxi University (Nat Sci Ed),2016,41(01):21-28.

Kitamura S , Morishita M . Design Method of Vertical Component Isolation System[C]// Asme Pressure Vessels & Piping Conference. 2002.

Zhiguang Zhou, Jenna Wong, Stephen Mahin. Potentiality of Using Vertical and Three-Dimensional Isolation Systems in Nuclear Structures[J]. Nuclear Engineering and Technology,2016,48(5).

James M. Kelly. Analysis of Fiber-Reinforced Elastomeric Isolators[J]. Ssd Block Fault Flat Ramp Flat Faults Barrandian, 1999, 44(3):1-8.

Syed M B , Patisson L , Curtido M , et al. The challenging requirements of the ITER anti seismic bearings[J]. Nuclear Engineering and Design, 2014, 269:212-216.

Kubo T , Yamamoto T , Sato K , et al. A SEISMIC DESIGN OF NUCLEAR REACTOR BUILDING STRUCTURES APPLYING SEISMIC ISOLATION SYSTEM IN A HIGH SEISMICITY REGION – A FEASIBILITY CASE STUDY IN JAPAN-[J]. Nuclear Engineering and Technology, 2014.

INTERNATIONAL ATOMIC ENERGY AGENCY, Seismic Isolation Systems for Nuclear Installations, IAEA-TECDOC-1905, IAEA, Vienna (2020).

US NUCLEAR REGULATORY COMMISSION, Technical Considerations for Seismic Isolation of Nuclear Facilities, NUREG/CR-7253, USNRC, Washington, DC (2018).

AVALLET, C., Seismic Cliff-edge Effects in the Primary Circuits of the European Fast Reactor. Part 1: Seismic Response of the Structures, Paper K18/5, SMiRT 14, Lyon(1977).

GB/T 51408-202, Standard for seismic isolation design of building[S].

Abstract: SMiRT 26
10 – 15 July 2022 in Berlin/Potsdam, Germany
Special Session: Seismic Isolation

A STUDY ON SEISMIC SSI ANALYSIS OF A BASE-ISOLATED STORAGE STRUCTURE FOUNDED ON FIRM SOIL

Dan M. Ghiocel[1], Victor Kostarev[2], Alex Kultsep[3] and Peter Nawrotzki[4]

[1] President, Ghiocel Predictive Technologies, Inc., New York, USA (dan.ghiocel@ghiocel-tech.com)
[2] President, CKTI-Vibroseism, Saint-Petersburg, Russia (victor.kostarev@gmail.com)
[3] Principal, CKTI-Vibroseism, Saint-Petersburg, Russia (alex.kultsep@cvs.spb.ru)
[4] Director, GERB Vibration Control Systems, Berlin/Essen, Germany (peter.nawrotzki@gerb.de)

ABSTRACT

The paper investigates the seismic SSI effects for a base-isolated reinforced concrete (RC) storage structure founded on firm soil. Three types of base-isolators are considered: 1) Lead-Rubber Bearing (LRB) isolators, 2) Triple Pendulum Friction (TPB) and 3) Base Control System (BCS) isolators including a combination of spring units and high-viscosity damper units. Two level of earthquake severity are considered: 1) 0.40g for DBE and 2) 0.60g for BDBE (1.5 DBE). Both deterministic and probabilistic simulations are considered. The paper also investigates the effects of motion incoherency on the SSI responses for base-isolated structure and shows that these effects are quite significant. The LRB and TPB isolators are modelled as hysteretic systems, while the BCS isolators are modelled using a combination of linear springs and frequency-dependent 3D high-viscosity damper (HVD) systems. Results highlight the significant additional benefits of the 3D-space BCS in comparison with the traditional 2D-space horizontal LRB and TPB systems, for reducing of the large structural amplifications due local vibration modes, reducing drastically the floor vertical vibrations, totally filtering out the detrimental amplifications due to the motion incoherency effects, and also reducing the structural moments more significantly than the other isolation systems.

INTRODUCTION

To perform the deterministic and probabilistic nonlinear seismic SSI analyses for the base-isolated auxiliary storage (AS) structure for the hysteretic LRB and TPB isolators, the ACS SASSI NQA software with advanced options PRO (probabilistic SSI) and NON (nonlinear hysteretic isolators) capabilities was used (GP Technologies, 2022). The ACS SASSI NQA also includes specialized frequency-dependent HVD finite elements that are defined as a combination of two parallel Maxwell chains (with 3-nodes each) including a total of four input parameters (Ghiocel, 2019, Kostarev et al., 2019, Nawrotski et al., 2019).

AUXILIARY STORAGE (AS) STRUCTURE MODEL

The two-level hypothetical AS structure FE model used in this study is shown in Figure 1. The structure has a square shape in horizontal plane with a size of 48m x 48m, and height of 22.5m. The total AS stracture weight is 48, 315 tons. The AS structure is like a stiff concrete box with four exterior walls including inside a separation wall and three frame structures for supporting the moving cranes in X-direction. The frames are designed to be not connected to the building exterior walls.

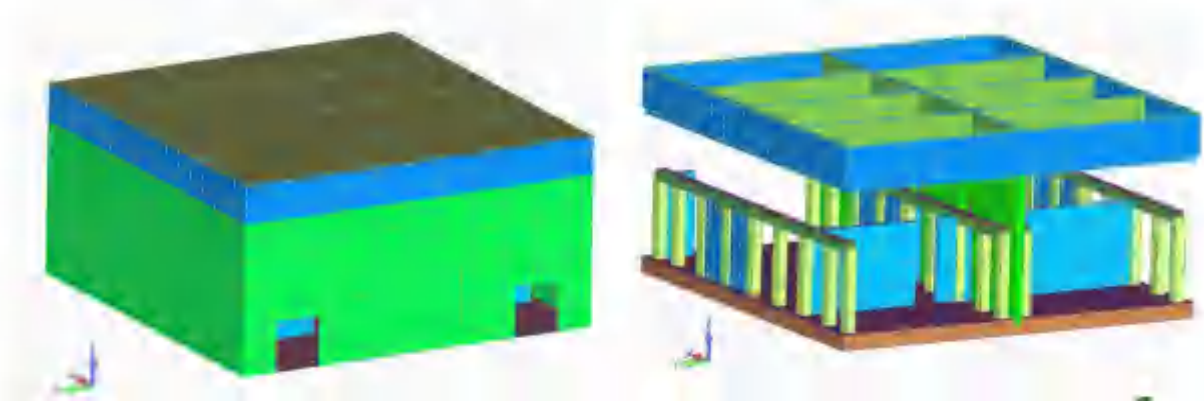

Figure 1 AS Structure FE Model; Exterior View (left) and Interior View (right)

The AS concrete box structure is very stiff with horizontal and vertical natural vibration frequencies above 10 Hz. However, the internal crane frames are more flexible having transversal vibration modes in Y-direction at about 4.4 Hz and 6.9 Hz frequencies.

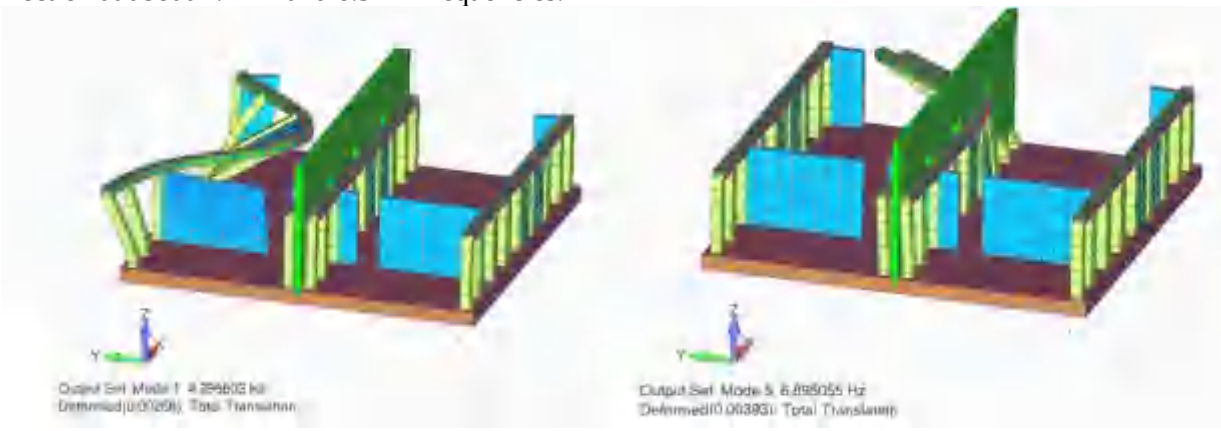

Figure 2 Transverse Vibration Modes of Crane Frames in Y-Direction

BASE ISOLATOR INPUT DATA

The isolators were uniformly distributed on the foundation mat area. A total of 121 isolators were considered equally spaces on a grid of 11 x 11 for all bearing types.

Lead-Rubber Bearing (LRB) Isolators

121 Bridgestone LH070G4 devices were selected. The LRB were modeled using nonlinear shear springs for horizontal direction, and very stiff linear axial springs for vertical direction. For nonlinear springs a set of back-bone curves (BBC) were defined for horizontal spring force as function of horizontal displacement. The characteristic parameters of the BBC are provided in Figure 3.

Do (mm)	Outer diameter	700
Kd (N/mm)	Post-yield stiffness	740.45
Qd (N)	Characteristic strength	62486
K1 (N/mm)	Initial stiffness	9675.9
Kv (N/mm)	Compressive stiffness	2243484.0

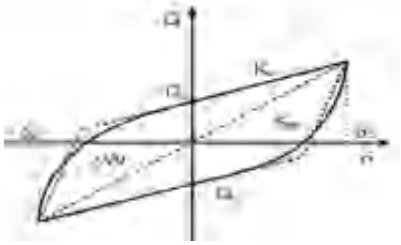

Figure 3. LRB Isolator Back-Bone Curve and Hysteretic Loop for Cyclic Motion

Triple Pendulum Bearing (TPB) Isolators

121 Standard TPB isolators were selected as shown in Figure 4 (Fenz and Constantinou, 2008). The TPB were modeled using nonlinear shear springs for horizontal direction, and very stiff linear axial springs for vertical direction. For nonlinear springs a set of back-bone curves (BBC) were defined for horizontal spring force depending on horizontal displacement. The BBC data is provided in Figure 5.

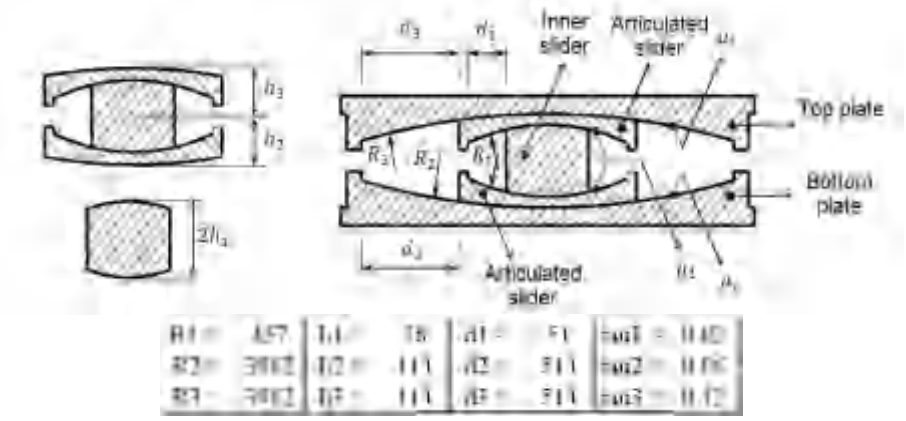

Figure 4 Standard TPB Isolator Characteristics

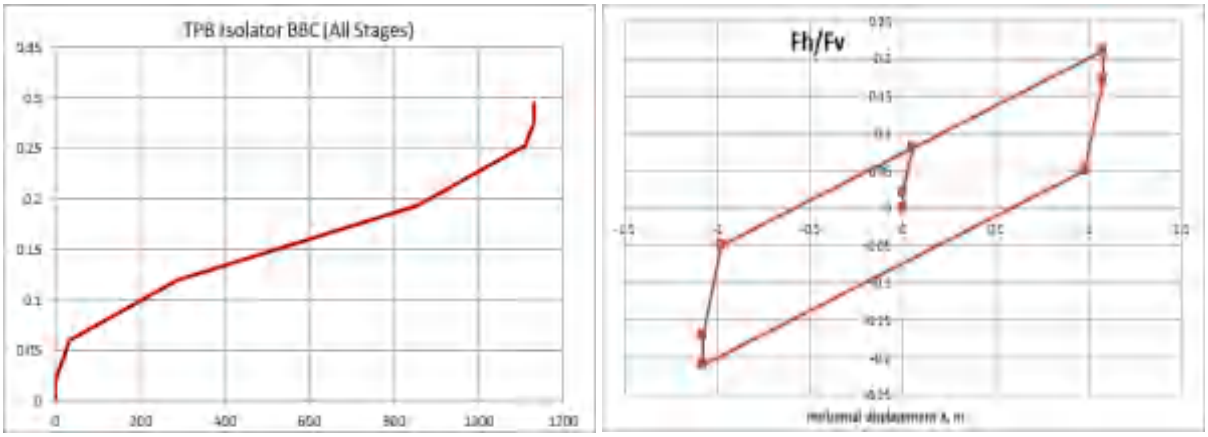

Figure 5 TPB Isolator Back-Bone Curve (All Stages) and Hysteretic Loop for Given Cyclic Amplitude

It should be noted that the BBC is a normalized curve to the vertical axial load in isolators, herein assumed to be constant and produced by the gravity load. The nonlinear spring modeling is simplified since it does not capture the TPB pendulum effects due to the concave geometry of the friction surfaces and friction dependency on instant force and velocity, which are expected to produce some high-frequency vibration components and tendency to uplift as shown against experiments (Fenz and Constantinou, 2008).

Base Control System (BCS) Isolators

121 FE-NI-BCS-02.2 GERB Spring Blocks modeled by linear axial spring elements and 121 viscous dampers modeled by frequency-dependent HVD elements. Dampers are placed nearby of spring blocks.

Type	Capacity (MN)	Kh (kN/mm)	Kv (kN/mm)	Static deflection under dead load (mm)	Limit horizontal displacement (mm)
FE-NI-BCS-02.2	3.85	6.65	71	50.1	150

The HVD unit properties (4 parameter Maxwell model with 2 chains) are as follows;

Type	Kh1 (kN/mm)	Kh2 (kN/mm)	Ch1 (kNs/m)	Ch2 (kNs/m)
VDVL-850/500/437-145/95-11 RHY	64.6	54.0	738.1	6372.0
	Kv1 (kN/mm)	Kv2 (kN/mm)	Cv1 (kNs/m)	Cv2 (kNs/m)
	58.0	24.6	549.1	1899.4

SEISMIC SSI ANALYSIS INPUTS

For the seismic DRS input is shown in Figure 6 was used for deterministic analysis and probabilistic analysis for BDBE level with 0.60g for horizontal directions and 0.40g for vertical direction. For DBE level, the DRS was scaled to 0.40g for horizontal and 0.27g for vertical direction. The soil condition was defined by a deep soil deposit with Vs=600 m/s. For the 60 probabilistic DRS simulations, the lognormal distribution was assumed and a c.o.v. of 20% was considered. For the 60 probabilistic Vs profiles, the lognormal distribution was assumed and a c.o.v. of 22% was considered. No probabilistic variations are considered for structure.

For the LRB and TPB hysteretic isolators, nonlinear SSI analysis was performed with the ACS SASSI Option NON software (GP Technologies, 2022) using nonlinear springs for isolator behavior modeling. Figure 7 shows two typical LRB and TPB isolator shear force hysteretic responses for the base-isolated AS structure for the 0.40g DBE input. The TPB isolators behave much stiffer than the LRB isolators.

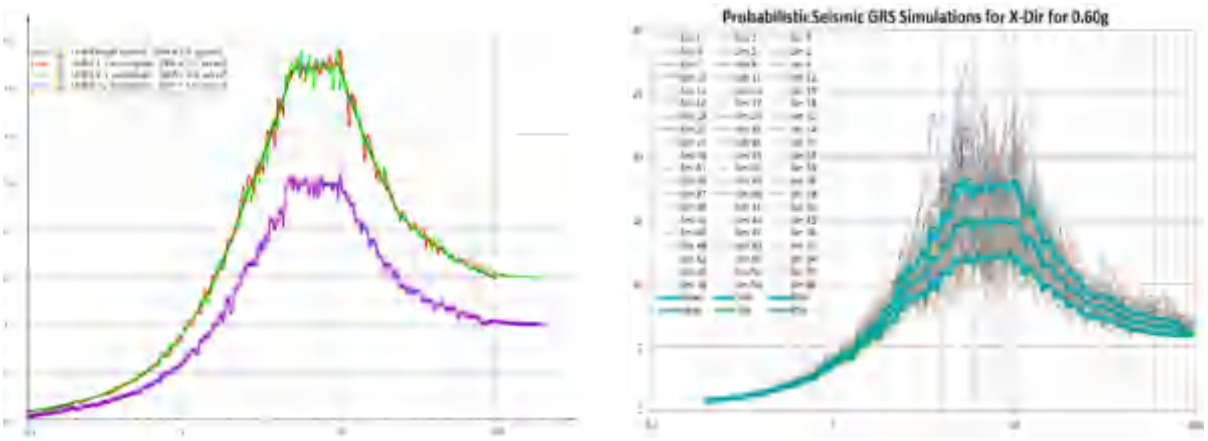

Figure 6 Seismic DRS Input Scaled at 0.60g; Deterministic (left) and Probabilistic (right) w/ 60 Samples

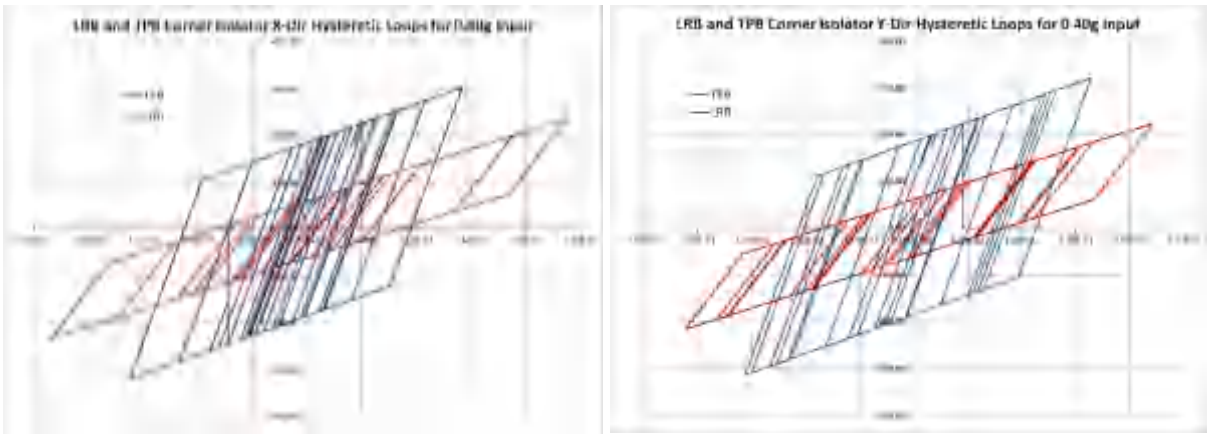

Figure 7 Nonlinear LRB and TPB Isolator Responses for X and Y Directions

SEISMIC SSI RESPONSES FOR COHERENT SEISMIC INPUT

The seismic SSI analyses were performed for the AS structure sitting on LRB, TPB or BCS isolators, and, for comparison, on perfectly rigid isolators. Figure 8 shows the selected seismic response locations. To investigate the AS structure motion, four node locations, specifically, nodes 803, 2620, 2640 and 4459, were considered (left). For evaluating the efficiency of base-isolation on reducing structural forces, two columns of a crane frame were selected (right).

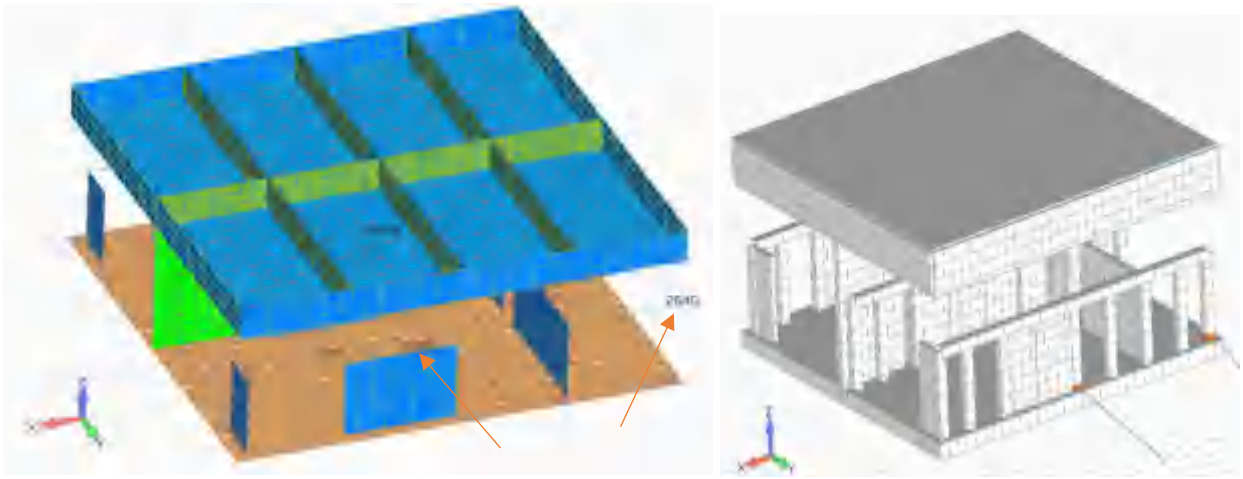

Figure 8 Outputs for SSI Response; Four Node Locations (left) and Two Base Columns (right)

Since the frame is along the X-direction, it is expected that large amplification local vibration modes will manifest in Y-direction (see also Figure 2).

Figures 9 and 10 shows computed ISRS at the top basemat above isolators (Node 803) and roof level (Node 4459) for 0.40g horizontal input. Nodes 803 and 4456 are on the AS main box structure. Computed results include the deterministic ISRS for LRB, TPB, BCS and Rigid isolators, but also the probabilistic simulation-based ISRS computed for the mean and 80% non-exceedance probability (NEP).

Figure 9 shows the top base ISRS for X-horizontal and Z-vertical directions. It should be noted that for horizontal direction the LRB isolators are the softest isolators, while the BCS isolators are the stiffest isolators. The ISRS amplitude reduction factors for the horizontal ISRS at the top basemat is about 2 for BCS and about 5 for LRB and TPB. For vertical ISRS, there is a 15-20% amplitude amplification for all LRB, TPB and BCS. The BCS isolators show a substantial reduced isolator stiffness in vertical direction in comparison the LRB and TPB isolators.

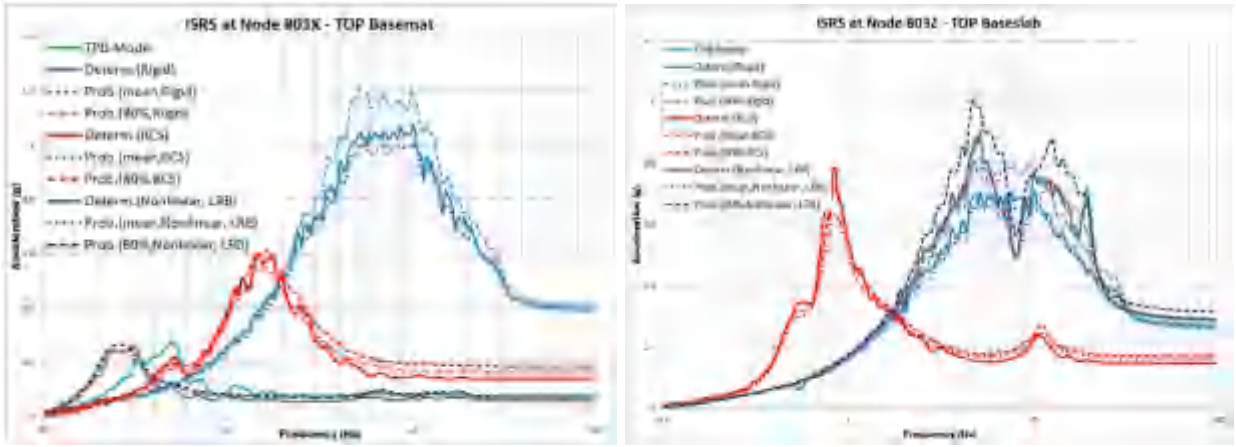

Figure 9 Comparative ISRS for Top Basemet Location (Node 803) in X and Z Directions

Figure 10 shows the roof ISRS for ISRS for Y-horizontal (left) and Z-vertical (right) directions. It should be noted the large benefit from all isolators for reduction the horizontal ISRS amplitudes. For the vertical direction, the BCS isolators are much more efficient since they reduce the floor vibration by few times more than the LRB isolators. From Figure 10, there is another aspect to be remarked, that the probabilistic-based mean and 80% NEP horizontal ISRS are significantly larger that the deterministic ISRS. However, herein, the deterministic ISRS was computed only for a single BE soil profile, not as an envelope of three ISRS for BE, LB and UB soils. If the 80% NEP ISRS are considered for deterministic design of base-isolated structures as discussed in ASCE 4-16 Chapter 1 Commentary, then, using multiple randomized seismic inputs simulations, as recommended in ASCE 4-16 Chapter 12, appears to be strongly justified.

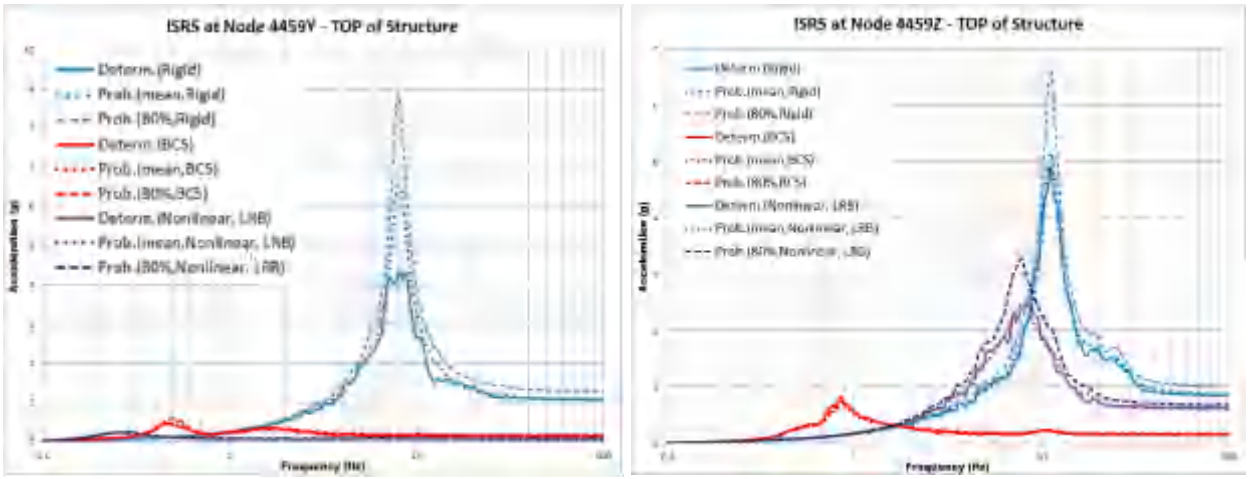

Figure 10 Comparative ISRS for Top Floor (Roof) Location (Node 4459) in X and Z Directions

As a note, it should be understood that the BCS system behavior can be signficantly improved if the viscous damper units are placed denser on the basemat perimeter to damp the rocking motion. Herein, as the initial part of the study, we considered the viscous dampers spatially uniformly distributed on the basemat.

Figure 11 shows the AS structure motion (frozen at a given time step) for the LRB (left) and BCS (right) base isolators under seismic coherent inputs. External walls are not shown. It should be noted that using the BCS isolators, there is basically no transmission of the basemat deformation into the structure. The BCS isolated structure moves a rigid body. However, this BCS rigid body behavior is only possible since the BCS vertical stiffness is much softer than the LRB vertical stiffness.

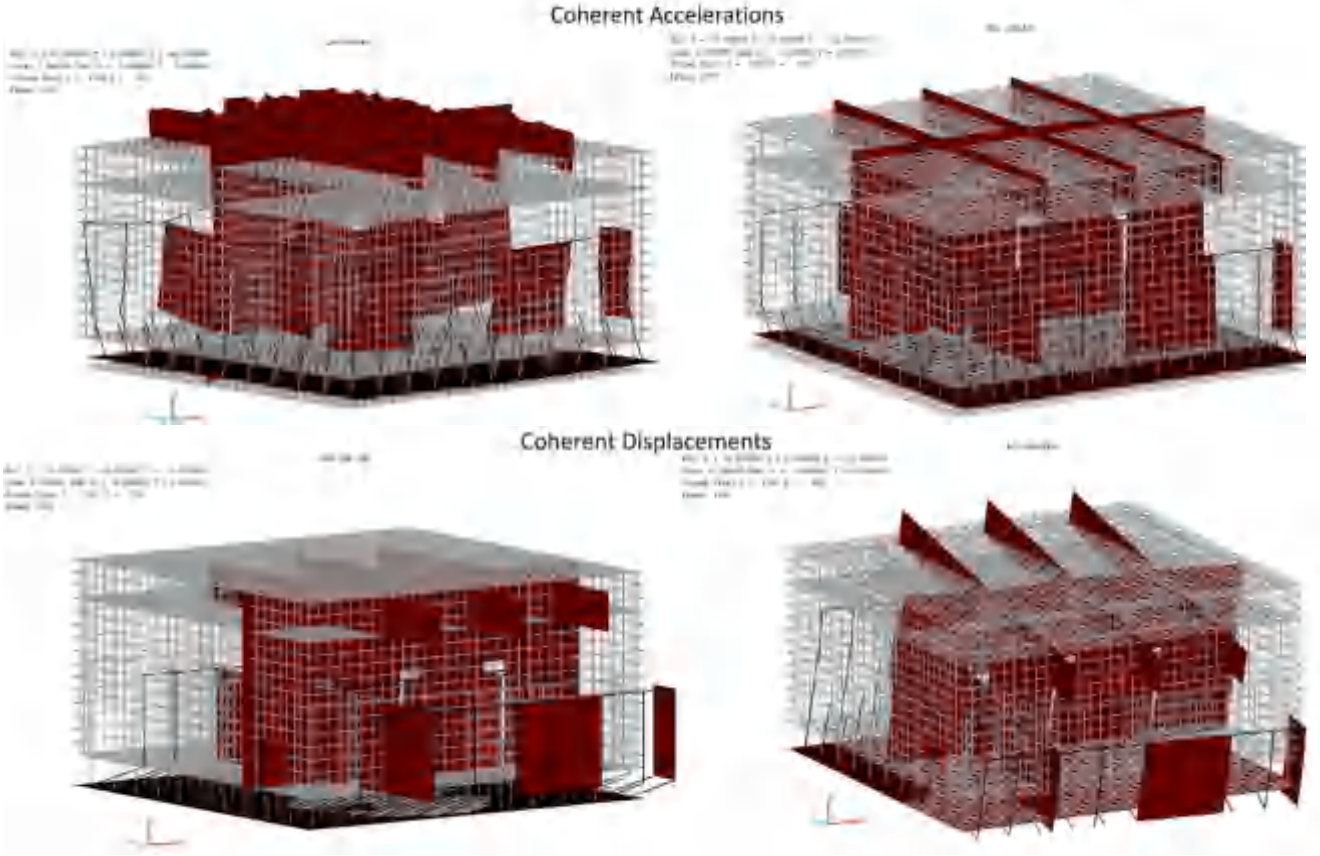

Figure 11 LRB (left) and BCS (right) Isolated AS Structure Motion at Given Time;
Acceleration (upper) and Displacements (lower)

Figures 12 and 13 show the ISRS on the top of the selected crane frame in the Y-transverse direction, at nodes 2620 and 2640 (see Figure 8 right for node locations). The left plots include the Rigid isolator case.

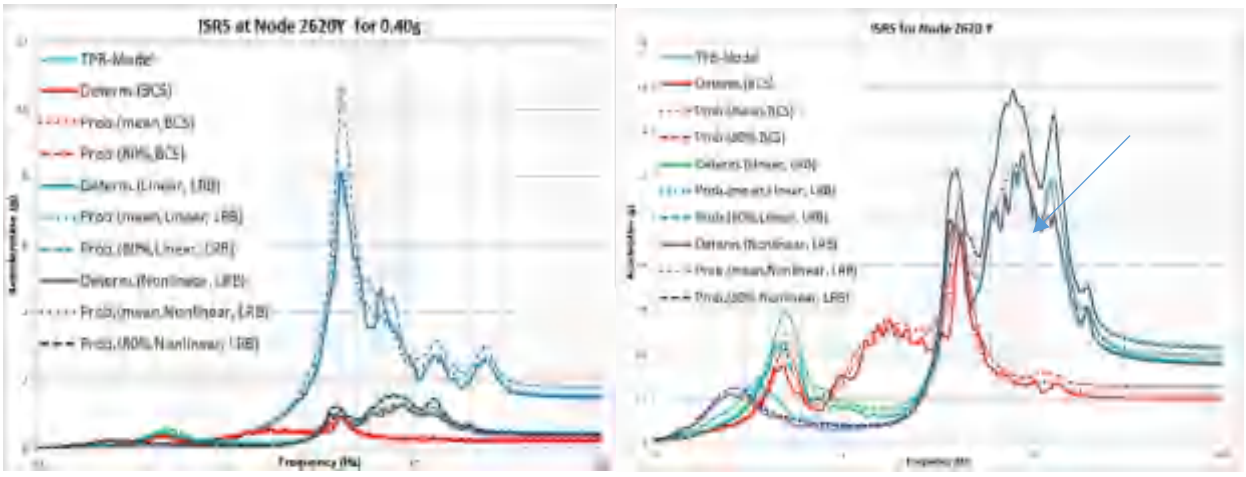

Figure 12 Comparative ISRS for Crane Frame Location (Node 2620) in Y Direction

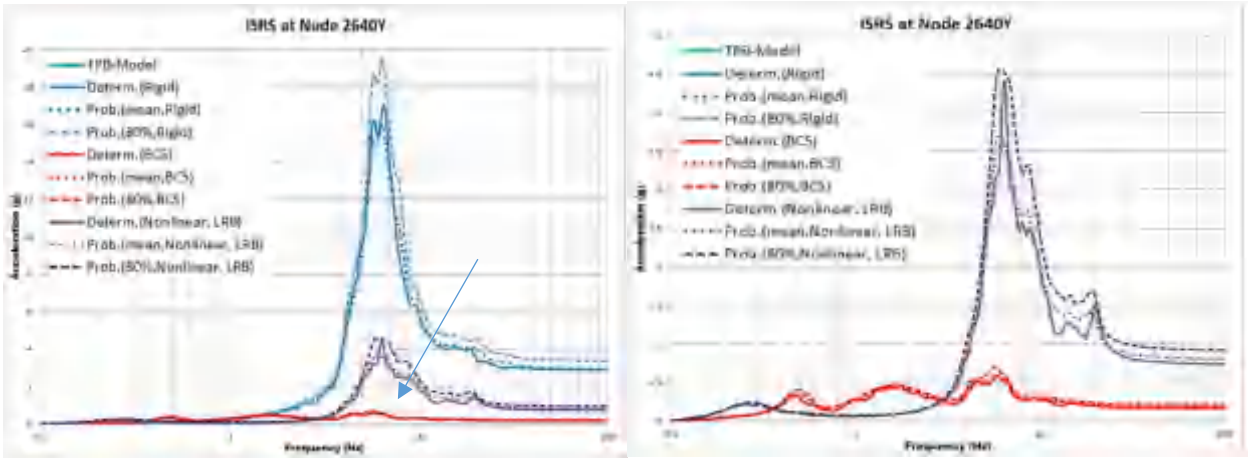

Figure 13 Comparative ISRS for Crane Frame Location (Node 2640) in Y Direction

In comparison with the Rigid isolator case, all isolator types, perform very well providing a deterministic ISRS peak reduction of at least 4 times for the 2640 node location, and 5-6 times for the 2620 node location. However, Figure 13 indicate that for the local vibration modes of the crane frame, the BCS isolators significantly outperforms the LRB and TPB isolators. For BCS isolators the 2640Y ISRS reduction is about 32 times, in comparison with LRB isolators for which 2640Y ISRS reduction is only 4 times, so that the ISRS peak has still a high amplitude of 4.5g.

Table 1 is a summary for the base-isolated AS structure displacement with respect to the bottom basemat center location below isolators. Both 0.4g and 0.6 input levels are included. As expected, the table results indicate for the BCS isolators smaller horizontal displacement amplitudes and much larger vertical displacement amplitudes. At the top basemat level, above isolators, the BCS horizontal displacement amplitude is 30.38 mm, which is about 6 times smaller than LRB and 3.3 times smaller than TPB isolators.

Table 1 Base-Isolated AS Structure Deterministic Maximum Displacement With Respect to Bottom Basemat center (Below Isolators)

		0.40g			0.60g		
		Bottom Base Center Node			Bottom Base Center		
	Nodal	Dx(mm)	Dy(mm)	Dz(mm)	Dx(mm)	Dy(mm)	Dz(mm)
RIGID	803	0.0835	0.0827	0.0856	0.0853	0.0841	0.0883
	2620	0.6984	15.0897	0.1118	1.0443	28.0265	0.1673
	2640	1.0155	13.3082	0.0167	1.5303	26.9569	0.0242
	4459	2.3573	4.156	1.6695	4.406	6.2343	2.4674
BCS	803	30.376	25.359	69.1061	45.5646	38.9384	104.62
	2620	28.4378	64.5371	115.725	102.203	96.8021	173.307
	2640	26.2556	61.7176	126.203	102.79	92.5774	188.612
	4459	102.083	89.5653	57.0814	153.119	134.348	85.376
LRB	803	186.069	219.186	0.1545	281.934	290.888	0.2377
	2620	166.94	220.369	1.0034	264.324	296.575	1.5279
	2640	169.571	219.086	1.2349	264.423	295.014	1.8494
	4459	186.848	219.849	2.4651	284.513	291.556	3.2872
TPB	803	102.239	130.002	0.1655	157.767	194.044	0.2604
	2620	101.043	131.044	0.9177	156.267	195.499	1.3489
	2640	101.887	125.047	1.1455	158.357	188.9	2.0353
	4459	102.539	129.739	2.2001	158.335	195.16	3.319

Table 2 shows the deterministic maximum moments computed in the two frame crane columns (see Figure 8 right) for 0.40g and 0.60g seismic input. Table 2 results indicate the efficiency of base isolation to reduce

structural component forces (kN) and moments (kN-m). The maximum largest moment M3 reduction factors are in the range of 6.2-15.2 for BCS, 5.1-6.7 for LRB and 5-6.1 for TPB.

Table 2 Base-Isolated AS Structure Crane Frame Column Deterministic Maximum Moments

		0.4g						0.6g					
		Point 1 (Element 190)						Point 2 (Element 224)					
		M1 TORSION SIS effect,		M2 SIS effect,		M3 SIS effect,		M1 TORSION SIS effect,		M2 SIS effect,		M3 SIS effect,	
Model	Node #	Mt, kN/ times=		Mt, kN/ times=		Mt, kNn times=		Mt, kNn times=		Mt, kNn times=		Mt, kNn times=	
RIGID	59 (Node	7.9		754.9		4360.5		11.8		1102.1		6540.6	
	1148 (No	7.9		744		3378		11.8		815.8		5068.8	
	1129 (No	146.8		103.2		3786.2		220.2		154.8		5679	
	40 (Node	146.8		496.2		2935.4		220.2		744.8		4 [illegible]	
BCS	59 (Node	0.7	11.3	[illegible]	[illegible]	319	13.9	1.1	10.7	292.7	3.9	4691	13.9
	1148 (No	0.7	11.3	681.8	8.1	221.8	15.2	1.1	10.7	1022.7	4.3	3326	15.2
	1129 (No	29.8	4.9	83.7	2.8	427.3	6.5	44.7	6.5	1255	2.4	6405	6.5
	40 (Node	29.8	4.9	156	3.1	475.1	6.2	44.7	4.9	2458	3.0	7122	6.2
LRB	59 (Node	2.2	3.6	147.7	6.2	897.7	4.9	3.2	5.7	1706	6.5	1294	5.1
	1148 (No	2.2	3.6	82.9	6.6	668.4	5.1	3.2	5.3	1202	6.8	975.1	5.2
	1129 (No	35.9	4.1	28.2	3.4	450.2	6.2	51.8	4.1	97.1	4.2	642.7	6.5
	40 (Node	35.9	4.1	69.3	7.1	457.7	6.4	51.8	4.3	100.2	7.4	655.3	6.7
TPB	59 (Node	2.2	3.8	182	5.7	880.7	4.9	3.3	5.8	1901.1	5.8	1210.3	5.0
	1148 (No	2.2	3.8	98.7	5.7	667.6	5.1	3.3	5.6	1320.6	6.2	984.1	5.1
	1129 (No	39	3.8	41.8	4.1	493	5.7	56	4.1	48.2	3.5	705.8	5.8
	40 (Node	39	3.8	75.8	4.8	498.2	5.9	56	3.9	109.6	6.8	714.1	6.1

Table 3 shows the deterministic maximum forces (kN) in isolators, including the Rigid isolator case as a reference case. It should be noted that the largest forces are in the corner isolators at the node 121. The BCS isolators, as expected, provide the maximum isolation benefits reducing the maximum isolator forces by about three times in comparison with the LRB and TPB isolators.

Table 3 Maximum Seismic Forces in the AS Structure Base-Isolators

		0.4g			0.6g		
Model	Element #	Axial Force Z	Shear Force X	Shear Force Y	Axial Force Z	Shear Force X	Shear Force Y
RIGID	Corner Element 1	6847.2	2718.2	3711	10270.6	4076.3	13066.7
	Corner Element 61	9175.5	2916	9522.7	13760.9	3924	14283.5
	Corner Element 121	27993	4533	32666.4	41973	6769.8	48993.8
BCS	Corner Element 1	203.2	68	208.1	304.7	294	304.7
	Corner Element 61	181.9	179.1	183.5	272.6	268.7	275.3
	Corner Element 121	974.3	296.3	1064.6	1454.3	443.3	1550.1
LRB	Corner Element 1	204.9	204.5	205.2	40.5	40.4	40.5
	Corner Element 61	233	235.2	238.6	33.4	33.6	33.9
	Corner Element 121	3252	2044.4	3460.6	483.1	2981.4	5126.8
TPB	Corner Element 1	236.6	249.6	281.6	563.2	562.6	564.4
	Corner Element 61	226.3	227.6	236.2	4065	4054	4043
	Corner Element 121	3215.9	2012.6	3450.7	5342.3	2981.8	5775.1

COMPARATIVE RESPONSES UNDER COHERENT AND INCOHERENT INPUTS

In this section, the effects on motion incoherency on the base-isolated AS structure are investigated for the 0.40g seismic input. To model motion incoherency the Abrahamson coherence function for soil condition was applied (Abrahamson, 2007). For incoherent SSI analysis, the Stochastic Simulation approach implemented in ACS SASSI with five incoherent motion simulations was used to compute the average incoherent seismic responses. Only the LRB and BCS isolators are included.

Figure 14 shows the effects of motion incoherency on the ISRS computed at the top basemat above isolators, node 803. The left plots include the Rigid isolator case. For the X-horizontal direction, it should be noted that for LRB isolators the incoherent ISRS is highly amplified in comparison with coherent ISRS. The incoherent ISRS amplification corresponds to the dominant frequency range of the seismic input

motion. However, for the BCS isolators this ISRS discrepancy due to incoherency effects is not visible. The vertical ISRS show not much effects of motion incoherency.

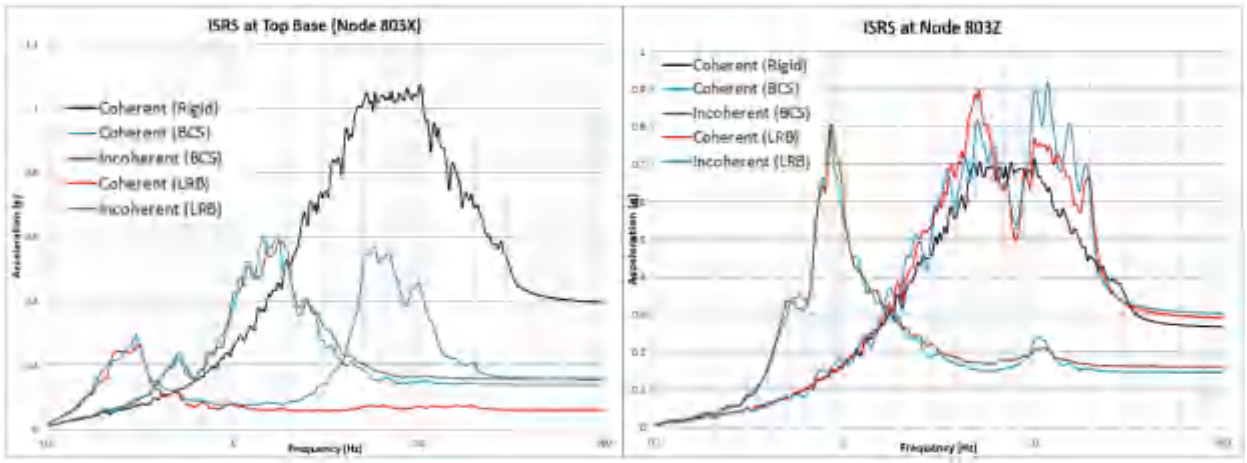

Figure 14 Comparative ISRS for Top Basemet Location (Node 803) in X and Z Directions

Figure 15 show the computed ISRS for roof level, node 4459 in X-direction. Left plots include the Rigid isolators case, while right plots do not include this case. Same incoherency effects as shown in Figure 14.

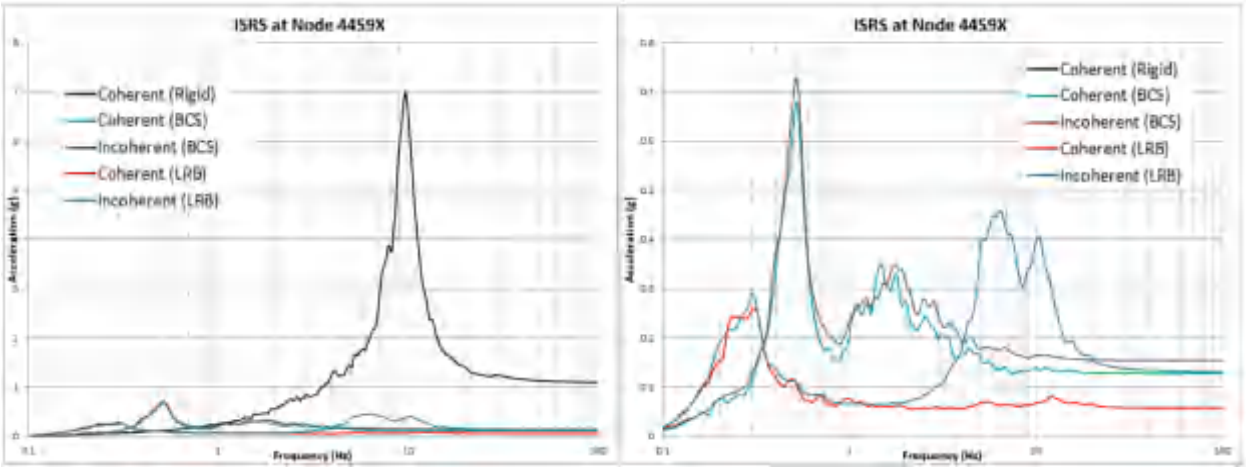

Figure 15 Comparative ISRS for Top Floor (Roof) Location (Node 4459) in X and Z Directions

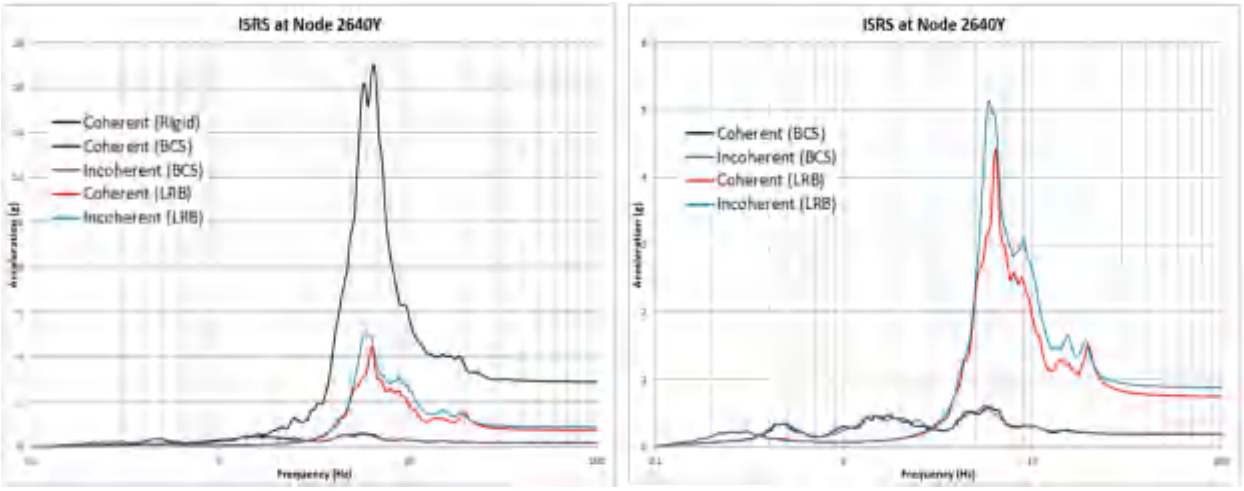

Figure 16 Comparative ISRS for Crane Frame Location (Node 2640) in Y Direction

Figure 16 shows the motion incoherency effects on the crane frame ISRS which is dominated by the local transverse vibration in Y-direction.

The BCS isolators again, under incoherent inputs, totally cut the ISRS amplification due to local vibration mode. This is a notable performance. The LRB isolators amplify slightly higher the horizontal ISRS due to the local mode effects under the incoherent inputs.

Figures 17 and 18 show for crane frame locations all the five incoherent ISRS simulations in comparison with coherent ISRS. The LRB results are shown in left plots, while the BCS results are shown in right plots.

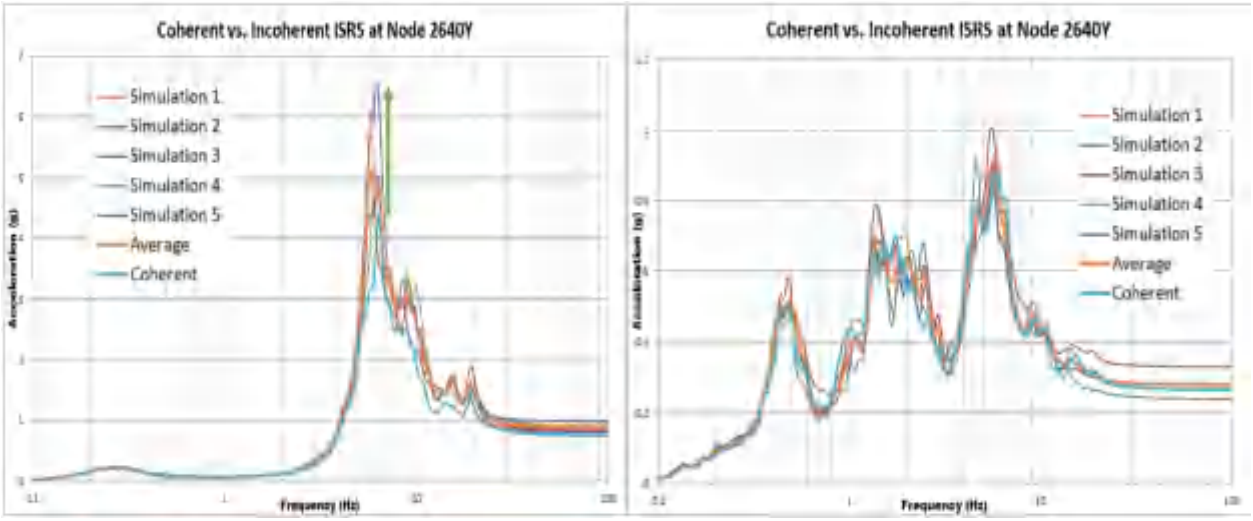

Figure 17 Incoherent ISRS Simulations for LRB and BCS Crane Frame Location (Node 2640) in Y Dir

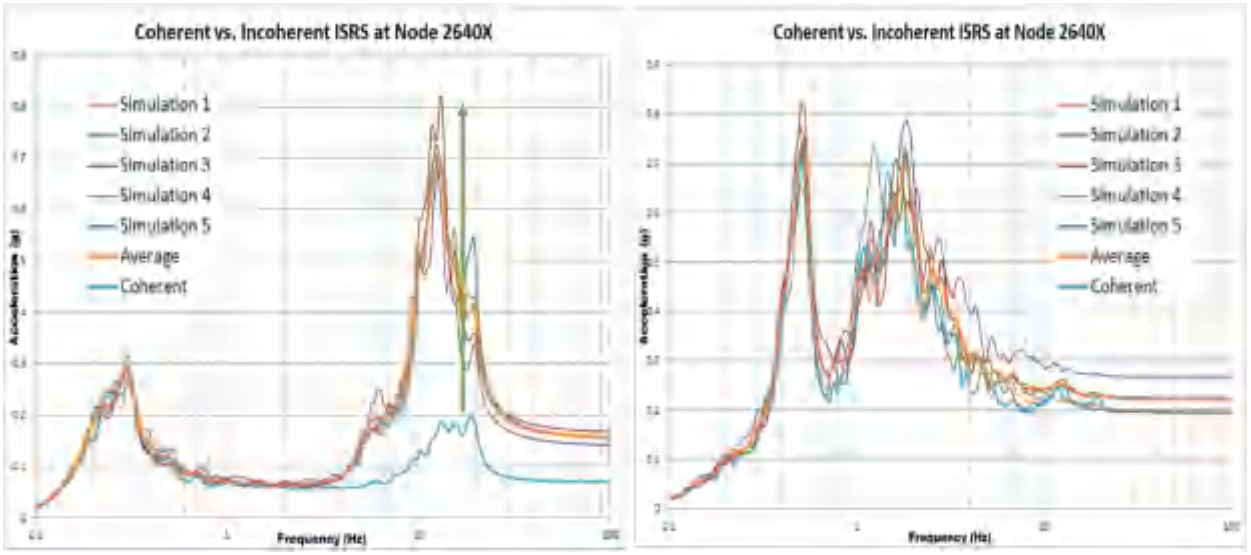

Figure 18 Incoherent ISRS Simulations for LRB and BCS Crane Frame Location (Node 2640) in X Dir

The green arrows in the LRB plots in Figures 17 and 18 show the ISRS spectral amplification due to motion incoherency effects. It should be noted that the BCS ISRS plots shows no visible ISRS amplification due to motion incoherency effects.

The effect of motion incoherency on AS structure response is visualized in Figures 19 and 20. Figure 19 shows the instant structural accelerations for LRB isolators for coherent (left) and incoherent (right) inputs. Apparently, there is a visible more global deformation of the AS structure due to incoherency.

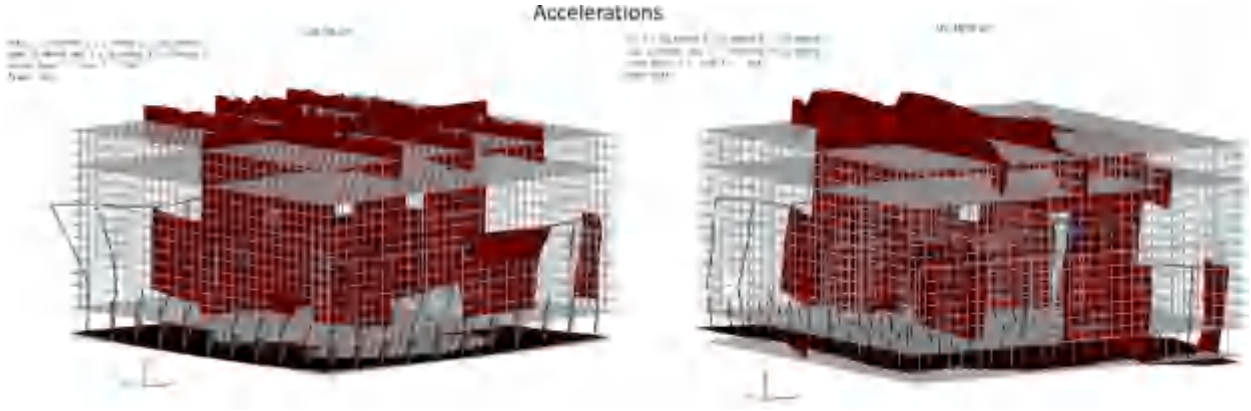

Figure 19 LRB Isolator Coherent (left) and Incoherent (right) Response Accelerations at Given Time;

Figure 20 shows the instant structural accelerations for BCS isolators for coherent (left) and incoherent (right) motion inputs. Apparently, there is no deformation of the AS structure due to incoherency.

Figure 20 BCS Isolator Coherent (left) and Incoherent (right) Response Accelerations at Given Time;

CONCLUDING REMARKS

The study results for the AS structure indicate significant benefits of the application of the 3D-space BCS isolation system in comparison with the traditional 2D-space horizontal LRB and TPB isolation systems. The BCS isolator system additional benefits in comparison with LRB and TPB systems include:

1) Reducing drastically the large ISRS amplifications due local vibration of the crane frame,
2) Reducing drastically the floor vertical vibrations due to its efficient vertical isolation,
3) Completely filtering out the detrimental amplifications due to motion incoherency effects, and
4) Reducing the structural base moments more significantly than the other isolation systems,

Future research studies will focus on the optimization of the BCS viscous damper unit distribution and locations with more units close to the perimeter edges of the basemat. An aspect of practical interest is also to improve the numerical modeling of the TPB isolators by including the pendulum effect and variable friction.

REFERENCES

Abrahamson, N. (2007).*Effects of Spatial Incoherence on Seismic Ground Motions*, Electric Power Research Institute, Palo Alto, CA and US Department of Energy, Germantown, MD, Report No. TR-1015110, December 20

American Society of Civil Engineers (2017), *Seismic Analysis for Safety-Related Nuclear Structures and Commentary*, ASCE 4-16 Standard

Fenz, D.M. and Constantinou, M.C. (2008). *Development, Implementation and Verification for Multi-Spherical Sliding Bearings*, Technical Report MCEER-08-0018, University of Buffalo, NY

Ghiocel, D.M. (2019) *Probabilistic Seismic SSI Analysis Sensitivity Studies for Base-Isolated Nuclear Structures Subjected to Coherent and Incoherent Motions*, the SMiRT25 Conference Proceedings, Division III, Charlotte, NC, August 4-9

GP Technologies, Inc. (2022). *ACS SASSI Version 4.3 User Manual, Including Advanced Options A-AA, NON, PRO, RVT-SIM and UPLIFT*, Revision 7, Pittsford, New York, January 31.

Kostarev, V., Nawrotzki, P., Vasilyev, P. and Vayndrakh, M. (2019) *Developing and natural scale testing of the 3D base isolation system*, 16th World Conference on Seismic Isolation. Energy Dissipation and active Vibration Control (16thWCSI), St. Petersburg

Nawrotzki, P., Siepe, D., and Salcedo. V. (2019). *Seismic protection of NPP structures using 3-D base control systems*. 25th International Conference on Structural Mechanics in Reactor Technology (SMiRT25), Charlotte, NC.

Transactions, **SMiRT-26**
Berlin/Potsdam, Germany, July 10-15, 2022
Division V

SEISMIC ISOLATION OF AN EMERGENCY DIESEL GENERATOR SYSTEM FOR NUCLEAR POWER PLANTS

Ricardo Bustamante[1], Gilberto Mosqueda[2]

[1] Ph.D. Student, University of California, San Diego
[2] Professor, University of California, San Diego (gmosqueda@ucsd.edu)

ABSTRACT

The post-earthquake functionality of an Emergency Diesel Generator (EDG) is critical for the safe shut down of Nuclear Power Plants (NPPs). The EDG performance requirements are embedded in the proposed seismic evaluation and qualification procedures of regulatory agencies, with both structural and functional failure modes considered. This paper evaluates the applicability of a 3D seismic protection system to enhance the seismic performance of an EDG under a relatively large seismic hazard. The proposed system consists of two isolation layers to decouple the seismic demand. The upper layer consists of linear springs and dampers to handle the vertical seismic demand, while the bottom layer consists of lead-rubber bearings to mitigate the horizontal seismic demand. The performance target is to reduce the EDG acceleration while limiting the isolation system lateral displacement based on the Engineering Demand Parameters (EDP) of the critical components. The isolation system design is challenged by the trade-off between reducing the acceleration response of the EDG and the displacement capacity across the isolation plan that can affect the performance of umbilical lines. The seismic performance of the seismically isolated EDG is examined under NCR R.160 seismic hazard imposing large accelerations and displacements at low periods and demonstrates that seismic isolation can be effectively reduce acceleration while limiting displacements.

INTRODUCTION

In the event of Loss of Offsite Power (LOOP), the functionality of Emergency Diesel Generators (EDG) is critical for the plant operation and, if necessary, safe shut down (Kančev et al., 2013). This function makes the EDG one of the most critical equipment within nuclear power plants required to maintain operations following an earthquake or other hazards and prevent potential core damage. These seismic performance requirements for EDGs considering independence, redundancy, and testability are embedded in the proposed seismic evaluation and qualification procedures (U.S. Nuclear Regulatory Commission, 2007, 2020). To maintain operation, both structural and functional failure modes have been considered for the EDG, with functional failure modes largely based on limited experimental data from testing on shaking tables (Jeong et al., 2019). A structural failure mode consists of stress damage to the equipment frame, the anchorage system, the pipelines, and ducts connected to the EDG. More generally, the EDG seismic performance and associated damage states have been related to Engineering Demand Parameters (EDP). Typically, the EDP used to assess the probability of damage has been the acceleration experienced by the EDG unit and accounts for functionality.

Past studies indicate the expected failure mode of an EDG during seismic shaking is anchor failure at the attachments; seismic isolation has been proposed as a solution to substantially reduce forces transferred to the anchor bolts and the foundation and increase the seismic capacity (Y.-S. Choun et al., 2007). In addition, a seismically isolated EDG can experience a significant reduction of the horizontal acceleration response, thus increasing the safety margin for critical EDP. Nevertheless, introducing seismic isolation imposes

additional challenges. The first is the vertical acceleration component, which can be amplified given the typical range of the natural vertical frequency of bearings, as evidenced in buildings (Ryan et al., 2013). The second challenge is related to the lateral displacement of the isolation system that should have sufficient clearance to move freely, and any umbilical crossing the isolation system must have sufficient deformation capacity. This introduces the need to consider an additional EDP based on lateral deformation of the isolation system. For example, the fuel pipeline is a critical umbilical line required for an EDG unit to remain functional. The third concern is related to the lateral deformation capacity of the bearings, typically expressed in terms of the shear strain, and can be characterized by a lateral displacement EDP.

A three-dimensional (3-D) seismic isolation system is designed for an EDG unit consisting of Lead Rubber Bearings (LRB), coils springs, and viscous dampers, merging the benefits of these devices to meet operational and seismic requirements. The 3-D isolation system is configured in two isolation levels considering the target design objective of decoupling the seismic demand in the horizontal and vertical directions. LRB are considered for isolation in the horizontal direction since they are widely accepted and applied in practice. Coil springs and dampers are considered for the vertical component, considering both the seismic and vibration operational demand though only seismic demands are examined here. The seismic isolation systems properties are determined, and bearing are designed to ensure feasibility. The proposed system is studied by performing a deterministic analysis using Engineering Demand Parameters to define and quantify its seismic performance.

SEISMIC ISOLATION OF EDG

Several authors have studied the application of base isolation to equipment and nonstructural components, including applications in the nuclear industry (Y.-S. Choun et al., 2007; Ebisawa et al., 2000; Furukawa et al., 2013; JAERI, 2000; Najafijozani et al., 2020). Different systems have been applied for vertical seismic demands, ranging from springs to dampers and a combination of both. The type of approach depends on how the horizontal isolation is considered. Najafijozani et al. (Najafijozani et al., 2020) studied adaptative vertical isolation of light-weight acceleration-sensitive equipment for a base-isolated NPP. Using a combination of springs and dampers, they achieve a reduction of the acceleration to meet the seismic capacity of the equipment. They focused solely on the vertical movement of the equipment, assuming the base isolation system of the NPP reduces the horizontal acceleration and suppresses any rocking. Since the Emergency Diesel Generator unit is typically located outside the NPP buildings, any seismic isolation system should isolate the unit horizontally and vertically.

Choun et al. (Y. Choun et al., 2006) experimentally studied the performance of the coil spring–damper unit under two different types of ground motions. Their study found amplification of the vertical acceleration of a given ground motion set and a reduction for another set, highlighting that the effectiveness of isolation is dependent on the natural vertical frequency of the coil spring-damper unit and the frequency content of the ground motion. A similar trend was found for the displacement response. Choun et al. (Y.-S. Choun et al., 2007) developed a base-isolated EDG numerical model and performed a numerical fragility analysis. The EDG was modelled as a single degree of freedom with the total weight lumped at mid-height of the equipment with a natural frequency is 34Hz. A fixed-base EDG model was developed for comparison purposes. They concluded that increasing the damping on the isolation system provides a lower failure probability. It was reported that the isolator would fail first before the EDG, while the EDG would fail at a lower PGA without isolation. The study showed that higher damping values would also decrease the lateral displacement of the system, reducing demands for the umbilical lines that cross the isolation interface. Ebisawa et al. (Ebisawa et al., 2000) studied the behavior of a horizontal isolation system and a horizontal and vertical isolation system. The latter consists of ball bearing units, coil springs, viscous dampers in the horizontal component, and air springs in the vertical direction. The vertical acceleration was reduced to

40% of the testbed acceleration. The study concluded that this isolation system effectively improves the seismic resistance and decreases the functional failure probability.

SEISMIC HAZARD AND LIMIT STATES

The effectiveness of seismic isolation is examined here for a relatively high seismic zone. The seismic input ground motions for the analysis consist of twenty dispersion-appropriate three-component ground motions that were used in a previous study for seismically isolated NPP (Schellenberg et al., 2015) following NRC RG1.60. Figure 1 shows the Pseudo Spectral Acceleration (PSA) and the ground motions, with a PGA=0.50g.

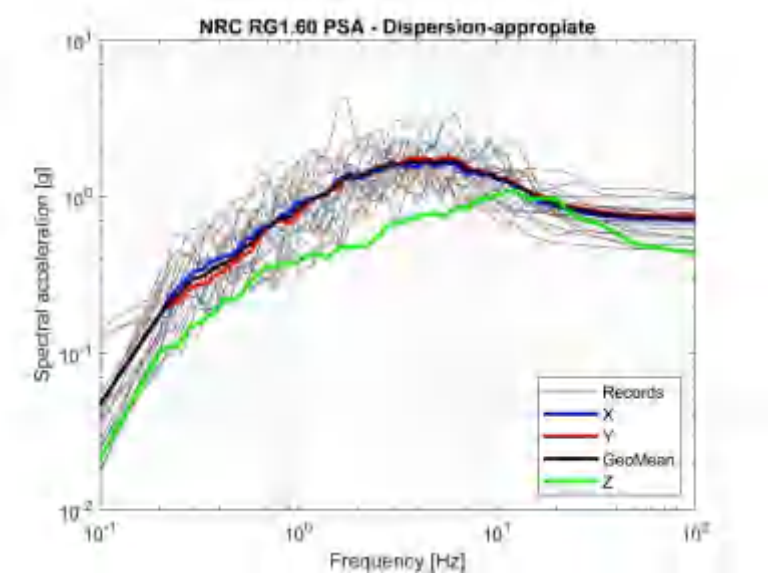

Figure 1. Pseudo Spectral Accelerations with records

The seismic performance of the equipment is evaluated based on Engineering Demand Parameters (EDP) reported in the literature. The probability of failure of an EDG unit can be characterized by the acceleration experienced by the unit. In contrast, the base isolation system and the umbilicals crossing the isolation plane are characterized by their displacement capacity. Therefore, two different types of capacities are examined, with the Limit States considered for each EDP listed in Table 1 with some of the values reported a High Confidence Low Probability of Failure (HCLPF).

Table 1: Engineering Demand Parameters for system components

EDP	Limit State	Value	Reference
Isolation Lateral Displacement	Pipeline	127mm	(Jeon et al., 2015)
	Bearing	250% shear strain	(JAERI, 2000)
EDG Acceleration	EDG	0.41g	(Liu & Aziz, 2007)

EMERGENCY DIESEL GENERATOR ANALYSIS MODEL

The study considers seismic isolation of an Emergency Diesel Generator with a weight equal to 150 Tf. Past studies (Bustamante et al., 2022) under a lower seismic hazard showed that a two-layer isolation system

can improve the seismic performance of the EDG. Figure 2 shows a schematic configuration of the EDG and seismic isolation system following (Bustamante et al., 2022).

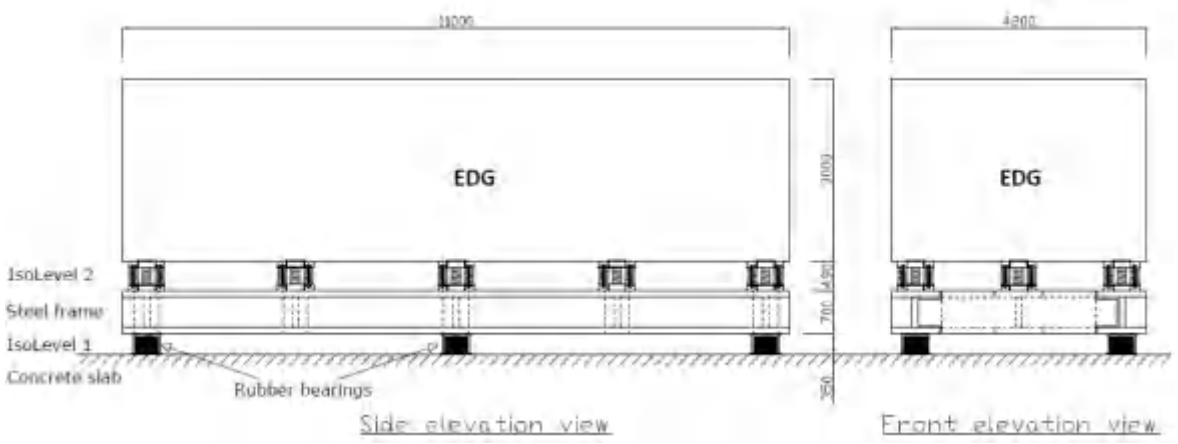

Figure 2. Configuration of the proposed seismic isolation system

The first isolation layer (IsoLevel 1) is intended to mitigate horizontal vibration transferred to the EDG from ground shaking and consists of LRB devices that can be designed to provide a range of effective stiffness and damping values to limit the lateral displacement. As previously mentioned, however, these devices are vertically stiff and can amplify the vertical shaking transmitted to the EDG. To address this concern and operational requirements, the second isolation layer (IsoLevel 2) consists of springs and damper supported on top of the LRB isolation layer. This system can mitigate the effect of vertical shaking by modifying the vertical frequency. A rigid frame is considered between the two isolation levels, assuming it provides an adequate rocking restraint system with vertical guides. The numerical model of the EDG and isolation system was developed in OpenSees (McKenna et al., 2020). The EDG is modelled as a single degree of freedom with the weight equal to 150 Tf at mid-height of the unit and a primary vibration frequency of 34 Hz [5].

The LRBs sizing is defined based on a target isolation system displacement and base shear transferred to the EDG. Using the procedure in FEMA P-751 (FEMA, 2009), assuming 5% damping, the criterion used in a previous study (Bustamante et al., 2022) was to choose the intersection of both curves shown in Figure 3, to reduce the acceleration while limiting the lateral displacement. If the same criterion is used for this seismic hazard, the effective period is 1.60s, as shown in Figure 3. Three options are explored for this seismic hazard and detailed in Table 2.

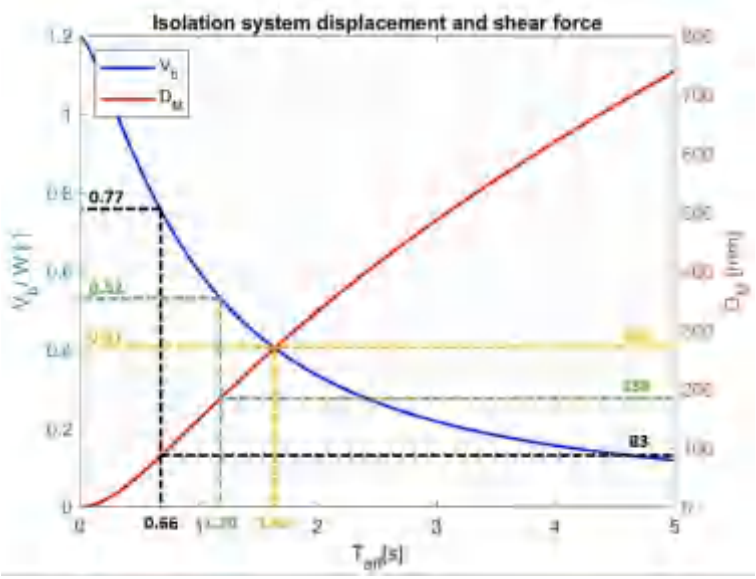

Figure 3. FEMA P-751 feasibility domain

Table 2: LRB sizing options using FEMA P-751

Option	T_{eff} [s]	V_b/W	D_M [mm]
1	1.60	0.41	263
2	0.66	0.77	83
3	1.20	0.52	188

It is assumed here that the target isolation displacement is limited by the pipeline Limit State of 127mm. While a flexible pipeline connection can be designed for larger displacements, this limit is considered here as a tested system reported in the literature related to this application. Option 1 leads to a large lateral displacement compared to the pipeline Limit State even though the LRB can provide additional damping. Option 2 significantly limits the lateral displacement, with the downside of forcing the isolation system to underperform in its capacity to reduce the EDG acceleration. The spectral acceleration is similar to the fixed base option for this case.

The design displacement of Option 3 is 188mm for 5% of critical damping. The lead rubber bearings provide an effective damping of 23.1% with an expected displacement reduction factor of about 1.5, reducing the design displacement to 125mm, below the pipeline Limit State shown in Table 1. Option 3 is considered to balance displacement and acceleration demands and is examined in more detail considering that a more rigorous iterative design process can lead to more optimal performance. The LRB are designed for Option 3 with the dimensions shown in Table 3. The LRB are modelled as bilinear assuming Shear Modulus of rubber G_R=0.4MPa and yield stress of lead of σ_{yL}=7.9MPa.

Table 3: Bearing dimensions and properties

# bearings	**D_{ext} [mm]**	**$D_{lead\ core}$ [mm]**	**t_r [mm]**	**# layers**	**β_{eff}**
6	470	100	8	16	23.1%

The coil springs are sized for operational vibration (vertical static deflection) and vertical frequency content of the ground motion, targeting a vertical frequency of less than 2.0 Hz and a static deflection of less than 200mm to satisfy both conditions. The coil springs' vertical frequency is 1.29 Hz with a static deflection of 150mm. Linear viscous damping is assumed and sized following a parametric study examining the reduction of the ground acceleration amplification, with a damping of 11% of critical.

Time-history analysis

A nonlinear time history analysis is performed of the EDG subjected to the 20 triplets of ground motions. The result from Record 8 are shown to examine the behavior of the system. Record 8 is representative of the mean isolation lateral displacement. Figure 4a compares shear force-lateral deformation hysteresis of the isolation system, while Figure 4b compares the orbital displacements. Figure 4a shows that the bearings exhibit limited nonlinear behavior for Record 8 with 31% shear strain in the rubber. The limited deformation was intended to reduce the lateral displacement of the system based on the capacity of umbilical lines, which causes the large shear force and acceleration transferred to the EDG unit.

The displacement response results for the 20 ground motions in shown in Figure 5. The average and 99th percentile displacement is added in Figure 5 considering ASCE 43(ASCE43-05, 2006) defines as goal for Design Basis Earthquake shaking to comply with 1% or less probability of unacceptable performance. Only one record exceeds this threshold, with also slightly above the pipeline Limit State deformation capacity considered equal to 127mm.

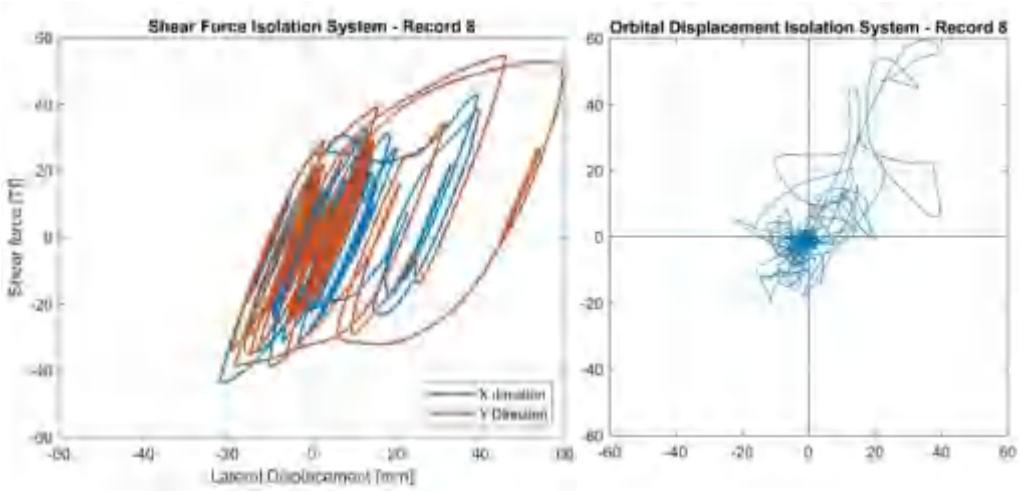

Figure 4: (a) Isolation level shear force – lateral displacement for Record 8 – X Direction (b) Plan view Orbital lateral displacement for Record 8

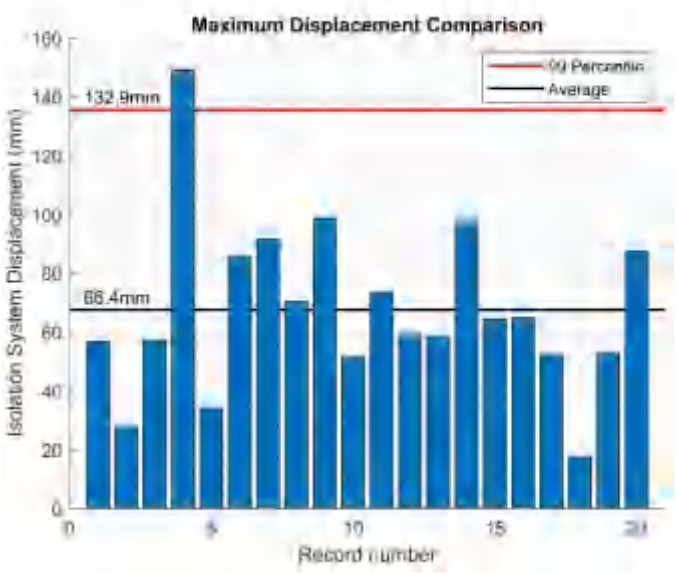

Figure 5: Maximum bi-directional horizontal displacement comparison for each record.

The acceleration time history of the EDG compared to input motion for Record 8 is shown in Figure 6. As shown in Figure 6a, the proposed seismic isolation system is able to reduce the peak acceleration by a factor of two. Figure 6b shows that the vertical acceleration experienced by the EDG is reduced slightly and not as effective as in the horizontal direction. The EDG acceleration is the most commonly reported Engineering Demand Parameter though typically specified as the PGA at the base with some amplification expected to non-seismically isolated systems. To contrast the performance of the isolation system, the bi-directional horizontal acceleration of the EDG unit is reported in Figure 7 for all the ground motions considered. The seismic hazard has a PGA equal to 0.50g, while the average EDG unit acceleration is 0.33g, showing that the isolation system effectively reduces the acceleration. Note that he 99 percentile acceleration shown no amplification in response.

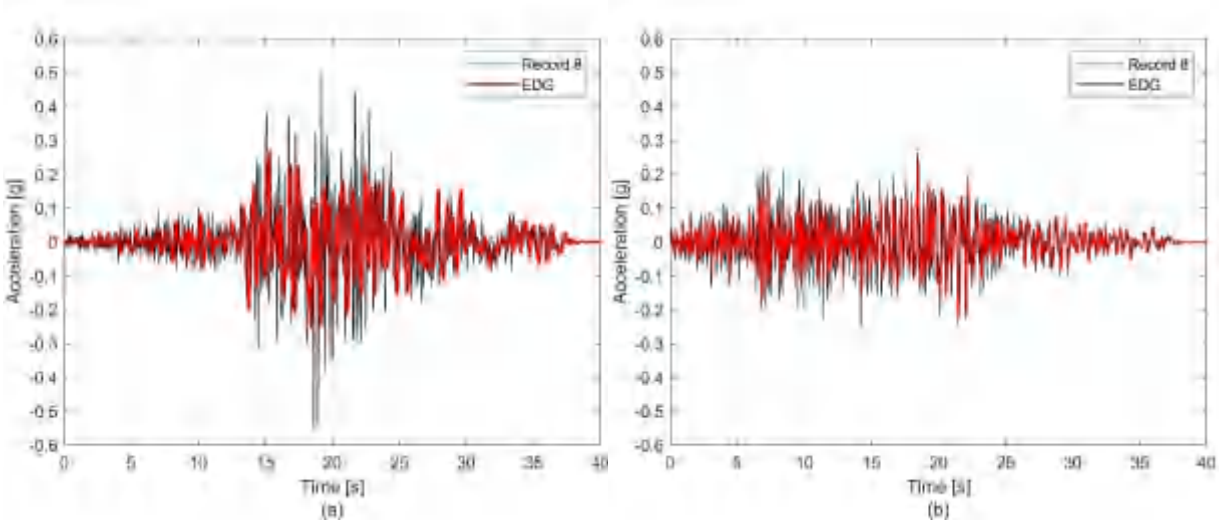

Figure 6: EDG acceleration time history response Record 8 (a) Horizontal direction 'X' (b) Vertical direction 'Z'

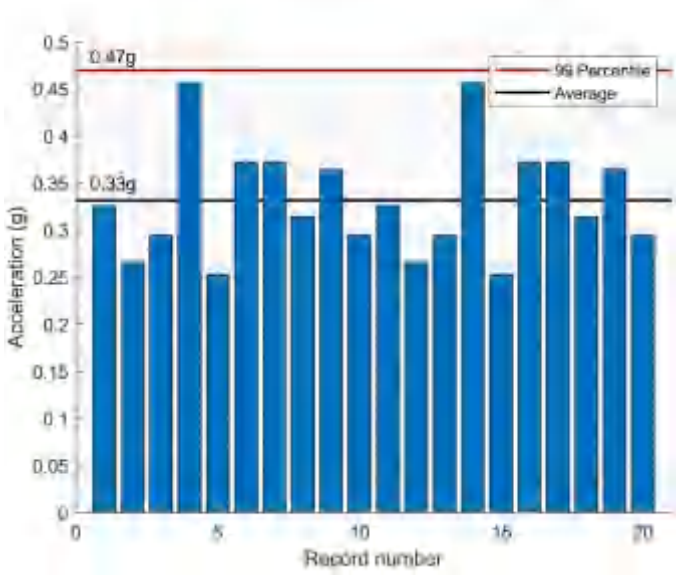

Figure 7: Maximum bi-directional horizontal EDG acceleration comparison for each record.

Figure 8 plots in grayscale the Pseudo Spectral Acceleration (PSA) corresponding to 5% of critical damping for all records at the EDG level for the horizontal and vertical directions. This is representative of the forces experience by electrical and mechanical components attached to the EDG. The ground motion PGA is shown for comparison to the average PSA at the EDG. The horizontal PSA in Figure 8a shows an amplification of the ground motion at 2 Hz, consistent with the effective period attained by Record 8. Figure 8b shows the vertical PSA for the EDG unit, which does not exhibit an overall acceleration amplification for any of the motions and a significant reduction in the average PSA.

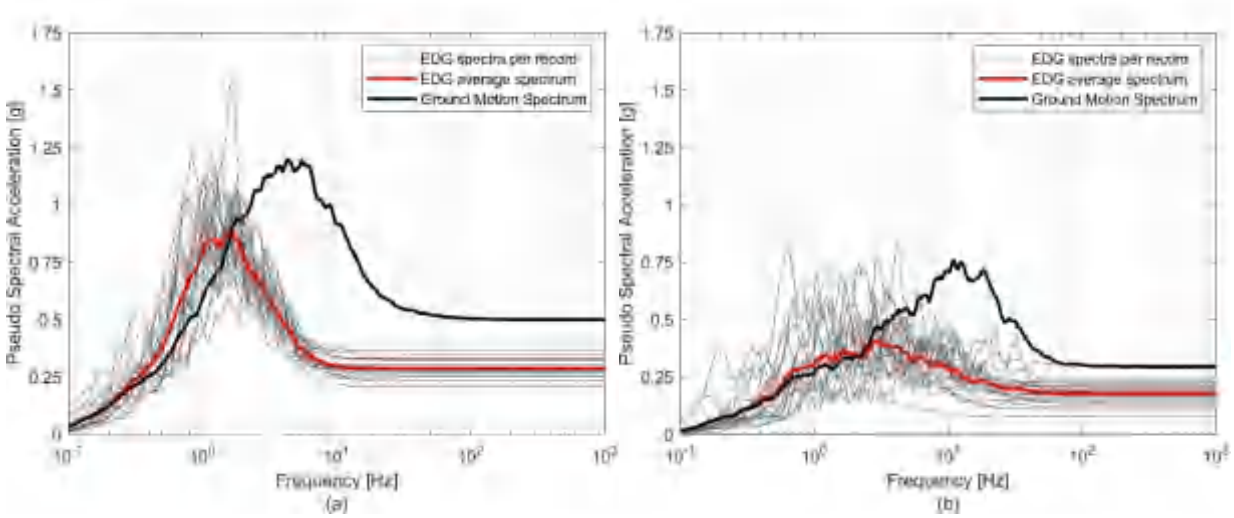

Figure 8: Spectral acceleration results for (a) horizontal direction (b) vertical direction 'Z'

CONCLUSION

The Emergency Diesel Generator at a Nuclear Power Plant site is essential to maintaining a safe shutdown after an earthquake. Potential failure modes of an EDG consist of failure of the equipment frame itself, damage to umbilical lines connected to the equipment, and damage to the support and anchorage system. Typical EDG seismic isolation systems are based on a vibration control solution developed for operational mode vibration isolation, consisting of coil springs, lateral restrainers, and/or dampers. This study demonstrates the feasibility of a three-dimensional isolation system that could meet the seismic performance requirements for a high seismic zone with a PGA=0.50g. The system has independent horizontal and vertical isolation systems that enhance the seismic performance of an EDG unit compared to the fix-based unit, reducing the acceleration while controlling the lateral displacement.

The system is designed to accommodate the limited deformation capacity of the fuel pipelines crossing the isolation interface based on the capacity reported in the literature. The proposed seismic isolation system can be improved by considering more flexible umbilicals to increase the displacement capacity of the system and further reduce the reduction of acceleration and forces transmitted to the EDG unit. To further examine this approach, experimental testing of fuel pipelines and other umbilical are needed to verify their capacity and increase the displacement capacity. Experimental data of an isolated EDG unit could provide better estimates for the acceleration that the EDG unit can withstand, as well for the uncertainty parameters, to better relate to reported values in the literature in terms of PGA.

REFERENCES

ASCE43-05. (2006). *Seismic Design Criteria for Structures, System , and Components in Nuclear Facilities*.

Bustamante, R., Mosqueda, G., & Kim, M. (2022). Enhanced Seismic Protection System for an Emergency Diesel Generator Unit. *Energies*, *15*(5), 1728. https://doi.org/10.3390/en15051728

Choun, Y.-S., Kim, M.-K., & Ohtori, Y. (2007). The use of a base isolation system for an emergency diesel generator to reduce the core damage frequency caused by a seismic event. *SMiRT*, *19*, 1–8.

Choun, Y., Kim, M., & Seo, J. (2006). *Seismic and Vibration Isolation of an Emergency Diesel Generator by Using a Spring-Viscous Damper System*. 8.

Ebisawa, K., Ando, K., & Shibata, K. (2000). Progress of a research program on seismic base isolation of nuclear components. *Nuclear Engineering and Design*, *198*(1), 61–74. https://doi.org/10.1016/S0029-5493(99)00279-4

FEMA. (2009). *FEMA P-751 - NEHRP Recommended Seismic Provisions for New Buildings and Other Structures*.

Furukawa, S., Sato, E., Shi, Y., Becker, T., & Nakashima, M. (2013). Full-scale shaking table test of a base-isolated medical facility subjected to vertical motions. *Earthquake Engineering and Structural Dynamics*, *42*(13), 1931–1949. https://doi.org/10.1002/eqe.2305

JAERI. (2000). *Characteristics and Dynamic Response Analysis of 3-D Component Base Isolation System Using Ball Bearings and Air Springs*.

Jeon, B., Choi, H., Hahm, D., & Kim, N. (2015). *Seismic Fragility Estimation of Piping System of Base-*. *2007*.

Jeong, Y. S., Baek, E. R., Jeon, B. G., Chang, S. J., & Park, D. U. (2019). Seismic performance of emergency diesel generator for high frequency motions. *Nuclear Engineering and Technology*, *51*(5), 1470–1476. https://doi.org/10.1016/j.net.2019.03.012

Kančev, D., Duchac, A., & European Commission. Joint Research Centre. Institute for Energy and

Transport. (2013). *European clearinghouse : events related to emergency diesel generators.* Publications Office.

Liu, W., & Aziz, T. S. (2007). *Seismic Capacity of Emergency Power Supply Diesel Generator Set for Candu 6*. 1–8.

McKenna, F., Fenves, G., & Filippou, F. (2020). *The Open System for Earthquake Engineering Simulation (OpenSees). Available online at: http:// opensees.berkeley.edu*.

Najafijozani, M., Becker, T. C., & Konstantinidis, D. (2020). Evaluating adaptive vertical seismic isolation for equipment in nuclear power plants. *Nuclear Engineering and Design*, *358*. https://doi.org/10.1016/j.nucengdes.2019.110399

Ryan, K. L., Coria, C. B., & Dao, N. D. (2013). *Large Scale Earthquake Simulation of a Hybrid Lead Rubber Isolation System Designed with Consideration of Nuclear Seismicity*.

Schellenberg, A. H., Sarebanha, A., Schoettler, M. J., Mosqueda, G., Benzoni, G., & Mahin, S. A. (2015). Hybrid simulation of seismic isolation systems applied to an APR-1400 nuclear power plant. *Peer 2015/05, April*, 379.

U.S. Nuclear Regulatory Commission. (2007). RG 1.208: A performace-based approach to the site-specific earthquake ground motion. In *RG 1.208* (Issue March).

U.S. Nuclear Regulatory Commission. (2020). Appendix A to Part 50 - General Design Criteria for Nuclear Power Plants. US Nuclear Regulatory Commission. In *Medical Dosimetry* (Vol. 13, Issue 2). https://doi.org/10.1016/0958-3947(88)90038-6

Transactions, SMiRT-26
Berlin/Potsdam, Germany, July 10-15, 2022
Division VII

Determination of Clearance to the Stop based on Performance Criteria of a Seismically Isolated Nuclear Power Plant

Minkyu Kim[1], Gyeonghee An[2]

[1] Principal Researcher, Korea Atomic Energy Research Institute, Daejeon, Korea
[2] Senior Researcher, Korea Atomic Energy Research Institute, Daejeon, Korea (akh425@kaeri.re.kr)

ABSTRACT

The clearance to the stop (CS), which refers to the horizontal distance between the superstructure of isolated NPP and the physical stop, is an important matter affecting the risk assessment of isolated NPPs. The objective of this paper is to evaluate the CS requirements based on the performance criteria. To satisfy these criteria, the CS has to be greater than the 90th percentile displacement of the structure under beyond design basis earthquake (BDBE) ground motions, and the isolation system needs to be designed to have 90% confidence or higher for the CS. The 90th percentile displacement under BDBE ground motions is analytically determined. The numerical model of a lead rubber bearing (LRB) was suggested based on the full-scale test results for reasonable seismic response. Capacity of isolator is experimentally determined. Failure probability can be calculated by maximum likelihood estimation using experimental results. The 10th percentile from the failure probability of isolator can be the upper bound of the CS to satisfy the performance criteria. Limitations of this study include insufficient numbers of experiments as well as analysis results that are dependent on the particular models, ground motions, and criteria selected. Further research is necessary to suggest more reasonable ranges of CS.

INTRODUCTION

In this research, an NPP model was built based on the APR1400 (Advanced Power Reactor 1400 MW) from the Republic of Korea with lead rubber bearings (LRBs) used for the isolation system. The structural model was initially developed by KEPCO E and C (Korea Electric Power Corporation Engineering and Construction Company), which is in charge of the APR1400 design, and later converted to OpenSees in collaboration with the University of California, Berkeley [Schellenberg et al., 2015]. The model was then modified for the current study as well as related research to include moat walls [Sarebanha et al., 2018] and advanced bearing models to capture the nonlinear characteristics of the LRBs [Mosqueda et al., 2019]. The bearing models focus on capturing experimental results at large shear strain to better reflect strong ground motions. In the present work, the response of an isolated NPP including the displacement of the isolation system and floor response spectra (FRS) is investigated using the analytical model combining both structural and bearing models.

The key objective of this paper is to examine the performance criteria of seismically isolated NPPs, particularly the clearance to the stop (CS), as suggested by NUREG [USNRC, 2019] and ASCE [2017]. A physical stop is necessary for seismically isolated NPPs to ensure the mean annual frequency of failure of the isolation system is very small. The CS, which refers to the horizontal distance between the superstructure of isolated NPP and the physical stop, is an important matter affecting the risk assessment of isolated NPPs, but few studies have evaluated CS. Kumar and Whittaker [2015] calculated CS considering responses from various ground motions but the capacity of the isolation system was not considered. In the current paper, both numerical simulations and the experimental results from the bearing

test program are considered in evaluating the range of CS. The lower and upper bounds of CS are suggested from the analytical displacement response and the experimental capacity of the isolators, respectively.

PERFORMANCE CRITERIA

The performance criteria for seismically isolated nuclear structures has been suggested in standards such as ASCE 4–16 [2017] and NUREG/CR-7253 [USNRC, 2019]. According to the standards, seismically isolated NPPs should allow for sufficient displacement of the isolation layer to reduce the acceleration induced by ground motions, while the failure probabilities of the superstructure, isolation systems, and umbilical lines remain at low levels, as specified below.

NUREG/CR-7253 gives performance and design recommendations for seismically isolated NPPs at two levels of ground motion: GMRS+ and BDBE GMRS. The first, GMRS+, covers RG1.208 GMRS and the minimum foundation input motion, while the second, BDBE GMRS, covers the UHRS (uniform hazard response spectrum) at a mean annual frequency of exceedance of $1 \times 10{-}5$ and 167% of GMRS+. The criteria under BDBE GMRS loading are normally critical. Isolation systems need to have 90% confidence of surviving without loss of gravity-load capacity, and the superstructure needs to have less than a 10% probability of contacting with a hard stop (moat wall) under BDBE GMRS loading. To satisfy these criteria, the CS has to be greater than the 90th percentile displacement of the structure under BDBE GMRS loading, and the isolation system and umbilical lines need to be designed to have 90% confidence or higher for the CS. The capacity of the interfacing components such as the umbilical lines is assumed in this work, and thus the failure of the umbilical lines is not considered at present.

CAPACITY OF THE ISOLATION SYSTEM

Experimental Setup

To obtain more data on the capacity of the LRBs, additional experiments were conducted on bearings smaller in size than those presented earlier for the model development. The dimensions of the LRB specimens are shown in Figure 1 [Kim et al., 2019]. The diameters of the LRB and lead core were 550 mm and 120 mm, respectively, and the total rubber thickness was 112 mm. Fifteen specimens, as listed in Table 1, were tested until failure. It should be noted that these specimens had experienced horizontal loading prior to the failed test and could have been slightly damaged; the LRBs were therefore classified as low damage (LD), moderate damage (MD), and high damage (HD) for previously experienced shear strain levels of 100%, 300%, and 400%, respectively. The fourth column in Table 1 lists the experimental variable P/Pd, which is the ratio of the axial load to the design axial load, ranging from 0 to 6. Each test was performed by horizontal displacement control loading under these axial loading conditions.

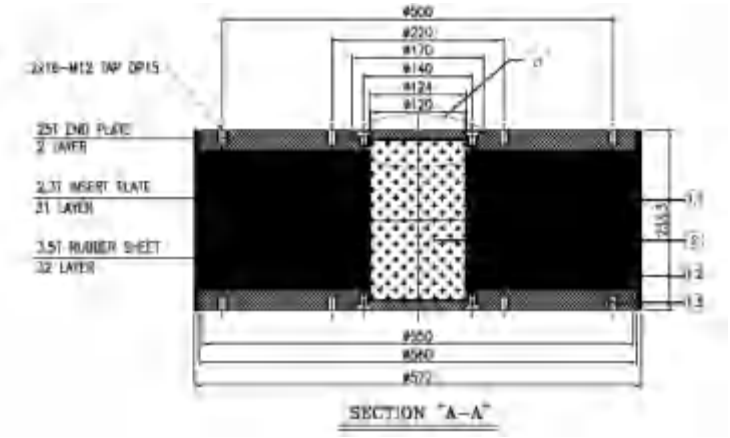

Figure 1. LRB specimen dimensions.

Table 1. Specimens for the ultimate property test.

Test Sequence	Specimen	Tag	P/P_d	Vert. Load (kN)	Buckling Load (kN)	Failure Load (kN)	Failure Disp. (mm)	Failure Disp. (%)
#1	UCSD300%(1)	MD-P1.0	1.0	2942		683	457	408
#2	UCSD300%(5)	MD-P1.0	1.0	2942		762	462	412
#3	UCSD Non(1)	LD-P1.0	1.0	2942		460	389	348
#4	UCSD400%(1)	HD-P1.0	1.0	2942	236	583	478	427
#5	SGS1.0Pd	MD-P1.0	1.0	2942		777	470	419
#6	UCSD Non(2)	LD-P6.0	6.0	17,649		245	67	60
#7	UCSD300%(3)	MD-P2.0	2.0	5883	232	766	480	429
#8	UCSD300%(7)	MD-P3.0	3.0	8825	311	666	476	425
#9	SGS1.5Pd	MD-P1.5	1.5	4412	287	761	467	417
#10	UCSD300%(4)	MD-P2.5	2.5	7354	214	614	457	408
#11	UCSD300%(8)	MD-P4.0	4.0	11,766	180	594	460	410
#12	SGS2.0Pd	MD-P5.0	5.0	14,708	126	666	483	431
#13	UCSD300%(2)	MD-P0.0	0.0	500		782	463	413
#14	UCSD400%(2)	HD-P0.0	0.0	500		597	477	426
#15	UCSD300%(6)	MD-P0.5	0.5	1471		763	469	419

Ultimate Property Diagram

The failure criteria of the LRBs can be represented by an ultimate property diagram (UPD). The vertical load on an LRB affects its failure mode and shear failure capacity; the UPD shows this relationship, namely between the axial load and the shear load or strain of the limit state. In this research, UPDs were predicted experimentally because of difficulties in numerical analysis.

Figure 2a and b show UPDs based on the failure load and failure strain, respectively, from the test results in Table 1. As can be seen in the figure, the failure strains of the specimens are rather consistent at about 420%, compared to the failure loads. Therefore, within a certain level of vertical load, the shear strain can be a failure criteria parameter.

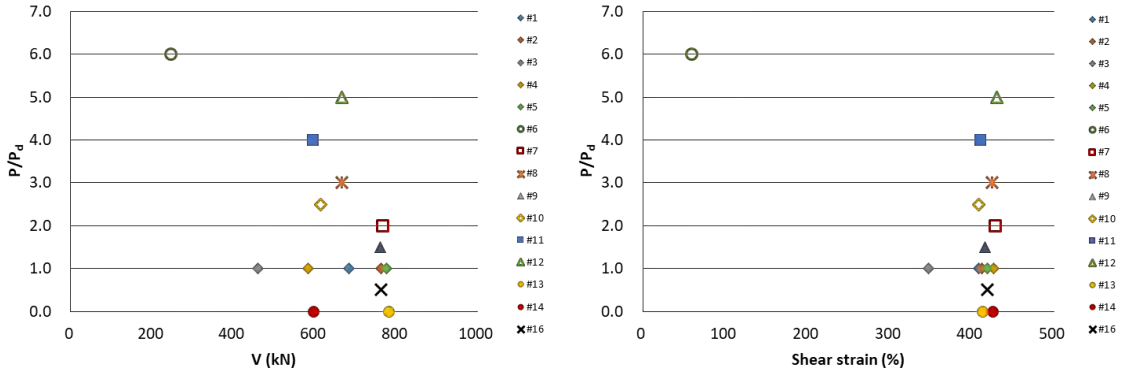

Figure 16. Ultimate property diagram in (a) shear force and (b) shear strain.

Models for Numerical Analysis

Structural Model of the APR1400

The structural model of the APR1400 including a seismic isolation system consisting of 486 bearings was initially developed in SAP2000 by KEPCO E and C. KEPCO, which is in charge of designing NPPs in Korea, developed a simplified Archetype Nuclear Test (ANT) stick model, as shown in Figure 3 [Mosqueda and Sarebanha, 2018]. The superstructure is modeled as beam–stick elements with lumped masses and the base mat is modeled using three dimensional solid elements. The reactor containment building (RCB) and the auxiliary building (AB) are located at the center of the model. The isolators are attached at the bottom of the base mat. The total weight of the nuclear island including base mat, reactor, RCB, and AB is 4732 MN. This SAP2000 model was then converted to an OpenSees format for hybrid simulations and parametric analysis [Schellenberg et al., 2015].

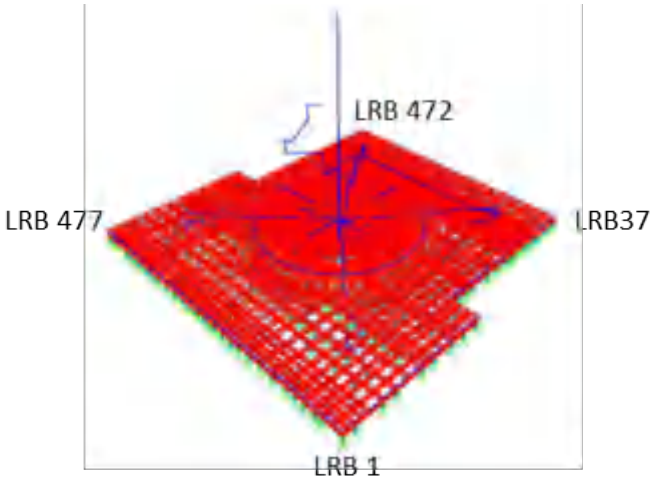

Figure 3. ANT model.

Isolator Model

KAERI conducted full-scale tests of LRBs designed for NPPs in 2014. As shown in the schematic in Figure 4, the diameters of the LRB and lead core were 1500 mm and 320 mm, respectively, with 32 layers of 7 mm thick rubber stacked to give a total rubber height of 224 mm. Two LRBs were tested,

where each specimen experienced various motions including sine wave motion, elliptical trace sinusoidal motion, and earthquake response motion. Shear strain up to 500% at three frequencies (0.01 Hz, 0.2 Hz, and 0.5 Hz) was tested at the design axial load, 22,000 kN. Detailed explanations of the experiments can be found in previous reports [Kim, M. et al., 2019, Kim, J. et al., 2019]; Figure 5 presents an example of experimental results obtained from the tests.

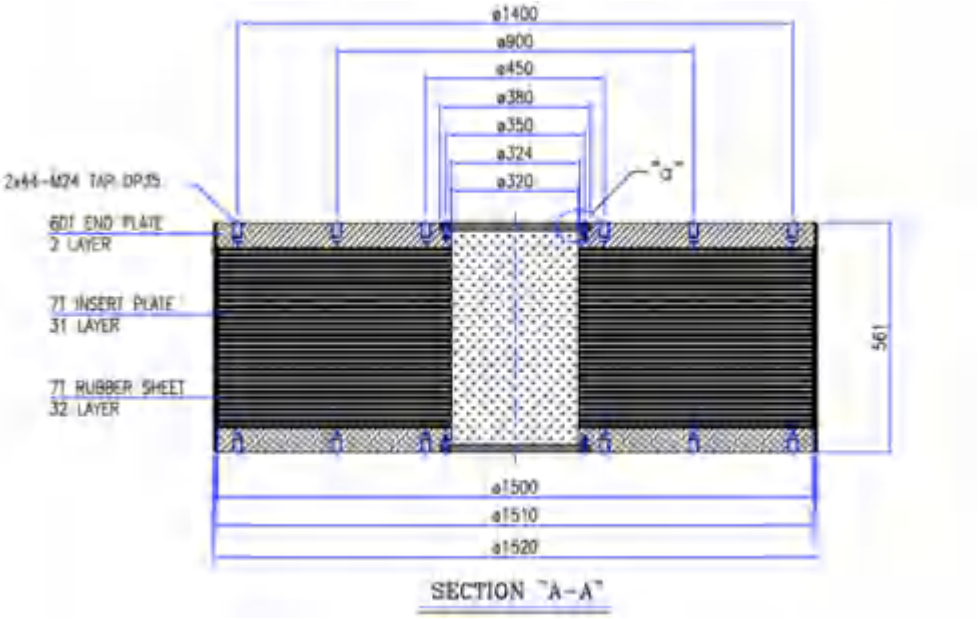

Figure 4. Dimensions of the test bearings (unit: mm).

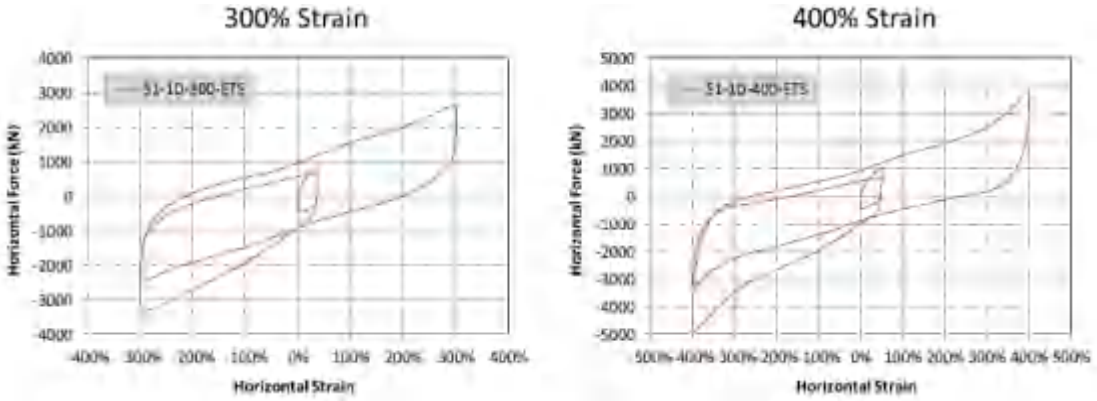

Figure 5. Strain-force curves in the unidirectional sinusoidal test [13].

A parallel numerical model of an isolator representing an LRB was suggested by Mosqueda, Marquez, and Hughes [2019]. The characteristic behaviors of the LRBs, such as a reduction in strength due to the heat of the lead and hardening at large strain, as shown in Figure 5, are modeled using three elements: an LRX element, a Bouc–Wen (hardening) element, and an HDR element, which are all separately available in OpenSees, as shown in Figure 6.

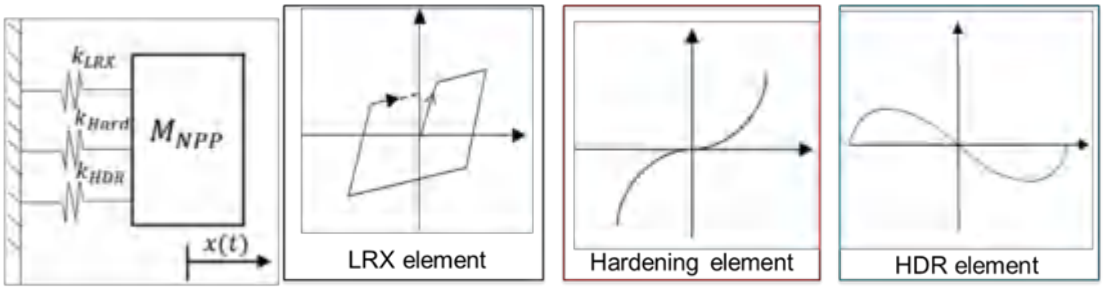

Figure 6. Parallel system of the bearing model.

Ground Motions

The Pacific Earthquake Engineering Research Center (PEER) published a technical report [Schellenberg et al., 2014] as the outcome of a research project conducted in tandem with KEPCO. In this project, a set of 20 ground motions were selected from the PEER NGA-West1 database, such that they match the mean and dispersion of a target response spectrum. Using RSPMatch, each of the selected dispersion-appropriate records was individually matched to a single target spectrum corresponding to 5% damping.

Response of an Isolated Nuclear Power Plant

Displacement of the Isolation System and Upper Structures

Figure 6 shows the force-displacement relation of an LRB (LRB #1) subjected to the same ground motion but at various PGA levels. This bearing, as depicted in Figure 3, is located at the corner of the base mat. According to Figure 7, the bearing model shows increased nonlinearity as the ground motion strengthens, similar to experimental observations, and thus it can be concluded that the bearing model is suitable for beyond design basis applications.

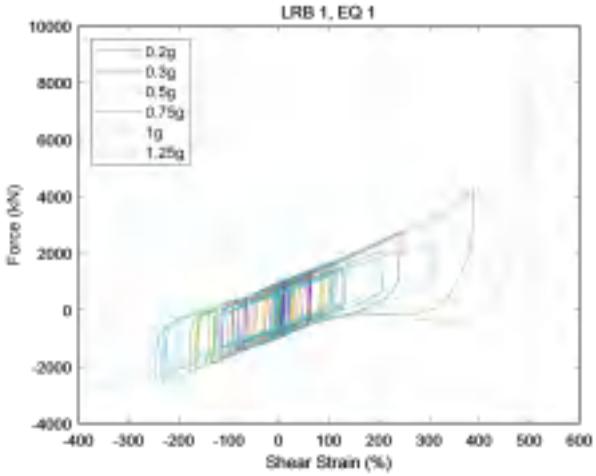

Figure 7. Hysteresis of LRB #1.3.2. Floor Response Spectra of an Isolated NPP.

The floor response spectra (FRS) is another essential aspect in the analysis of the seismic fragility of equipment as well as risk assessment. Figure 8 shows a comparison of the FRS from both base-isolated and non-isolated RCBs. The isolation system reduces the overall responses of the structure, with the

isolated RCB only slightly exceeding the non-isolated RCB in the region near the natural frequency of the isolation system.

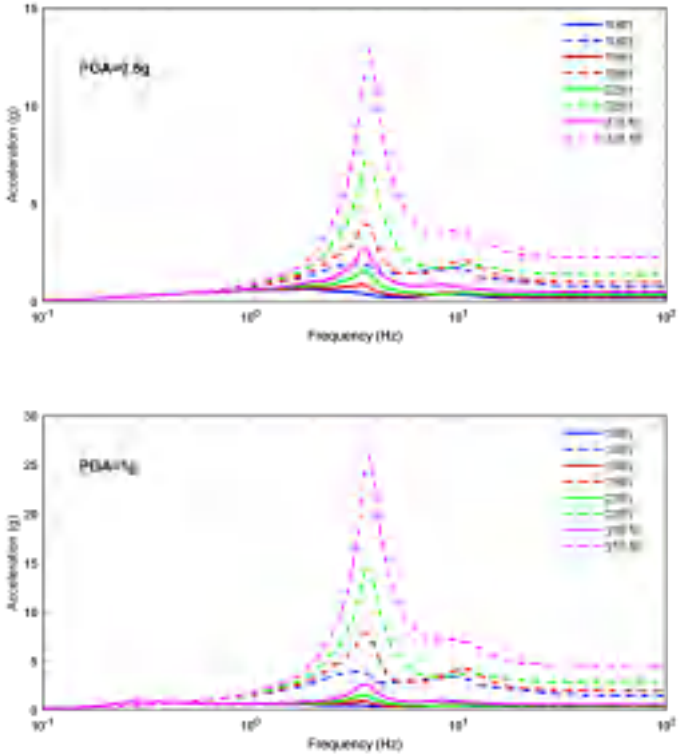

Figure 8. Comparison of FRS at different PGA from isolated (solid lines) and non-isolated (dashed lines) RCBs.

If there exists a stop (moat wall) in accordance with the evaluated CS, the FRS of the base-isolated RCB can be amplified due to a collision between the wall and the base mat, especially for ground motions exceeding BDBE ground motion response spectra (GMRS). Therefore, further research for the modeling of the moat wall, backfill soil, and impact is necessary to evaluate FRS considering moat wall impact at strong ground motions.

DETERMINATION OF CLEARANCE TO HARD STOP

Lower Bound of CS from Displacement Response

The RG1.60 design spectrum with PGA = 0.5g can be regarded as the GMRS in the present work because a specific target site was not designated, and therefore the 20 ground motions detailed in Section 2.3 were selected for the analysis. An amplification factor AR was calculated to be about 2 because the ratio of the peak ground acceleration at an annual frequency of exceedance of 10−4 and 10−5 is about 2 based on a related hazard analysis in Korea [Kim. et al., 2012]. Therefore, the BDBE GMRS is assumed as the RG1.60 design spectrum with PGA = 1.0 g.

Figure 9 shows a histogram of the maximum displacements of the AB at ground level (height = 100 ft) subjected to 20 ground motions for BDBE GMRS loading (PGA = 1.0 g).

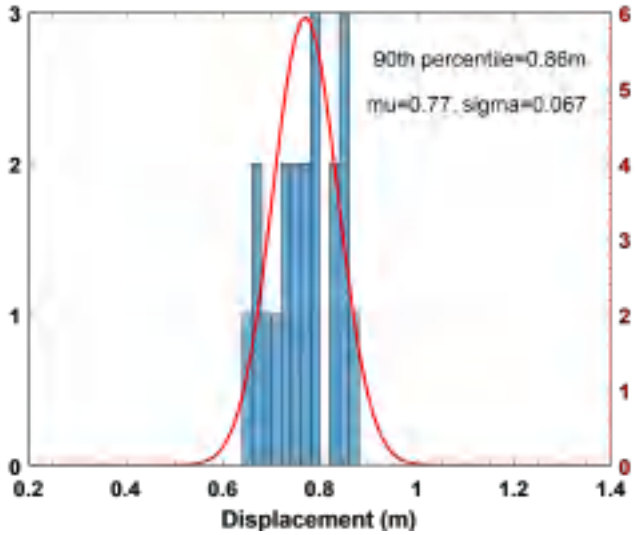

Figure 9. Displacement of the auxiliary building under BDBE ground motion response spectra (GMRS) (PGA = 1.0 g).

As shown in Figure 9, the mean maximum displacement was about 0.77 m. If a normal distribution is assumed, the 90th percentile of the displacement is about 0.86 m (2.81 ft). The superstructure has less than a 10% probability of contact with a hard stop (moat wall) under BDBE GMRS loading, as the codes suggested. In other words, the lower bound of the CS is about 0.86 m in this case.

Upper Bound of CS from UPD

In this research, a fragility curve for the LRBs was estimated from the maximum likelihood method suggested by Shinozuka et al. [2000]. The empirical fragility curve of the LRBs is assumed as a cumulative distribution function of the lognormal distribution, as shown in Equation (1),

$$F(e) = \Phi\left[\frac{\ln(e/e_m)}{\beta_c}\right] \tag{1}$$

where e and e_m are the shear strain (%) and the median value of the strain, respectively, β_c is the log-standard deviation, and $\Phi[\cdot]$ is the cumulative standard normal distribution function.

The likelihood function for the estimation can be defined as Equation (2),

$$L = \prod_{i=1}^{N} [F(e_i)]^{x_i} [1 - F(e_i)]^{1-x_i} \tag{2}$$

where e_i is the shear strain (%) to which the ith LRB is subjected, x_i= 1 or 0 depending on whether the LRB failed or not, and N is the total number of tested LRBs.

Two parameters, e_m and β_c, are estimated from Equation (3), which finds the parameters to maximize the likelihood function L.

$$\frac{d \ln L}{de_m} = \frac{d \ln L}{d\beta_c} = 0 \tag{3}$$

The median shear failure strain and log-standard deviations were about 413% and 0.051, respectively. Figure 18 shows the empirical fragility curve. The test results in Figure 16 with the highest axial load (Test #6) was not included in this failure probability estimation because it exceeded the range of interest.

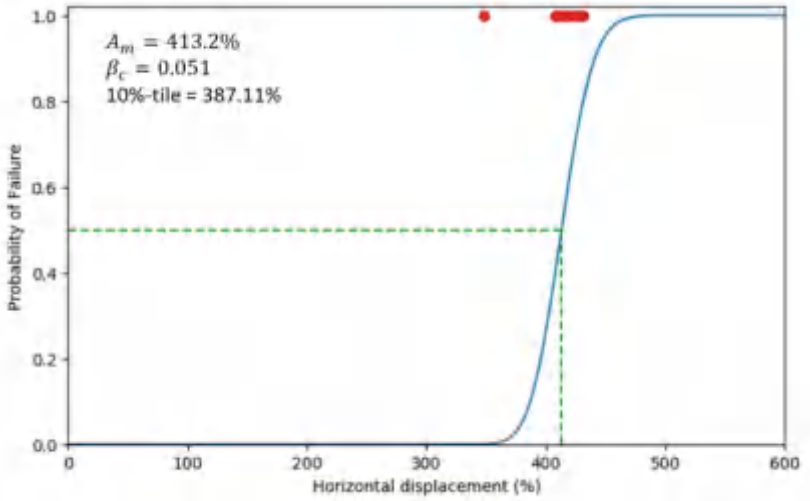

Figure 10. Probability of shear failure.

The failure probability of a prototype LRB in an isolated NPP is assumed to be the same as the small-scale LRBs despite size effects, considering the practical difficulty to conduct ultimate property tests of prototype LRBs. This assumption is considered to be acceptable based on the fact that the shear failure of the full-scale LRB specimen occurred at approximately 515% shear strain level [Kim, J., et al, 2019]. From the fragility curve, the 10th percentile of the failure strain is about 387% or 0.87 m for a full-scale LRB with 0.224 m rubber thickness. Thus, 0.87 m can be the upper bound of the CS to satisfy the performance criteria that the isolation system should have 90% confidence of surviving without loss of gravity-load capacity.

CONCLUSION

In this paper, we integrated NPP and LRB structural models to investigate the response, capacity, and clearance to the stop of an isolated NPP based on given performance criteria. From the experimental results and analysis, the following conclusions are drawn.

(1). If a normal distribution is assumed for the analysis results of the maximum displacement under BDBE GMRS loading, the 90th percentile of the displacement was about 0.86 m. In this case, CS should be greater than 0.86 m based on the performance criteria that the superstructure has less than a 10% probability of contact with a hard stop (moat wall) under BDBE GMRS loading.

(2). The shear strain of the LRB can be failure criteria within a certain level of vertical loading based on the UPD, which represents the results of bearing capacity experiments. Failure probability using the shear strain parameter can be calculated by maximum likelihood estimation. The median failure strain was about 413%, and the 10th percentile was about 387% from the estimation. The 387% shear strain means 0.87 m for a full-scale LRB, which can be the upper bound of the CS to satisfy the performance criteria that the isolation system should have 90% confidence of surviving without loss of gravity-load capacity.

Acknowledgments
This work was supported by a National Research Foundation of Korea (NRF) grant funded by the Korean government (NRF-2017M2A8A4014829).

REFERENCES

ASCE. Seismic Analysis of Safety-Related Nuclear Structures, ASCE/SEI Standard 4-16; ASCE: Reston, VA, USA, 2017.

Kim, J.; Kim, M.; Choi, I. Experimental study on seismic behavior of lead-rubber bearing considering bi-directional horizontal input motions. Eng. Struct. 2019, 198, 109529.

Kim, M.; Hahm, D.; Kim, J. Development of probabilistic seismic risk assessment methodology for seismically isolated nuclear power plants. In Transactions, SMiRT-25; Charlotte, NC, USA, 2019.

Kim, M.; Kim, J.; Choi, I. Investigation of Performance Objectives for Seismic Isolation Systems of Nuclear Power Plants, KAERI/TR-4667; 2012.

Kim, M.; Kim, J.; Hahm, D.; Park, J.; Choi, I. Seismic performance assessment of seismic isolation systems for nuclear power plants, PVP2016-63742 (Pressentation only). In Proceedings of the ASME 2016 Pressure Vessels and Piping Conference PVP2016, Vancouver, BC, Canada, 17–21 July 2016.

Kumar, M.; Whittaker, A.S. On the calculation of the clearance to the hard stop for seismically isolated nuclear power plants. In Transactions, SMiRT-23; Manchester, UK, 2015.

Mosqueda, G.; Marquez, J.; Hughes, P. Modeling of base-isolated nuclear power plants subjected to beyond design basis shaking. In Proceedings of the 25th Conference on Structural Mechanics in Reactor Technology, Charlotte, NC, USA, 2019.

OpenSees. Available online: http://opensees.berkeley.edu (accessed on).

Sarebanha, A.; Mosqueda, G.; Kim, M.; Kim, J. Seismic response of base isolated nuclear power plants considering impact to moat walls. Nucl. Eng. Des. 2018, 328, 58–72.

Schellenberg, A.; Baker, J.; Mahin, S.; Sitar, N. Investigation of Seismic Isolation Technology Applied to the APR 1400 Nuclear Power Plant; 2014.

Schellenberg, A.H.; Sarebanha, A.; Schoettler, M.J.; Mosqueda, G.; Benzoni, G.; Mahin, S.A. Hybrid Simulation of Seismic Isolation Systems Applied to an APR-1400 Nuclear Power Plant; Pacific Earthquake Engineering Research Center: Berkeley, CA, USA, 2015.

Shinozuka, M.; Feng, M.; Lee, J.; Naganuma, T. Statistical Analysis of Fragility Curves. J. Eng. Mech. 2000, 126, 1224–1231.

U.S.NRC. Technical Considerations for Seismic Isolation of Nuclear Facilities; NUREG/CR-7253; 2019.

Transactions, SMiRT-26
Berlin/Potsdam, Germany, July 10-15, 2022
Division V

3D SEISMIC ISOLATION SYSTEMS FOR THE NUCLEAR INDUSTRY LAYOUT, DESIGN & QUALIFICATION

Peter Nawrotzki[1], Victor Kostarev[2], Daniel Siepe[3], Frank Barutzki[4], Victor Salcedo[5]

[1] Director, GERB Schwingungsisolierungen GmbH&Co.KG, Berlin, Germany (peter.nawrotzki@gerb.de)
[2] President, CKTI-Vibroseism Ltd., St. Petersburg, Russia
[3] Seismic Group Manager, GERB Schwingungsisolierungen GmbH & Co.KG, Essen, Germany
[4] Director, GERB Schwingungsisolierungen GmbH & Co.KG, Berlin, Germany
[5] President US Operations, GERB Vibration Control Systems, Inc., Lisle, IL, USA

ABSTRACT

This contribution presents general layout procedures, important design issues as well as general remarks regarding the qualification of the corresponding devices. The complete layout process for an exemplary 3D earthquake protection system is also described. Lastly, corresponding details of executed projects are discussed; including qualification by full-scale testing of 3D devices under different performance levels.

INTRODUCTION

Nuclear islands, reactor and auxiliary buildings and similar seismic category 1 structures in nuclear facilities must be protected against seismic demands. The most common seismic isolation systems consisting of rubber bearings (e.g. LRBs), and friction pendulum bearings (FPS) are effective for protection against horizontal earthquake excitation. However, vertical ground motion and other possible dynamic impacts on the structure should be included in the performance assessment based on internationally recognized standards as ASCE, etc. Therefore, systems have been developed that work in all three spatial directions. Together with the well-known horizontal systems mentioned above, these 3D isolation systems are briefly described in the IAEA TECDOC-1905 (2020).

At first, adding vertical elasticity may not seem that difficult, but there are some important details to consider. After defining the vertical target frequency, the arrangement and stiffness parameters of the devices should be chosen to achieve the corresponding vertical displacement under permanent loads. Here, it is important to consider the elasticity of the sub and superstructures, if it has a significant influence on the resulting frequencies and mode shapes. This first step is followed by a partly iterative process until the desired performance of the 3D seismic protection system, the superstructure and the foundation / soil system is achieved. In general, the procedure requires an experienced designer and willingness to work with the manufacturers as early as possible in the project development process. The horizontal and vertical stiffness properties, as well as the corresponding load and displacement capacities of the devices must be discussed to ensure design and production feasibility.

Already during the initial design of a 3D isolation system, all important load scenarios, e.g.: BDBE (Beyond Design Basis Earthquake), CS (Clearance to the Stop) and FM (Failure Mode), must be considered in addition to the “basic” SSE (Safe Shutdown Earthquake) case. This not only includes the calculations but also the planning of the corresponding tests and quality assurance measures. Qualification tests are one of several important topics to be addressed with the regulator at an early project stage. For example, if

newer test methods are applied, that allow a test of full-scale devices subjected to dead load and seismic displacements as described in Nawrotzki et al. (2019), and described later in this paper.

LAYOUT OF A 3D SEISMIC PROTECTION SYSTEM

The layout of a suitable seismic protection system requires experience from the designer. This section describes the corresponding procedure for a Base Control System (BCS) as an example. These systems consist of spring elements, which are arranged below the base plate of the structure. Additionally, highly efficient viscous dampers are also arranged. The system is flexible in the horizontal directions, but possesses also vertical elasticity. The dampers supply absorption forces in all spatial directions. The implementation of spring elements and dampers modifies the fundamental model characteristics of the structure, whereby the predominant frequency of the system is reduced (=elongation of the fundamental period) and the corresponding mode shape exhibits a significant damping ratio increase. A typical view of such a system is shown in Figure 1.

Figure 1. Viscous damper (left) and spring element (right) below concrete superstructure.

When selected appropriately the BCS elements will significantly improve the seismic performance of the 3D base isolated structure. It is very important to choose, arrange, design, qualify and install the elements in an appropriate manner. Thus, it is recommended to contact the manufacturer of the devices as early as possible in the project development process. This approach will help to reduce the numbers of iterative steps and will ensure the general feasibility of the desired element parameters. The following

development steps are suggested to achieve desired performance of the BCS, the superstructure and the foundation / soil system below:

Step 1: Choose the target vertical support frequency based on the properties of the structure, the sub-structure and requirements of the desired performance of the BCS under the given seismic input.

Step 2: Position spring elements level between the superstructure and the substructure (e.g. pedestals on base mat).

Step 3: Check that single springs should have the same or similar vertical displacements under permanent loads. A uniform vertical displacement is recommended to ensure the chosen vertical frequency. Figure 2 shows a simplified sketch. The picture on the left side shows a certain tilting. This can be reduced by adjusting the spring stiffness at each location or by changing the location of the spring devices.

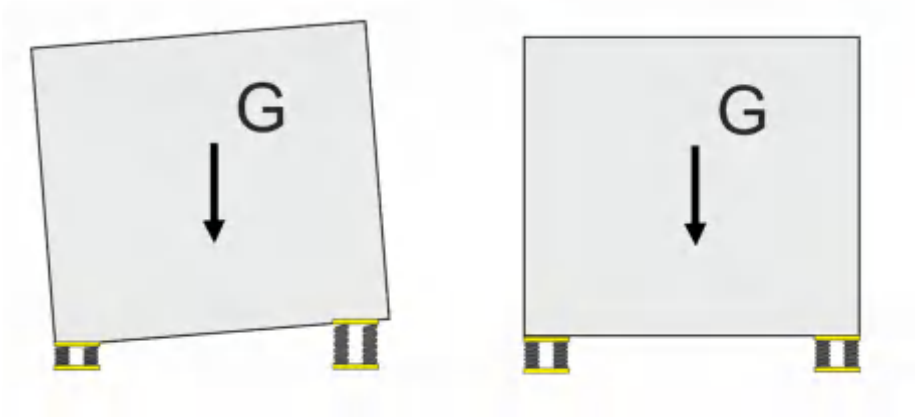

Figure 2. Tilting (exaggerated) of structure (left) due to non-uniform vertical displacement, optimized layout (right).

For a system which is almost rigid, the entire mass and centre of gravity plays an important role for the positioning of the elements. For flexible structures the support positions are regarded individually. Required vertical stiffness values can be calculated for each support location.

Step 4: Choose the ratio between horizontal and vertical stiffness of the spring elements considering the seismic vertical and horizontal isolation requirements as well as the mechanical feasibility of the spring design.

Step 5: Calculate all relevant frequencies and mode shapes of the entire system. For structures which are almost rigid six rigid body modes exist. For flexible structures like many conventional buildings, the elasticity of the superstructure plays an important role on the resulting frequencies and mode shapes.

Step 6: Check all target frequencies and mode shapes as well as of feasibility and capacity of suitable spring elements. If results are not favourable, repeat process from *Step 1*.

Step 7: Choose the horizontal and vertical damping resistance of single dampers. Select the damper quantity & distribution below the superstructure in order to limit the BCS seismic relative displacements to a demand amplitude and optimized isolation efficiency.

Step 8: Check for damping ratios corresponding to the rigid body modes; 6 mode shapes & frequencies exist. For elastic structures, damping of the elastic modes might be considered ("composite modal damping") when determining the damping ratios for the governing mode shapes / frequencies.

Step 9: Check the structural seismic performance (acceleration, stress & strain levels, support reactions, displacements, etc.) by dynamic analysis for different seismic input levels (DBE, BDBE, CS, etc.). Use linear modal analysis, linear time-domain investigations and/or non-linear time domain analysis, if necessary. Corresponding regulations must be checked. If performance targets are not achieved, start again at *Step 7* or even at *Step 1*.

Step 10: Check the feasibility/capacity of damper elements. If not feasible, start from *Step 7*.

Step 11: Perform a detailed design of corresponding hardware, i.e. spring elements and dampers. Analytically check the relative displacements and stress levels in these elements under the different seismic input levels.

Step 12: Establish pre-qualification criteria for hardware (springs, spring elements, dampers) by static and dynamic testing according to current regulations, at least under DBE, BDBE conditions.

Step 13: Develop production quality assurance programs.

Step 14: Develop installation, inspection and maintenance manuals.

The designer should already have an insight into steps 12 and 13 during the first steps of the layout procedure. Coordination with the manufacturer of the spring and damper elements, the customer and, if necessary, authorities or external test institutes is strongly recommended, and in most cases required. Depending on the project specific requirements, certain qualification procedures have to be used. Helical steel springs can be calculated and designed according to DIN EN standards. Prototype tests are also possible. Calculating the damper properties is generally not possible, usually requiring the performance of prototype tests to ensure and verify the design values of these devices. Special tests may be required to consider the influence of different temperature conditions, humidity, corrosion and/or radiation. For nuclear facilities it is essential to choose a suitable damper in regard to radiation effects. Figure 3 shows a typical example of viscous dampers in an NPP.

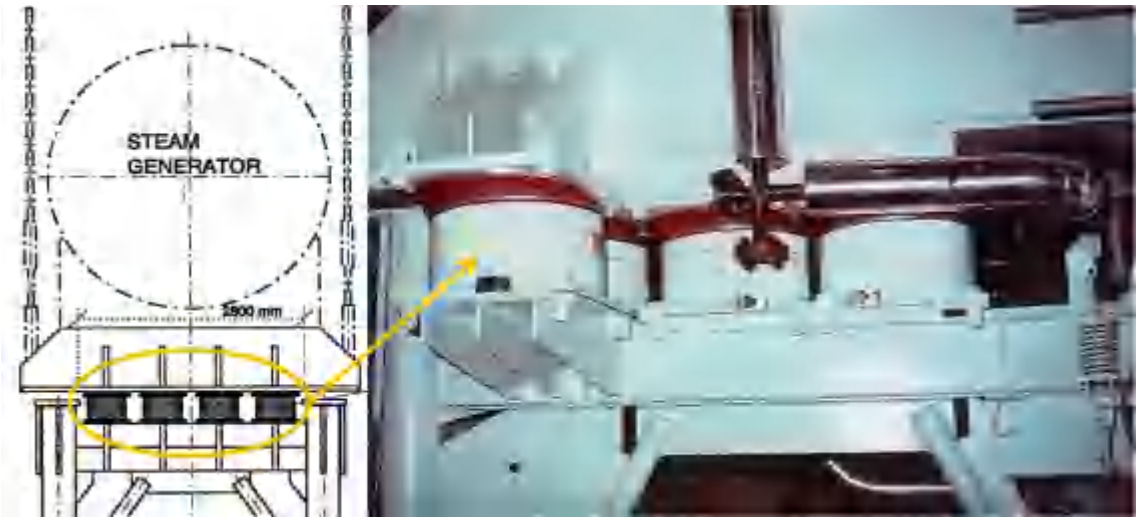

Figure 3. Seismic Protection of Steam Generator in NPP Bohunice, Slovakia.

In addition to the required documents regarding the general qualification of the supplier of spring and damper devices it is at least mandatory to provide Quality Assurance Plans. These plans have to been taken as a basis for ensuring the quality assurance of the devices. The general qualification could consist of the following components:

- prototype testing / qualification,
- production testing / quality assurance,
- certification of Quality Management Standard,
- certification of Environmental Management Standard,
- certification of Occupational Health and Safety Management System,
- documentation of the delivery capacity,
- documentation of the required test equipment for the spring elements and damping devices,
- test stands required for pre-qualification / and quality assurance.

BUILDING IN ARGENTINA

The stepwise procedure for the layout of seismic protection system, as described in the previous chapter, was applied successfully to many projects during the last decades. In general, each structure and corresponding project specific conditions (in terms of seismic input and requirements) are different. For a wide variety of structures (buildings, machine foundations, equipment) the parameters of the seismic protection devices are optimized. More information about the optimization procedure can be found in Nawrotzki and Siepe (2017). Based on the gained experience it is feasible to summarize some general design criteria. These are presented in Table 1.

Table 1: Layout criteria for earthquake protection projects.

Characteristic		Comment
Vertical Frequency [Hz]	1.0 – 3.0	Typical support frequency
Horizontal Frequency [Hz]	0.5 – 2.0	Very efficient reduction of seismic demands
Damping Ratio [%]	>10/20	Vertical/horizontal – reduction of seismic demands & control of relative motions

A corresponding example is the project of two identical apartment buildings, built in 2004 at Mendoza, Argentina. The first building consists of a conventional “rigid” foundation, and the second, adjacent building is supported by a Base Control System. Figure 4 shows the structures. Both buildings consist of three floors of reinforced concrete and masonry infill. After commissioning the National Technological University of Mendoza installed seismic accelerometers in both buildings. It has been possible to directly compare the seismic responses of both buildings during the same seismic excitation. Figure 4 presents the measured results at the roof of each building during an earthquake in 2005 with a peak ground acceleration of about 0.12 g.

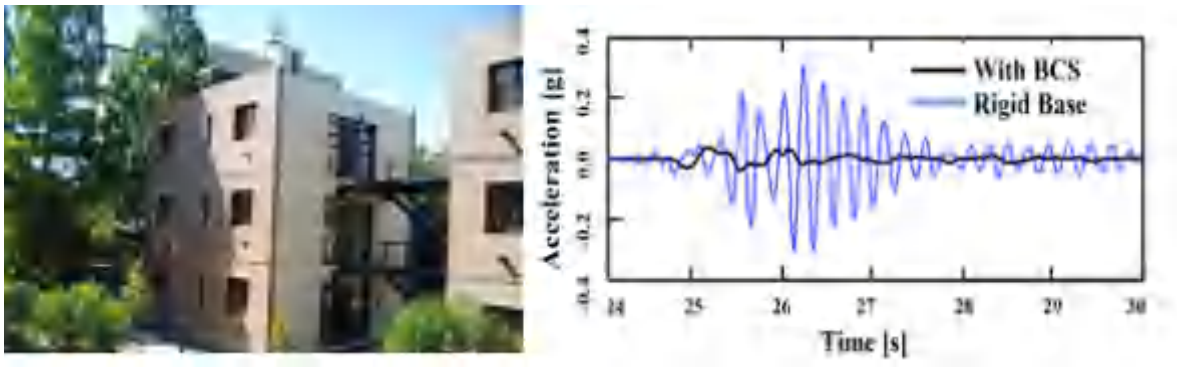

Figure 4. View of buildings and measured absolute accelerations at roof levels.

The efficiency of the BCS can be seen by comparing the measured results. The horizontal maximum acceleration at top of the building was reduced by more than 70 %. The measured data was also used to adjust the initial analysis model. It is shown in Stuardi et al. (2008) that similar to the acceleration reduction also the corresponding structural responses like internal forces and subsoil reactions could be reduced significantly.

TEST STAND IN ST. PETERSBURG

The project specific developments and solutions are backed with theoretical as well as practical investigations. More than 15 years ago extensive shaking table tests have been performed at IZIIS (Institute of Earthquake Engineering and Engineering Seismology) in Skopje, North Macedonia. Their biaxial shaking table is able to generate an acceleration input up to 3.0 g for the horizontal direction, as well as a vertical acceleration input up to 1.5 g. These values are applicable for zero pay load. The 5.0 x 5.0 m table possesses a maximum pay load of about 40 metric tons. A five story, three bay steel frame model with a total mass of about 24 metric tons has been tested with and without Base Control System on the described shaking table.

The efficiency of the mitigation system has been studied by simulating a set of ten different earthquake records for both test-configurations. Evaluating the large number of recorded time history responses in terms of absolute accelerations, axial and bending strain at different locations of the structure it can be concluded that the BCS reduces the structural responses by more than 50 % compared to the unprotected structure. More detailed information can be found in Rakicevic et al. (2006).

Beside the tests on typical shaking tables it is nowadays also possible to test elements of a BCS and/or other seismic isolation devices at a new test stand, erected in St. Petersburg, Russia. Here, a special inverse test rig (SIST) was developed for test performance of real structures with seismic isolation systems at full scale. In contrast to typical shaking tables, the inverse approach implies that the substructure is not shaking but the superstructure is shaking at its natural frequencies with amplitudes resulting from gravity and full seismic loading. The principle of the general test-setup is shown in Figure 5.

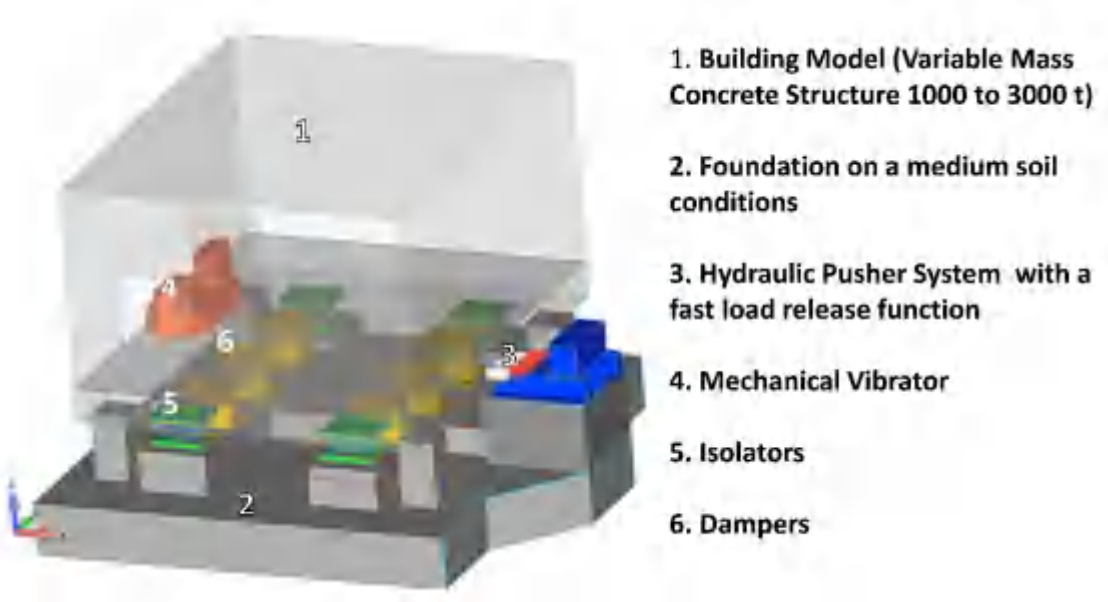

Figure 5. Configuration of the test stand.

The test setup consists of a superstructure with a mass between 1000 and 3000 metric tons and a hydraulic system that is able to push the structure to the desired maximum displacement and ensures a quick-release of the pushing mechanism to allow free movement of the supported structure. The superstructure placed on 4 isolators and a variable number of damping devices. Figure 6 shows the setup at the site in St. Petersburg before the first tests were performed in December 2017.

Figure 6. General view of SIST.

The initial tests verified the general functionality and operability of the test rig. Afterwards extensive tests of the 3D Base Control System were performed. The results show that the spring elements and viscous dampers provide previously defined optimal parameters to the superstructure, as presented in Kostarev et al. (2018). The corresponding test series was accompanied by previous individual static and dynamic testing of the devices at different test facilities, as discussed in Kostarev et al. (2019). The test rig was presented to the public during the 16th World Conference on Seismic Isolation, Energy Dissipation and Active Vibration Control of Structure in St. Petersburg in 2019.

CONCLUSION

The presented outline of layout principles and development steps for a 3D seismic control system generally shows a methodical approach towards a successful implementation. However, the chosen parameters are subject to the frequency content of horizontal and vertical ground shaking, as well as the displacement capacities of the selected devices. Hence, collaboration between designers, suppliers and end users is critical to avoid tedious iterations in selecting system parameters. Furthermore, a typical example of a BCS protected structure was discussed, where the calculated and measured responses show the applied control system yields a very significant reduction of seismic demands. The use of a BCS and the proposed layout process should be further investigated for practical application in Nuclear Facilities.

REFERENCES

International Atomic Energy Agency (2020). *Seismic Isolation Systems for Nuclear Installations, IAEA-TECDOC-1905*, IAEA, Vienna, Austria.

Kostarev, V., Nawrotzki, P., Vasilyev, P. and Vaindrakh, M. (2018). "Seismic dynamic analysis, optimization, testing and probabilistic safety assessment of an innovative 3D seismic base isolation system for important structures," *Proc., TINCE-2018 – Technological Innovations in Nuclear Civil Engineering*, Paris, France, 1-12.

Kostarev, V., Nawrotzki, P., Vasilyev, P. and Vaindrakh, M. (2019). "Developing and natural scale testing of the 3D BCS Base Isolation System," *Proc., 16th World Conference on Seismic Isolation, Energy Dissipation and Active Vibration Control of Structure*, DOI 10.13753/2686-7974-2019-16-460-472, 16WCSI, St. Petersburg, Russian Federation, 460-472.

Nawrotzki, P. and Siepe, D. (2017). "Optimisation of 3-D Base Control Systems for the Seismic Protection of Power Plant Machinery, Equipment and Buildings," *Proc., 24th Conference on Structural Mechanics in Reactor Technology – SMiRT-24*, Busan, Korea, 1-10.

Nawrotzki, P., Kostarev, V., Siepe, D. and Morozov, D. (2019). "3-D Base Control Systems for the Seismic Protection of Structures," *Proc., 16th World Conference on Seismic Isolation, Energy Dissipation and Active Vibration Control of Structure*, DOI 10.13753/2686-7974-2019-16-591-599, 16WCSI, St. Petersburg, Russian Federation, 591-599.

Rakicevic, Z., Jurukovski, D. and Nawrotzki, P. (2006). "Analytical modelling of dynamic behaviour of a frame structure with and without Base Control System," *Proc., 4th World Conference on Structural Control and Monitoring*, San Diego, USA, 1-18.

Stuardi, J. E., Suarez, L. E. and Nawrotzki, P. (2008). "Comparative seismic performance of a Base Control System based on measured and calculated responses," *Proc., 14th World Conference on Earthquake Engineering*, Beijing, China, 1-8.

Transactions, SMiRT-26
Berlin/Potsdam, Germany, July 10-15, 2022
Special Session

3-D SUPPORT SYSTEMS FOR THE SEISMIC CONTROL OF NPP STRUCTURES

Peter Nawrotzki[1], Daniel Siepe[2]

[1] Director, GERB Schwingungsisolierungen GmbH&Co.KG, Berlin, Germany (peter.nawrotzki@gerb.de)
[2] Seismic Group Manager, GERB Schwingungsisolierungen GmbH & Co.KG, Essen, Germany

ABSTRACT

At present, it seems that more and more Nuclear Power Plants are under construction or will be constructed in areas of high seismicity. For countries such as Turkey, Bangladesh, or even regions in the south of France, earthquake risk certainly plays a very important role. In addition to high PGA values of more than 0.3 g, subsoil conditions are also not optimal at certain locations. Thus, relatively soft soils or soils sensitive to uneven settlements are additional challenges. This article illustrates the application of 3-dimensional support systems for the earthquake protection of NPP structures. A step-by-step description of the layout process for a 3-d system is first provided. Subsequently, the application of these steps to the layout of a Base Control System is explained using project examples. Details of these projects and corresponding results of numerical investigations document the effectiveness of the presented seismic protection strategies. Due to its vertical flexibility and the possibility to use pre-stressable spring elements the proposed system provides the possibility of adjusting the building height during the entire lifetime and can easily and reliably compensate all uneven soil settlements that could happen during the structures long-term operation. Selected pictures are used to illustrate the general applicability of the mitigation system. Furthermore, some general recommendations regarding the parameters of these systems are given. As the devices of the system vary especially in the bearing capacity, in the horizontal and vertical stiffness properties, in the ratio between horizontal and vertical stiffness and in the damping resistance, a certain optimisation process is required. In addition, typical parameters are provided in tabular form to have appropriate starting values.

INTRODUCTION

The most common seismic isolation systems, like lead rubber bearings, rubber pads and friction pendulum systems are effective only for protection against horizontal earthquake excitation. The corresponding devices provide a large stiffness in vertical direction and yield an entire transmission of the vertical earthquake component into the supported structure. Furthermore, the corresponding coupling phenomenon of horizontal and vertical components could amplify the horizontal accelerations in higher frequency modes, as presented in Ryan et al. (2012). Therefore, the demand and requirement regarding three-dimensional seismic control of important structures is increasing significantly.

In literature several examples of 3-D base isolation systems can be found, typically consisting of combinations of 2-D devices with vertical 1-D devices. IAEA (2020) describes additionally a different approach: systems with helical steel springs and viscous dampers. These systems provide flexibility in horizontal and vertical directions and damping forces in all spatial directions. The corresponding 3-dimensional support systems are frequently used to reduce seismic demands. At the same time these systems yield vibration isolation efficiency as well as protection against other catastrophic events, such as aircraft impact or shock loads. It is shown in Nawrotzki et al. (2013) that these systems lead to a significant

reduction of accelerations, internal stresses, soil reactions and the values of the in-structural response spectra. Machinery (e.g. Turbo-generator Sets, Emergency Diesel Generators, etc.), equipment (e.g. spent fuel storage tank) in nuclear power plants already benefit from the mentioned advantages. Also outside the NPP sector, there are several examples of base-controlled structures.

Based on the previously mentioned experience it is no longer unthinkable that a complete nuclear island structure will be supported by a 3-d support system, as illustrated in Figure 1. This concept is supported in the meantime by newer test methods, allowing a full-scale testing of devices subjected to full dead load and seismic displacement, as described in Nawrotzki et al. (2019).

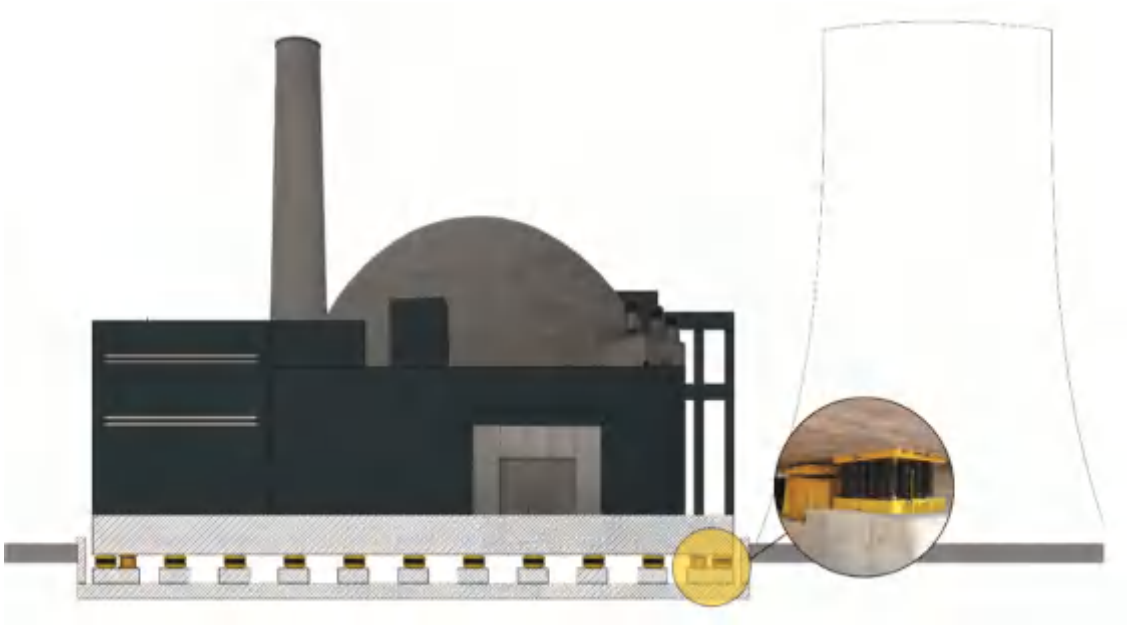

Figure 1. 3-D Base Control System below NPP building.

This paper presents basic layout criteria and efficiency analysis for the 3-D support system for typical NPP structures. Details of corresponding executed projects are presented to illustrate the theoretical investigations.

LAYOUT PRINCIPLES

The layout of a suitable seismic mitigation system requires experience from the responsible designer. This section describes the corresponding procedure for a Base Control System (BCS) as an example. A BCS systems consist of spring elements, which are arranged underneath the base plate of the structure. Highly efficient viscous dampers are arranged in parallel to the elastic support devices. The system is flexible in both horizontal directions, but possesses also vertical elasticity. The dampers supply damping forces in all spatial directions. Due to the implementation of spring elements the mode shape of the structure is changed and the predominant frequency of the system is reduced (=increase of fundamental period of vibration). The arrangement of dampers yields a significant damping ratio of the important mode shapes. A typical view of such a system is shown in Figure 1.

Figure 1. Viscous damper (left) and spring element (right) below concrete building

The use of the shown devices might have several advantages on the seismic performance of the structure when the BCS elements are chosen, arranged, designed, qualified and installed in an appropriate manner. Thus, it is recommended to contact the manufacturer of the devices as early as possible in the project process. This approach will help reducing numbers of iterative steps and will ensure the general feasibility of the chosen element parameters. The following steps are suggested for a successful performance of the BCS, the superstructure and the foundation / soil system below:

#1: Based on properties of the structure, the sub-structure and requirements of the desired performance of the BCS under the given seismic input, the vertical target frequency of the support system is chosen.

#2: The positions of the spring elements are selected at the level between the superstructure and the supports of the devices.

#3: The single springs should have the same or similar vertical displacements under permanent loads. A uniform vertical displacement is recommended to ensure the chosen vertical frequency. For a system which is almost rigid, the entire mass and centre of gravity plays an important role for the positioning of the elements. For flexible structures the support positions are regarded individually. Required vertical stiffness values can be calculated for each support location.

#4: The ratio between horizontal and vertical stiffness of the spring elements is chosen considering the seismic vertical and horizontal isolation requirements as well as the mechanical feasibility of the spring design.

#5: All the relevant frequencies and mode shapes of the entire system are calculated. For structures which are almost rigid six rigid body modes are existing. For flexible structures like, for instance, many buildings, the elasticity of the superstructure plays an important role on the resulting frequencies and mode shapes.

#6: Check of all target frequencies and mode shapes as well as of feasibility and capacity of suitable spring elements. If results are not favourable, repeat process from #1.

#7: Choice of horizontal and vertical damping resistance of single dampers. Selection of damper quantity & distribution below the superstructure in order to limit the BCS seismic relative displacements to a demand amplitude.

8: For rigid bodies 6 mode shapes & frequencies are existing as well as the corresponding damping ratios. For elastic structures, damping of the elastic modes might be considered ("composite modal damping") when determining the damping ratios for the governing mode shapes / frequencies.

#9: Check of structural seismic performance (acceleration, stress & strain levels, support reactions, displacements, …) by dynamic analysis for different seismic input levels (DBE, BDBE, CS, etc.). Use of linear modal analysis, linear time-domain investigations and/or non-linear time domain analysis, if necessary. Corresponding regulations must be checked. If performance targets are not achieved, start again at #7 or even at #1.

#10: Check of feasibility/capacity of damper elements. If not feasible, start from #7.

#11: Detailed design of corresponding hardware, i.e. spring elements and dampers. Analytical check of relative displacements and stress levels in these elements under the different seismic input levels.

#12: Pre-qualification of hardware (springs, spring elements, dampers) by static and dynamic testing according to current regulations, at least under DBE, BDBE conditions.

#13: Development of production quality assurance programs.

#14: Development of Installation, Inspection and Maintenance Manuals.

PORTA NUOVA BUILDING IN MILAN

A good project example for the previously described procedure is presented in this chapter. The Porta Nuova project in Milan, Italy includes several building complexes, a new metro station, parks and some underground parking. The building "D" is located in close proximity to the southern subway tunnel that passes under the site. The subway line may cause vibration and structure-borne noise problems within the building. By elastically supporting the building, these effects can be significantly minimized. For this purpose, a vertical system frequency of approximately 3.1 Hz was proposed by the consultant. Thus, the Step 1 of the layout process was finished. Due to the seismic risk at site it was already obvious that the spring elements should be combined with viscous dampers. Figure 2 shows a section of the arrangement of the elements below the building. Here, the elements are placed on a concrete base about 2.0 m high. This means that the space below the floor slab can also be used by the building's occupants.

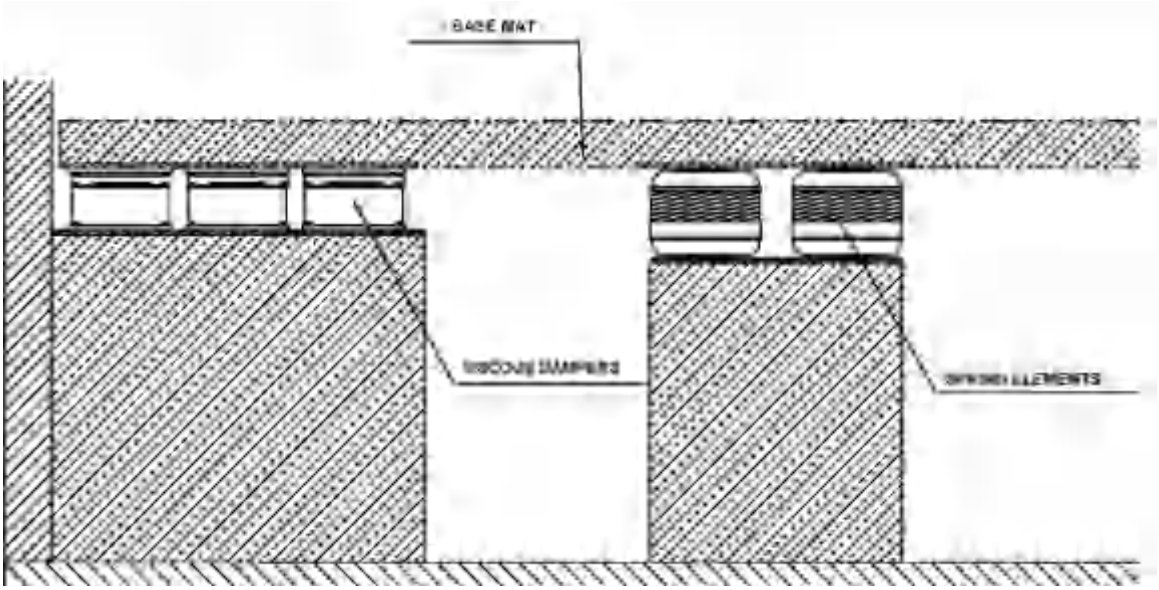

Figure 2. Devices below the floor slab of the building.

The building is approximately 22.0 m long, with a width of about 28.0 m and a height of 60.0 m. The total weight is estimated with 25500 metric tons. The seismic excitation can be described by the peak ground acceleration of approx. 0.07 g and a plateau range between 2.63 and 7.14 Hz with an amplification factor of 2.65. The selection of the element type and the arrangement of the elements were initially made considering the mentioned static building loads and the local space conditions. The elements vary in the bearing capacity, in the horizontal and vertical stiffness properties, in the ratio between horizontal and vertical stiffness and in the damping resistance values, as described in Siepe and Nawrotzki (2015). These features allow the adjustment of the element parameters in regard to the specific requirements of each projects. For several projects it is an advantage to use a higher stiffness ratio of the spring in a range of about 6 and 8. This parameter is used to control the seismic motion of the elastic supported system and could lead to a significant reduction of acceleration amplification.

After some preliminary calculations have been carried out it was decided to place the structure on 276 spring elements. The used type of spring exhibits a high stiffness ratio between vertical and horizontal stiffness of about 7. Thus, a low horizontal natural frequency and a corresponding mode shape with a low rocking component could be achieved. Parallel to the spring elements, 32 viscous dampers were arranged to increase the structural damping while limiting the relative motions of the building to the environment. A view of the building can be seen in Figure 3

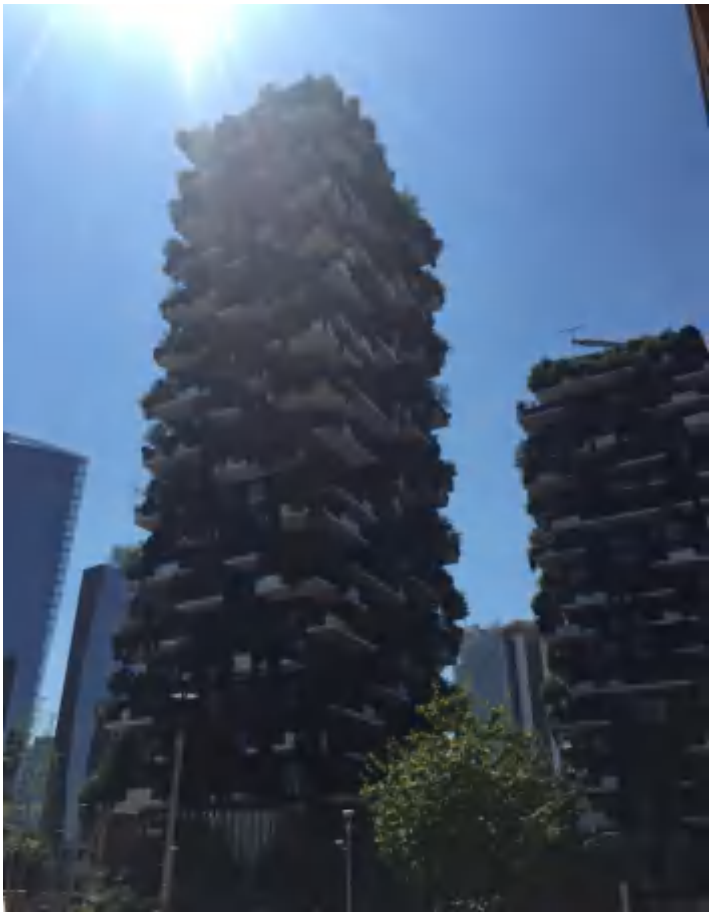

Figure 3. View of building.

The elements can safely support the static loads and provide sufficient margin for additional movements occurring in all three spatial directions as a result of dynamic loads (e.g. due to earthquakes). Completion of the project, which began in 2009, was in 2014. Together with the experience of several other projects, like important machinery and a spent fuel storage tank, as presented in Nawrotzki and Siepe (2015), it appears possible to install a complete NPP building (e.g. Reactor building and/or even the complete Nuclear Island) on top of a spring-/damper system. More details are discussed in the next chapter.

NPP BUILDINGS

Entire buildings or some parts of buildings in nuclear power plants have to be protected against possible seismic events and other extraordinary load cases. So far, there are more than 100 buildings worldwide nowadays supported on helical steel spring elements. In most of these cases the elastic support is required to provide vibration isolation efficiency, e.g. if there is a train passing by closely. The high-frequency excitation in vertical direction, which may disturb or endanger the structure, is filtered out by the low vertical support frequency. At seismic sites this support strategy is modified and optimized to consider also the effects of earthquakes, as already described in this contribution.

The seismic efficiency of a Base Control System has been proven in real earthquakes. For instance, in 2005 it was feasible to measure the seismic response of a base-controlled apartment building in Argentina in comparison to an identical, adjacent building without protection measures. The effect of the BCS can be

seen by comparing the measured results. The horizontal maximum accelerations at top of the building are reduced by more than 70 %. It is presented in Stuardi et al. (2008) that similar to the acceleration reduction also the corresponding structural responses like internal forces and subsoil reactions could be reduced significantly.

Thus, it seems absolutely possible to install the a complete NPP building on top of a Base Control System. To assess the reduction effect of such a system on an NPP structure such as the reactor building, numerical calculations of a structure, weighing approximately 150.000 metric tons were performed. It is shown in Nawrotzki et al. (2013) that the proposed control system leads to a significant reduction of the accelerations, base reactions and the values of the floor response spectra. An example for the comparison of in-structural response spectra is given in Figure 4.

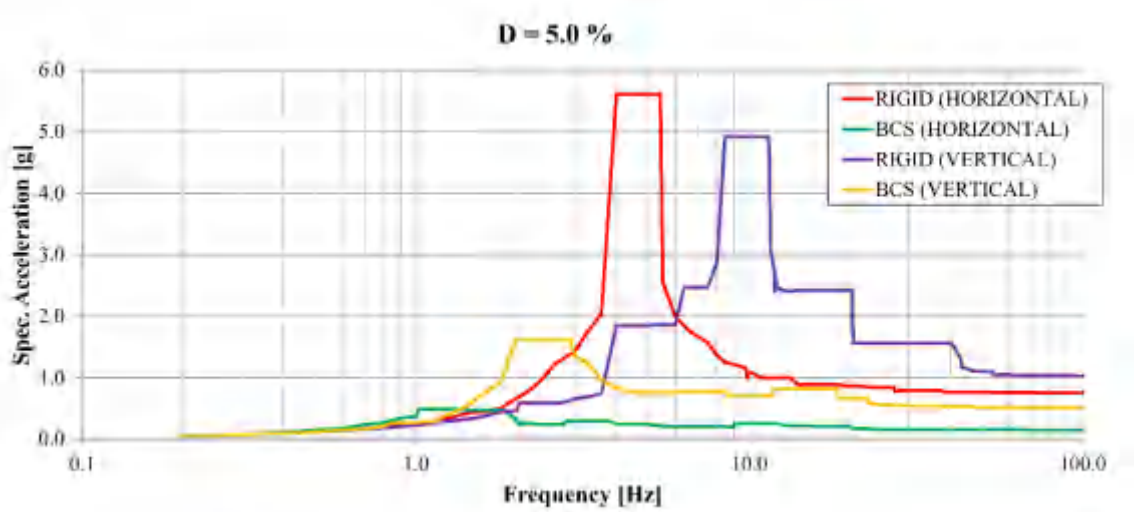

Figure 4. View of building.

The shown spectra are generated considering that the peak accelerations are assumed to be constant for a frequency range of ±15 % of the corresponding frequency (frequency widening). Having a look at these results it can be summarized that the application of a BCS leads to a significant reduction of the spectral values of the floor response spectra in a wide frequency range in horizontal and vertical directions. In comparison to other (e.g. horizontal protection systems) it should be noted that only small values of relative displacements between building and vicinity are expected. The corresponding connections, e.g. pipework systems, have to be designed to withstand such relative motion. Thus, it is important to optimize the parameters of the seismic protection system – to find an optimum between reduction of accelerations and occurring relative displacements. Having a look at executed projects (e.g. buildings, machine foundations, equipment) it was found that vertical support frequencies in a range of 1.0 to 3.0 Hz combined with horizontal frequencies within 0.5 and 2.0 Hz are typical layout criteria. The corresponding damping ratio amounts to about more than 10 % in vertical direction and to about more than 20 % in horizontal direction to reduce the seismic demands and to control the relative motions.

Beneath using the aforementioned general layout parameters, it is also possible to apply a more complex optimisation process, based on a “goal function”. Kostarev et al. (2017) proposed a goal function based on the peak accelerations at the support level and the maximum relative displacements at the isolator units. This criterion was applied successfully for the investigation of the parameter optimization for the

seismic isolation of a PWR Reactor Building having approximately 80 meters in height. The results, presented in Kostarev et al. (2019), are presented it Table 1.

Table 1: Optimum layout criteria for a typical reactor building.

Characteristic		**Comment**
Vertical Frequency [Hz]	around 3.0	quite typical support frequency
Horizontal Frequency [Hz]	around 0.9	Very efficient reduction of seismic demands
Damping Ratio [%]	within a range from 20 to 40	reduction of seismic demands & control of relative motions

It could be concluded that these results are in very good consistence with the described values from other studies and projects.

CONCLUSION

After a short introduction into the layout process of a three-dimensional seismic control system, some corresponding examples for earthquake protection were discussed especially using Base Control Systems. Seismic demands like absolute accelerations, internal forces, support reactions and floor response spectra can be significantly reduced if these systems are applied. The use of a 3-dimensional Base Control System should be further investigated for practical application in NPP structures including planning ahead for future challenges, such as climate change. Stendel and Christensen (2002) mentioned that under warmer climatic conditions the permafrost terrain would be vulnerable to subsidence. Here, too, the pre-stressable spring devices can be used for adjustments and levelling, as for the already mentioned well-known soil settlements (e.g. due to mining subsidence or soft soil conditions).

REFERENCES

International Atomic Energy Agency (2020). *Seismic Isolation Systems for Nuclear Installations, IAEA-TECDOC-1905*, IAEA, Vienna, Austria.

Kostarev, V.V., Vasilyev, P.S. and Nawrotzki, P. (2017). “A new approach in seismic base isolation and dynamic control of structures,” *Proc., 2017 NZSEE Conference*, Wellington, New Zealand, 1-9.

Kostarev, V., Nawrotzki, P., Vasilyev, P. and Vaindrakh, M. (2019). “Developing and natural scale testing of the 3D BCS Base Isolation System,” *Proc., 16th World Conference on Seismic Isolation, Energy Dissipation and Active Vibration Control of Structure*, DOI 10.13753/2686-7974-2019-16-460-472, 16WCSI, St. Petersburg, Russian Federation, 460-472.

Nawrotzki, P., Salcedo, V. and Siepe, D. (2013). “3-D Base Control Systems for the Seismic Protection of Power Plant Equipment and Buildings,” *Proc., 22nd Conference on Structural Mechanics in Reactor Technology SMiRT-22*, Transactions, San Francisco, CA, USA, 1-8.

Nawrotzki, P. and Siepe, D. (2015). “Seismic protection of machinery, buildings and equipment of nuclear power plants by using 3-D Base Control Systems,” *Proc., 23rd Conference on Structural Mechanics in Reactor Technology SMiRT-23*, Transactions, Manchester, United Kingdom, 1-10.

Nawrotzki, P., Kostarev, V., Siepe, D. and Morozov, D. (2019). “3-D Base Control Systems for the Seismic Protection of Structures,” *Proc., 16th World Conference on Seismic Isolation, Energy Dissipation and Active Vibration Control of Structure*, DOI 10.13753/2686-7974-2019-16-591-599, 16WCSI, St. Petersburg, Russian Federation, 591-599.

Ryan, K. L., Dao, N. D., Sato, E., Sasaki, T. and Okazaki, T. (2012). "NEES/E-defense base-isolation tests: interaction of horizontal and vertical response," *Proc., 15th World Conference on Earthquake Engineering 15WCEE*, Lisbon, Portugal, 1-10.

Siepe, D. and Nawrotzki, P. (2015). "Horizontal and vertical isolation of seismic and aircraft impact," *Proc., 14th World Conference on Seismic Isolation, Energy Dissipation and Active Vibration Control of Structures WCSI*, San Diego, CA, USA, 1-10.

Stendel, M. and Christensen, J. H. (2002). "Impact of global warming on permafrost conditions in a coupled GCM," *Geophysical Research Letters, Vol. 29, No. 13, 1632, DOI 10.1029/2001GL014345*.

Stuardi, J. E., Suarez, L. E. and Nawrotzki, P. (2008). "Comparative seismic performance of a Base Control System based on measured and calculated responses," *Proc., 14th World Conference on Earthquake Engineering*, Beijing, China, 1-8.

Transactions, SMiRT-26
Berlin/Potsdam, Germany, July 10-15, 2022
Special Session

2019-11-11 LE TEIL EARTHQUAKE - THE ULTIMATE MISSING PIECE OF EXPERIENCE FEEDBACK RELATED TO A NUCLEAR POWER PLANT BUILT ON SEISMIC BASE ISOLATION: A REAL EARTHQUAKE

Emmanuel Viallet[1], Julien Berger[2], Paola Traversa[3], Elias El Haber[3], Estelle Hervé-Secourgeon[4], Guillaume Hervé-Secourgeon[4,7], Loic Zuchowski[5], Guillaume Dupuy[6]

[1] Seismic Risk Fellow Expert, EDF, DIPNN/DT, Lyon, France
[2] Earthquake Engineering Proficient Engineer, EDF, DIPNN/DT, Lyon, France
[3] Seismologist PhD, EDF, DIPNN/DI, Aix-en-Provence, France
[4] Research Engineer, PhD, EDF, R&D/EDF-Lab, Paris-Saclay, France
[5] Earthquake Engineering Proficient Engineer, EDF, DIPNN/CNEPE, Tour, France
[6] Seismic Risk Engineer, EDF, DPN/UNIE, Paris, France
[7] Associate Professor, Université Paris-Saclay, CentraleSupélec, CNRS, ENS Paris-Saclay, LMPS - Laboratoire de Mécanique Paris-Saclay, Gif-sur-Yvette, France

ABSTRACT

Cruas Nuclear Power Plant is a three-loop 900 MW Pressurized Water Reactor designed and built at the end of the seventies. At the original stage of the design of French PWRs, EDF has decided to design series of plants, in order to get identical Structures, Systems and Components (SSCs) for the whole series under consideration. However, when Cruas site was selected, both soil conditions and seismic hazard were identified as non-standard design conditions. For this reason, EDF decided to build the plant on seismic base isolation, in order to keep the nuclear island identical to the rest of the series. The base isolation technology used is the so-called “laminated steel-neoprene bearing” that was already largely used in conventional buildings and bridges.

The plant has now almost forty years of operation and no issue has been identified in relation with this laminated steel-neoprene bearing seismic base isolation technology. This technology is therefore matured for use in nuclear industry and supported by Standards that address design and construction as well as manufacturing and maintenance. The only missing piece of experience feedback was the impact of the occurrence of a real earthquake on the plant, in order to give the opportunity to confirm that the design process (already supported by multiple analyses and test campaigns) provides adequate design margins, based on a real full-scale event.

Le Teil magnitude 4.9 (Mw) earthquake occurred on November 11, 2019 at approximately 15 km from Cruas NPP and led to a ground motion shaking between 0.02 and 0.05 g on site (Peak Ground Acceleration, free field). Although this ground motion level is not very high compared to the DBE of the Plant (0.3 g), due to operational procedures, the plant was shut down and post-earthquake inspections were performed before restart. In this context, the objective of this paper is first to introduce Le Teil earthquake in terms of seismological characteristics, then to describe what was done by the operator in the hours, days and weeks after the earthquake, and to present what was observed on site, especially the actual seismic records compared to analyses. Finally, the paper will put forward the current and further actions that are under progress and/or may start in a close future, including international benchmarks in order to share experience feedback and lessons learnt with the largest international community.

INTRODUCTION: STANDARD DESIGN PRINCIPLES FOR FRENCH NPP AND FOCUS ON CRUAS PLANT

Standard design principles for French NPPs

French Nuclear Power Plants (NPPs) currently under operation are Pressurized Water Reactors (PWRs) that have been designed since the 70's. At the time of the design of these plants, EDF decided to follow a standard design approach for series of plants in order to duplicate main Structures, Systems and Components (SSCs) and keep them identical from one site to another belonging to the same series. In this purpose, regarding seismic design, standard conditions were defined, mainly based on soil conditions and seismic hazard, in order to envelope most of the expected sites (that were not yet known at the early design stage). This standard design principle, as illustrated in Figure 1, also shows that at this stage some site-specific conditions were also anticipated (such as non-standard soil conditions or non-standard seismic level) and could be addressed through specific features (such as special foundation systems or seismic base isolation).

Figure 1. French NPPs standard design principles

Based on these principles, 4 series of plants were designed and built:

- 900 MWe – 3 loop series,
- 1300 MWe – 4 loop series,
- 1450 MWe – 4 loop series,
- EPR 1650 MWe – 4 loop series.

Focus on Cruas NPP

In the case of Cruas NPP, site investigations revealed that the site was mainly composed of limestone with stiff characteristics corresponding to hard rock. In addition, seismic hazard analyses indicated that the site could be subjected to moderate magnitude but near field earthquake with both a higher PGA (0.3g) and a higher frequency content compared with the standard design PGA (0.2g) of the 900 MWe series (see illustration in Figure 4). Then, naturally, EDF decided to build Cruas NPP on seismic base isolation in order to keep the design of all SSCs from the Nuclear Island (NI) identical to the rest of the plants of the series.

In practice, four units are built on Cruas site. A single "upper" basemat supports all NI buildings of a pair of units, as illustrated on Figure 2 (left). This upper basemat is supported by the seismic base isolation system, which is built in a prior phase of the construction, as illustrated in Figure 2 (right).

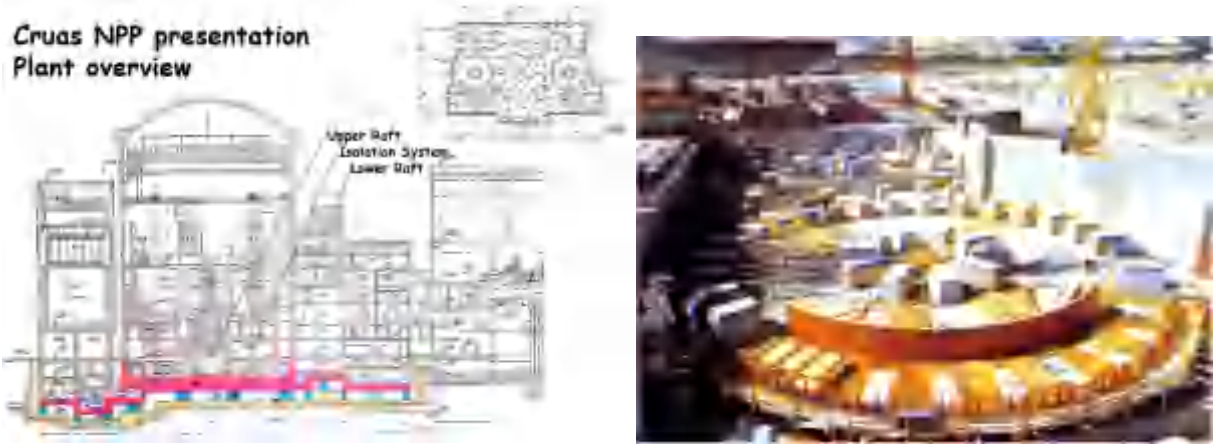

Figure 2. Cruas NPP layout (left) and seismic base isolation system during construction phase (right)

Some more detailed information regarding available seismic base isolation technologies and design approaches for NPPs are provided in an IAEA Tecdoc (IAEA, 2020).

Anti-seismic bearings technology description

The seismic base isolation system which was selected at the time of the design was the so-called laminated steel-neoprene bearing, as described in Figure 3. The main reasons for this choice were i) the well-known technology associated with a large feedback of experience (especially from bridges) and ii) the well-characterized ageing process and kinetic (stiffness of the laminated steel-neoprene bearing increases with time) which allowed to predict long-term evolution since the early design stage.

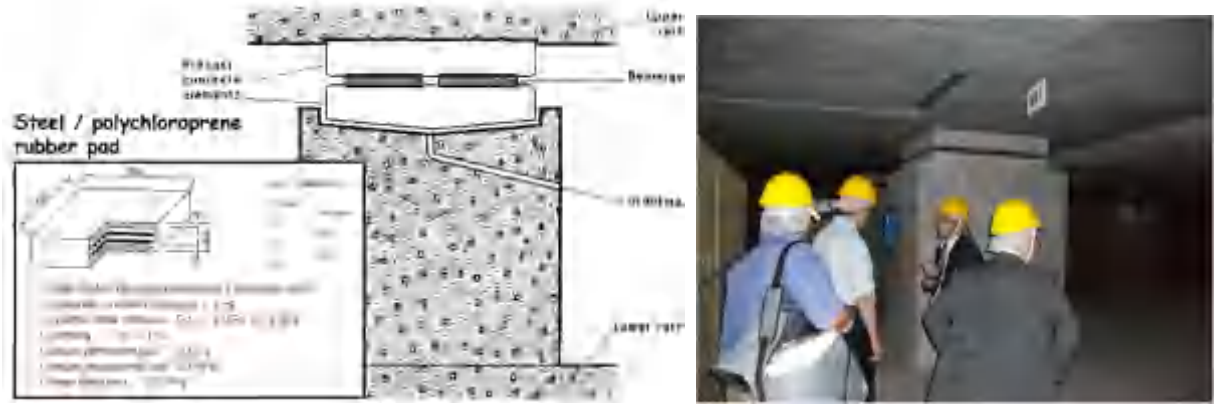

Figure 3. Laminated steel-neoprene bearing description: drawings (left) and actual view (right)

Seismic design principles of Cruas NPP

On the basis of the site conditions and design solutions introduced in the previous sections, the choice was made to design anti-seismic bearings characteristics in order to scale the main horizontal eigenfrequency of the whole isolated system (NI buildings) at 1 Hz for Design Basis Earthquake (DBE) level, including ageing prediction. This target eigenfrequency was selected in order to get a spectral acceleration of the isolated system close to the Peak Ground Acceleration (PGA) of the standard DBE (0.2 g), as illustrated in Figure 4.

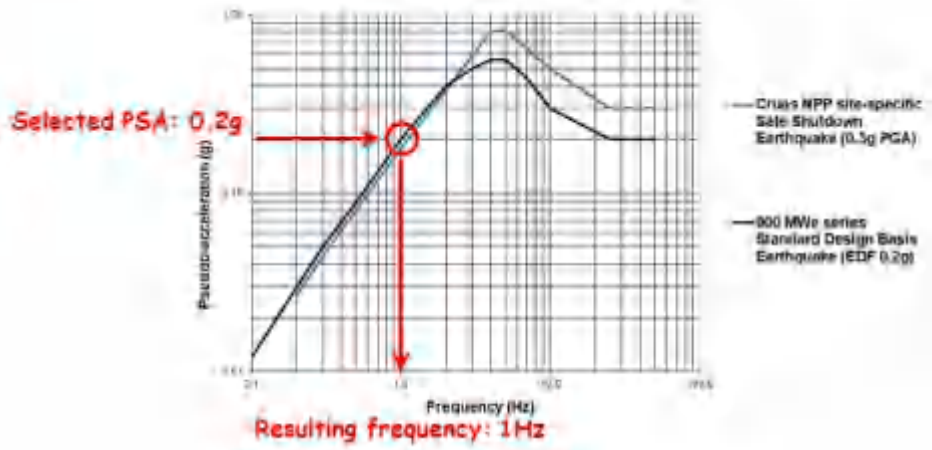

Figure 4. Illustration of Cruas NPP seismic based isolation design principles

2019/11/11 LE TEIL EARTHQUAKE DESCRIPTION

The 2019-11-11 Le Teil earthquake (Mw = 4.9, reverse focal mechanism) occurred in a low to moderate seismicity area within the lower Rhône river valley. In spite of its moderate magnitude, the earthquake caused significant damages to residential buildings in the epicentral area, presumably related to its very shallow focal depth (about 1 to 1.5 km, as described below). The maximum macroseismic intensities reported in the epicentral area are between VII and VIII EMS-98 (Sira et al., 2020).

Satellite radar interferometry images (InSAR) revealed a rupture zone along La Rouvière fault (red line in Figure 5, Ritz et al, 2020).

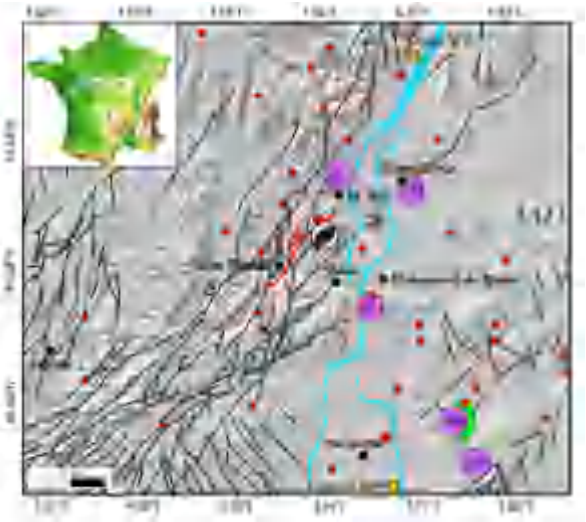

Rupture Parameters	Values
Earthquake magnitude	4.9 (Mw)
Epicenter location	4.6688°, 44.5208°
Hypocenter depth	1 Km
Rupture dimensions	5 x 1.75 Km^2
Strike	50°
Dip	58°
Rake	89°
Stress drop	2 MPa
Rupture velocity (Vr)	1800 m/s
Anelastic attenuation parameters	$Q_0 = 347 \pm 4$
(Q_0 and α)	$\alpha = 0.31 \pm 0.005$
Geometric spreading parameter (β)	1.02 ± 0.02

Figure 5: To the left, Seismotectonic map of the region around the 11 November 2019 Mw 4.9 earthquake. The red and purple circles are instrumental and historical seismicity, respectively; the yellow squares represent the Nuclear Power Plants in the region (Cruas and Tricastin NPP). The black lines are faults from the Aubenas geological map (Elmi et al., 1996) with the La Rouvière Fault (LRF) in red. The shaded DTM is from BD ALTI 25m (IGN); MC and Al in the inset are Massif Central and Alps, respectively. (Figure form Ritz et al., 2020). To the right, the main rupture parameters of the Le Teil earthquake found in the literature and used in the ground motion simulations benchmark (see next sections).

The seismic source of this earthquake was studied in detail (Delouis et al., 2019, Cornou et al., 2021, Ritz et al., 2020, De Novellis et al., 2020, Mordret et al., 2020). The rupture area was very shallow, with a length of ~5km and a width of 1.75 km. The rupture reached the surface, inducing surface deformation, which is unusual for earthquakes of such moderate magnitude. Up to 15 cm of uplift was observed on the SE side of the fault (Delouis et al., 2021). Based on the analysis of the seismological network records, the earthquake hypocenter was located on the NW portion of the La Rouviere fault at a depth in the range of 1–1.5 km (Cornou et al., 2020, Delouis et al., 2021).

The ground motion produced by Le Teil earthquake was widely recorded by the seismic stations of the RESIF consortium national network (RESIF 1995a, 1995b) and by the seismic stations installed at Nuclear Installation sites. Figure 6 shows Peak Ground Accelerations (PGA) recorded by accelerometric and broad-band seismic stations within 500 km as function of distance and Eurocode 8 site classification.

In France, EDF's NPP sites dispose of two different types of seismic instrumentation, with two different goals. On one hand, five sensors constitute the seismic safety monitoring system (EAU), including one free field sensor and four sensors installed within the main structures of the plant (see next section for more details). On the other hand, the RAN seismological network includes at least one accelerometer and one broad-band sensors installed at free-field condition at all NPP. The aim of this latter network is to provide continuous recordings that can be used in seismological analyses and seismic hazard studies.

Cruas NPP is located at 15 km distance from Le Teil epicenter. The RAN broad-band sensor saturated during the shaking, while the accelerometer provides the closest high-quality record of the Le Teil earthquake ground motion.

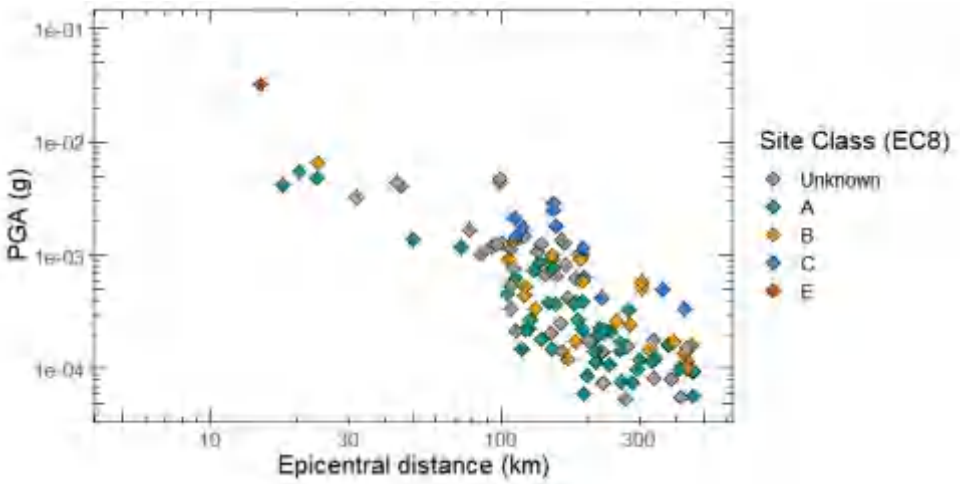

Figure 6: PGA (Peak Ground Acceleration) recorded at seismic stations during Le Teil earthquake as function of epicentral distance and site class (according to the EC8 classification).

Figure 7 shows the time histories recorded by this sensor.

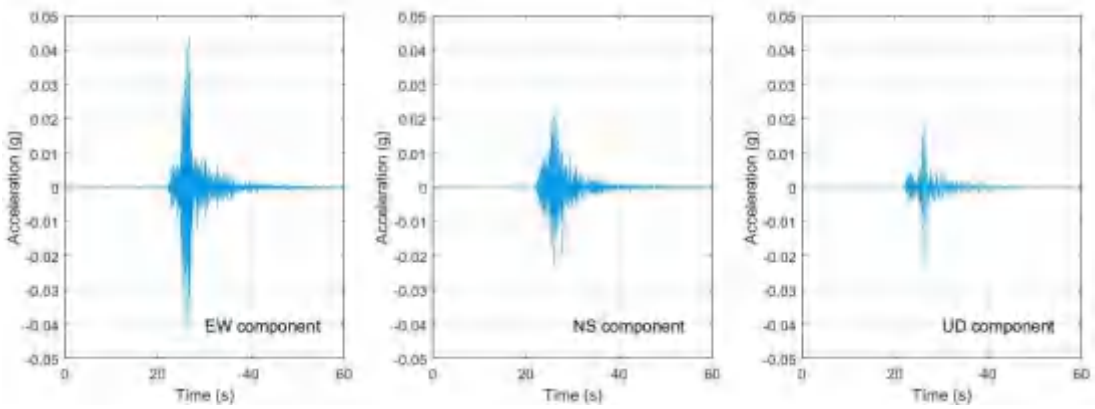

Figure 7: Time histories recorded at Cruas RAN free-field accelerometer.

The ground motion recorded at Cruas free field is characterized by a resonance peak around 9 Hz. This is related to the presence of a thin sediment layer (7 m thick) above stiff rock for the free-field surface condition (see more details in next sections).

2019/11/11 LE TEIL EARTHQUAKE: IMPACT ON CRUAS NPP (SHUTDOWN, INSPECTIONS AND RESTART)

This section describes the actions that were performed by the Cruas NPP operators and their engineering supports in a chronological manner, from the earthquake occurrence time until the restart of the units.

November 11th: Immediate actions by operators and decisions

According to French nuclear basic safety rule RFS I-3-b (ASN, 1984), a seismic recording system (called "EAU") is implemented on each NPP site. This system is triggered with a first threshold scaled to 0.01g that, when reached, simultaneously sends a warning message to operators (in main control room) and records acceleration time histories in 5 locations (free field, basemat of the reactor building, main floor at +20m in the reactor building, basemat of the nuclear auxiliary building and ASG tank building) for 3 components (X, Y and Z plant main axis).

At 11:53 am local time, seismic warning system appeared in main control room and operators immediately launched the seismic event operating procedure coded as "I-EAU", which mainly consist of i) confirming that an earthquake was felt by a large part of NPP staff, then ii) launching immediate plant walkdowns to identify any damage or any seismic-induced situation and finally iii) get and post-process seismic records from the five locations given above.

From 11:53 am to 4:00 pm local time, previous actions were implemented. No specific issues were reported by plant walkdown teams. However, one of the records (ASG tank building, vertical component) indicated that the maximum recorded acceleration was 0.037g, which exceeded the Inspection Earthquake threshold defined at 0.05g in horizontal direction and scaled at 0.033g (2/3 x 0.05g) in vertical direction. Due to this record and according to I-EAU procedure, the 3 units that were under operation when the earthquake occurred (Units 2 to 4) where manually shutdown by the operators. This was progressively done in the afternoon and evening of the same day.

From November 12th to November 20th: Post-earthquake walkdowns and conclusions

According to RFS I-3-b, in case of plant shutdown due to an earthquake, authorization of restarting the plant should be given by the regulator based on a detailed investigation report provided by the operator.

Then, post-earthquake investigations were performed by the operator and its engineering support following international guidelines (IAEA, 2011) and (EPRI, 2015). Despite the relatively low recorded seismic level and the absence of any seismic related issue from immediate plant walkdown which would have led to an immediate restart of the plant according to these previous references, post-earthquake walkdowns covered a large panel of SSCs, including safety-related and non-safety-related ones, civil structures, mechanical and electrical equipment and SSCs outside of the base-isolated structures. These investigations were documented, as illustrated in Figure 8.

Figure 8: Illustration of post-earthquake plant walkdown.

The conclusions of these extensive plant walkdowns, confirmed by a Peer Review, established that the earthquake did not induce any damaged to any of the SSCs of the plant. The detailed investigation report was sent to the French Regulator (ASN) on November 22.

From November 22nd to December 6th: Assessment by the Regulator

The French Regulator (ASN) and its Technical Support Organization (TSO) IRSN assessed the reports sent by the operator and performed their own plant walkdown. These actions led to some requests for clarifications that were addressed by the operator.

At the end of this process, authorization of restarting the plants was given by the French Regulator on December 6. Finally, Cruas units 2 to 4 progressively restarted between December 7 to 13.

EMPIRICAL AND NUMERICAL SIMULATIONS APPLIED TO THE TEIL EARTHQUAKE

Within the SIGMA2 project (https://www.sigma-2.net/), four different simulation techniques (two empirical and two physics-based techniques) were used to reproduce the Le Teil earthquake. The four simulation techniques are:

- The **Irikura recipe**: (Irikura and Miyake, 2011) a strong ground motion methodology mainly developed and used in Japan, which is based on a kinematic description of the source. This empirical technique is based on small events corrections to generate Empirical Green's Functions (EGFs) and on large event source definition using asperities representing the rupture slip distribution. The summation over the rupture area of the convolution between EGFs and elementary slip on the fault allows to simulate the Ground Motion of the large event.
- The **Dujardin et al. (2020) technique** that is similar to the Irikura recipe: ground motions of a large event are simulated by summing the recordings of small events. This technique differs from the previous technique in the summation and the slip distribution generation techniques.
- A **1D Physics-Based Simulation** : where ground motions are calculated through the tensor product between the tensors of the earthquake source and the Green's function of the medium (including the soil layers) crossed by the seismic waves (Fasan, 2017; Magrin, 2012; Panza et al., 2012). The technique has been successfully applied and validated against past events and available ground motion prediction equations (Fasan, 2017; Fasan et al., 2016; Hassan et al., 2020; Magrin et al., 2016; Panza et al., 2012).
- A **3D Physics-Based Simulation** using the open-source high-performance computer code SPEED (http://speed.mox.polimi.it/, Mazzieri et al., 2013). In order to increase the frequency resolution, the SPEED signals have been enriched a posteriori at high frequencies using a technique based on ANN trained on strong ground motion recordings (Paolucci et al. 2021a and 2021b).

The common assumptions used by the different techniques are summarized in Figure 5 (right).

The analysis of seismic ground motion parameters in both, time and frequency domains, was performed at 5 stations (ADHE, CRU1, OGLP, TRI2 and A192B) that recorded the main event and the aftershocks. Two of these stations (CRU1 and TRI2) are located next to the Cruas and Tricastin NPP, respectively. Figure 9 compares the Fourier Amplitude Spectra of acceleration time histories computed through the different simulations at the CRU1 and TRI2. Knowing that a perfect match between simulations and recordings cannot be reached, overall, the FAS simulated using the different techniques approach the observed ground motion features with different accuracy levels, depending on the frequency band and the considered technique. Empirical Green's function techniques are particularly good at reproducing specific features of site response (i.e. the 8-9 Hz amplification peak observed on ground motion recorded at CRU1 station EW component), because site-response features are included in the recordings used as EGF. Physic-based simulations, particularly the 3D approach, allow to well reproduce lower frequency patterns of observed ground motion (below 1 Hz), where EGF-based simulations perform worse due to the poor signal-over-noise ratios of the small events.

In additional to the Fourier spectrum, simulated ground motions are analyzed in the time domain using four ground motion intensity measures: the peak ground acceleration (PGA), the peak ground velocity (PGV), the Arias Intensity (AI) and the corresponding duration (D5-95).

In two different frequency bands: [1-10Hz] for the empirical techniques and [0.2-2Hz] for the PBS techniques, Figure 10 shows the Goodness of Fit (GoF) between simulated and recorded data, calculated for the five ground motion indicators (PGA, PGV, mean(|FAS|), AI and D5-95), for the three components

of CRU1 and TRI2 stations. The GoF is defined as $log_{10}\left(\frac{Simulated}{Recorded}\right)$ and a GoF equal to 0 means excellent agreement between the recorded and simulated data.

The estimated GoF are sensitive to the GM indicator, the station and the azimuth. For selected stations, a non-negligible variability is found also between approaches belonging to the same class of methods (i.e. the two EGFs and the two PBSs), because of the assumptions and constraints at the basis of the approaches.

At TRI2 station, all methods show higher performance, with relatively a smaller variability. However, closer to the fault and located to the north-west of the fault, CRU1 exhibits a larger variability of results.

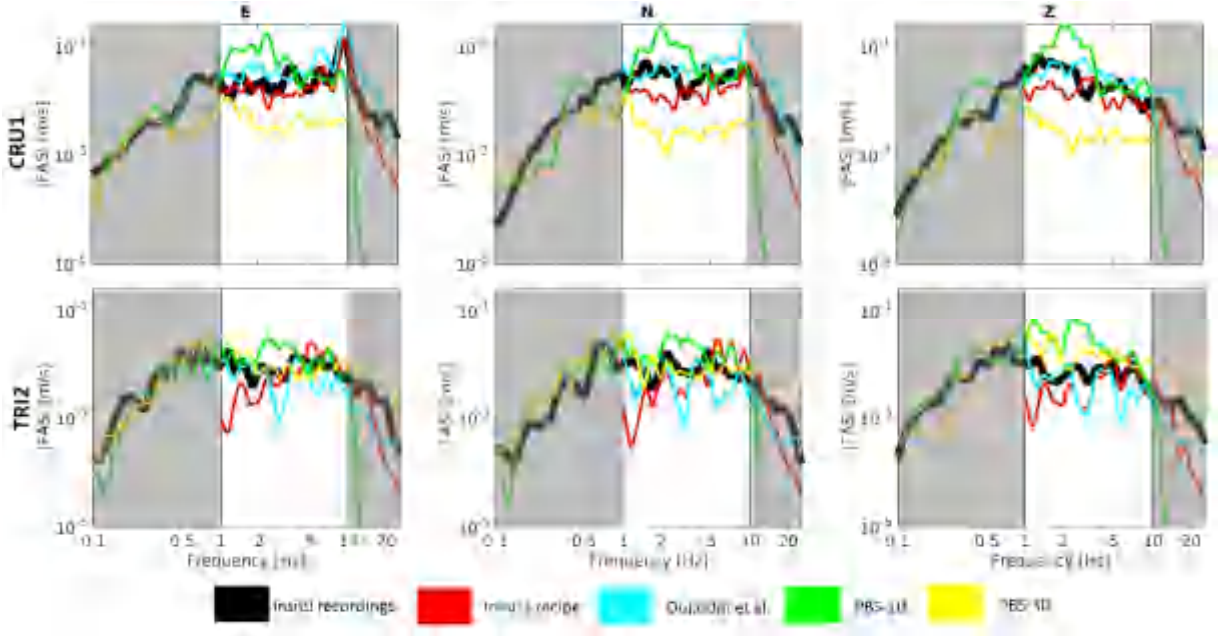

Figure 9: The Fourier Amplitude Spectrum (FAS) of three-component (E: East-West; N: North-South; Z: Up-Down) acceleration time histories calculated by the four different simulations (Irikura in red, Dujardin modified in cyan, PBS-1D in green, PBS-3D in yellow) and smoothed with the Konno and Ohmachi (b=40; Konno and Ohmachi, 1998), at CRU1 and TRI2. The thick black lines correspond to the recordings FAS.

The results of this simulation benchmark show that the different simulation techniques considered in this study are complementary to each other: while EGF-based simulations are reliable in the high frequency range (above 1 Hz), the 3D-physics-based simulations provide reliable ground motion in the low frequency range (below 2 Hz). The former techniques are limited by the availability and the quality of earthquake records to be used as EGF, while the latter techniques need to be complemented by other approaches in the higher frequency range. They can therefore be used to complement each other as hybrid simulations to obtain broad-band ground motion. Even more, 3D simulations could be used to generate synthetic Green's functions in regions where no small events are recorded.

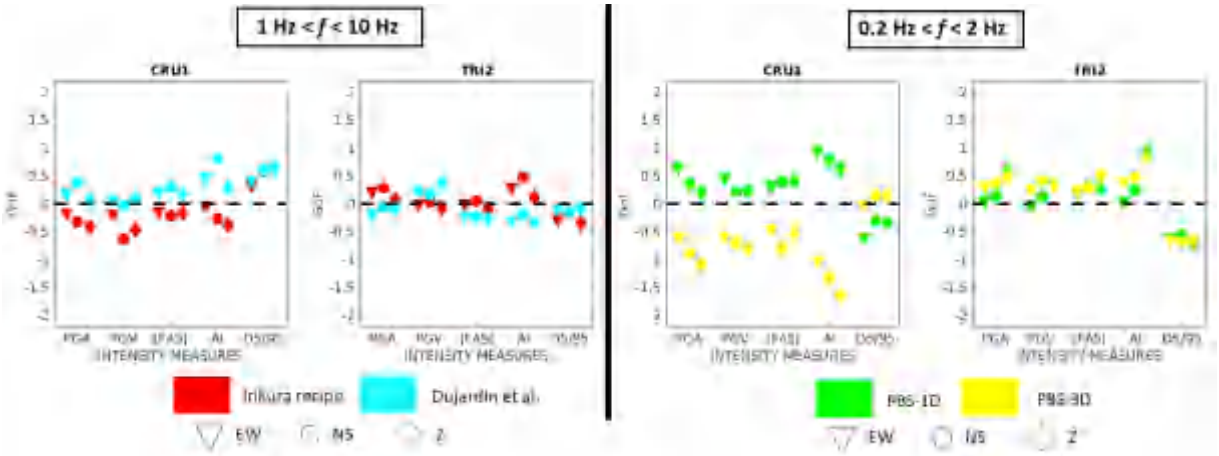

Figure 10: The Goodness of Fit (GoF) between simulated and recorded accelerograms calculated for the five ground motion intensity measures (PGA, PGV, FAS, Arias Intensity and Duration) estimated using the empirical techniques at high frequencies ([1-10Hz]) and the PBS techniques at low frequencies ([0.2-2Hz]). The results are shown for CRU1 and TRI2 stations in the 3 directions.

CURRENT STATUS OF ASSESSMENTS: STRUCTURAL BEHAVIOR AND SEISMIC RESPONSE OF THE PLANT

The locations of EAU sensors within Cruas NPP, inside or near Nuclear Island #1, are shown in Figure 11.

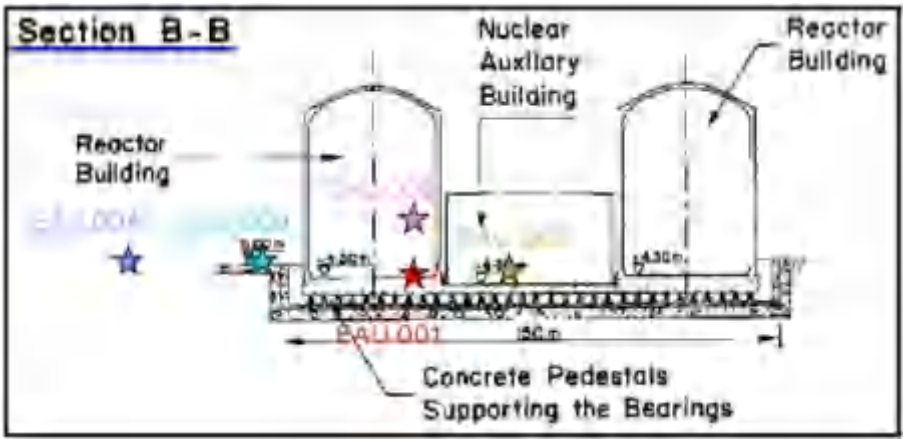

Figure 11: Location of EAU sensors within Cruas NPP.

The response spectra computed from the acceleration time histories registered at these positions, as well as the RAN sensor accelerations at free field conditions, are not presented in this paper because of the coming international benchmark (see conclusion) which will include a blind prediction phase. However, they highlight the frequency shift of the seismic signal within the isolated structure roughly between 1.5 and 1.8 Hz, whereas other sensors spectra display a rich frequency content between 5 and 15 Hz. This base-isolation effect is illustrated and commented in a different way in the next paragraphs.

Continuous wavelet transforms (Erlicher, 2007) were used to analyze the time histories frequency content. On RAN sensor time histories, the superficial alluvial layer mode located around 9 to 10 Hz is visible in Figure 12, as well as other frequencies, especially within the 5 to 15 Hz range.

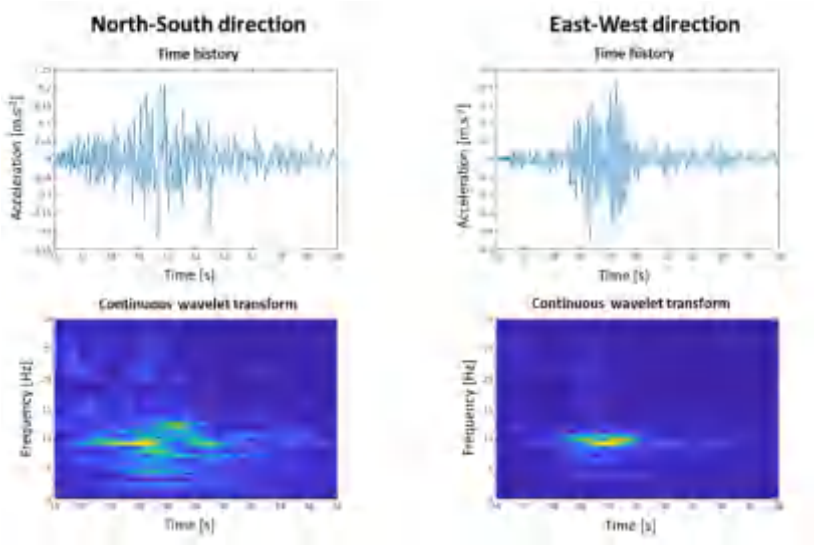

Figure 12: Frequency analysis of RAN sensor time histories, using continuous wavelet transform

Similar analysis applied to EAU sensors located within the isolated structure show a very different frequency content, with a single eigenfrequency highlighted in Figure 13 for the two sensors located within the lower levels, and still visible at +20m level even if other structural eigenfrequencies are visible in this case. The base isolation of the nuclear island has played a filter role, exactly as it was designed to behave, lowering the main eigenfrequency of the nuclear island to a very low value. Nevertheless, the vertical seismic movement is not filtered, and is responsible for both vertical and in some cases horizontal movements with higher frequencies within the higher levels, visible on EAU-002 time histories analysis.

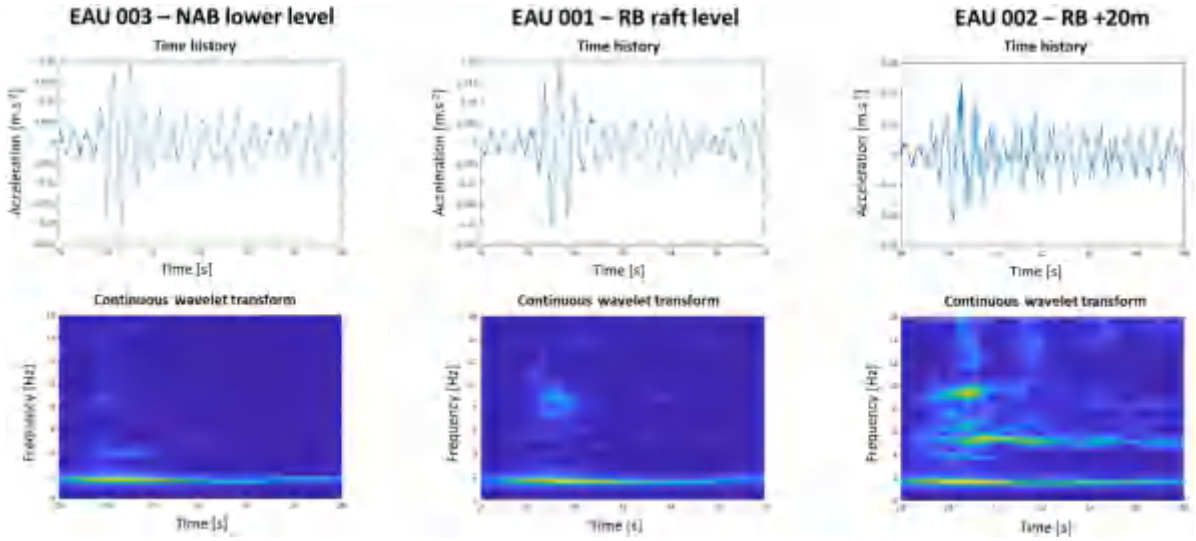

Figure 13: Frequency analysis of EAU 001 to 003 sensors' time histories in one horizontal direction, using continuous wavelet transform

Ridge detections techniques are used to follow up this frequency, which is shown to vary between 1.5 and 1.8 Hz during the main phase of the seismic motion, as shown in Figure 14. It is further plotted as a function of the acceleration level, as the neoprene bearings ensuring the base isolation are known to be slightly nonlinear, even at low amplitude. A least square regression is computed according to a power law, fitting rather well with the registered data from the 3 sensors, in the two horizontal directions. It is consistent

with a main eigenfrequency varying between about 2 Hz at a very low level of excitation to around 1 Hz for earthquakes with an acceleration amplitude of about 10 times the ones recorded during Le Teil earthquake (Safe Shutdown Earthquake is defined at 0.3g PGA for Cruas site).

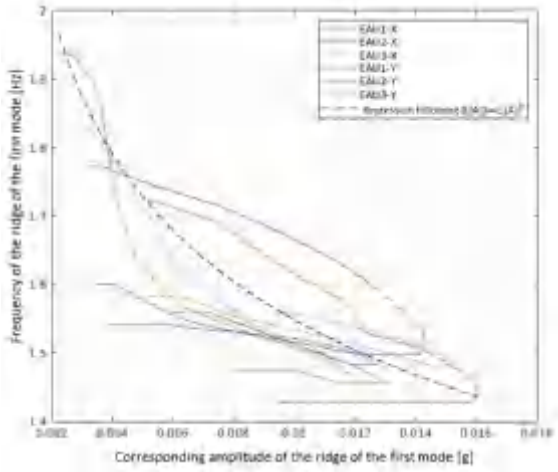

Figure 14: EAU 001 to 003 main ridge frequency follow-up as a function of the associated amplitude of the ridge

CONCLUSIONS AND PERSPECTIVES

Le Teil magnitude 4.9 (Mw) earthquake occurred on November 11, 2019 at approximately 15 km from Cruas NPP, a three-loop 900 MW Pressurized Water Reactor built on seismic base isolation. This earthquake led to a ground motion shaking between 0.02 and 0.05 g on site (Peak Ground Acceleration, free field). Although the ground motion level is not very high compared to the DBE of the Plant (0.3 g PGA), due to operational procedures, the plant was shut down and post-earthquake inspections were performed before restart. The conclusions of these extensive plant walkdowns, confirmed by a Peer Review, established that the earthquake did not induce any damaged to any of the SSCs of the plant. Finally, Cruas units NPP units progressively restarted less than one month after the event.

This seismic event, that was largely assessed and documented on the seismological aspect, also provides the ultimate missing piece of experience feedback regarding the actual behavior of a NPP built on seismic base isolation, in terms of dynamic behavior of the anti-seismic bearings themselves and in terms of dynamic behavior of the plant. This was achieved thanks to the records that allow to compare design studies that were performed 40 years ago to actual observations. Additional pieces of experience feedback, analyses and lessons learnt regarding this earthquake were also shared in the framework of the French Society for Nuclear Energy, (SFEN, 2020).

Finally, in order to move forward and to share this unique experience feedback with the largest community, EDF and IRSN have decided to organize an international benchmark. This benchmark, organized under the auspices of OECD/NEA, will include a first phase related to seismic ground motion characterization at Cruas site location and will also include a second phase related to assessing the seismic response of the plant including seismic base isolation system. EDF and IRSN are looking forward to share experience feedback with the largest international community in order to promote this optimized seismic design solution in the future, not only for current generations of plants but also for new ones such as SMRs or advanced reactors.

REFERENCES

ASN (1984). RFS I-3-b, Conception générale de la centrale et principes généraux applicables à l'ensemble de l'installation - Principes généraux de conception et d'installation - Instrumentation sismique. https://www.asn.fr/l-asn-reglemente/rfs/rfs-relatives-aux-rep/rfs-i-3.b.-du-08-06-1984

Causse, M., Cornou, C., Maufroy, E., Grasso, J. R., Baillet, L., & El Haber, E. (2021). Exceptional ground motion during the shallow M w 4.9 2019 Le Teil earthquake, France. *Communications Earth & Environment*, *2*(1), 1-9.

Cornou, C., Ampuero, J. P., Aubert, C., Audin, L., Baize, S., Billant, J., ... & Weng, H. (2020). Rapid response to the M_w 4.9 earthquake of November 11, 2019 in Le Teil, Lower Rhône Valley, France.

Delouis, B., Ampuero, J. P., Audin, L., Bernard, P., Brenguier, F., Grandin, R., ... & Voisin, C. Rapport d'évaluation du groupe de travail (GT) CNRS-INSU sur le séisme du Teil du 11 novembre 2019 et ses causes possibles, 2019 http://www.cnrs.fr/sites/default/files/ press_info/2019-12.*Rapport_GT_Teil_phase1_final_171219_v3. pdf (35 p., in french)*.

Delouis, B., Oral, E., Menager, M., Ampuero, J. P., Trilla, A. G., Régnier, M., & Deschamps, A. (2021). Constraining the point source parameters of the 11 November 2019 Mw 4.9 Le Teil earthquake using multiple relocation approaches, first motion and full waveform inversions. *Comptes Rendus. Géoscience*, *353*(S1), 1-24.

De Novellis, V., Convertito, V., Valkaniotis, S., Casu, F., Lanari, R., Monterroso Tobar, M. F., & Pino, N. A. (2020). Coincident locations of rupture nucleation during the 2019 Le Teil earthquake, France and maximum stress change from local cement quarrying. *Communications Earth & Environment*, *1*(1), 1-10.

Dujardin, A., Hollender, F., Causse, M., Berge-Thierry, C., Delouis, B., Foundotos, L., ... & Shible, H. (2020). Optimization of a simulation code coupling extended source (k− 2) and empirical green's functions: Application to the case of the middle durance fault. *Pure and Applied Geophysics*, *177*(5), 2255-2279.

Elmi, S., Busnardo, R., Clavel, B., Camus, G., Kieffer, G., Bérard, P., & Michaëly, B. (1996). Notice explicative, Carte Géologique France 1/50000, feuille Aubenas (865). *Orléans: BRGM*.

EPRI (2015). Guidelines for Nuclear Power Plant Response to an Earthquake. Report 3002005284. https://www.epri.com/research/products/3002005284

Erlicher, S., Argoul, P. (2007), Modal Identification of Linear Non-Proportionally Damped Systems by Wavelet Transform , Mechanical Systems and Signal Processing 21, no 3, pp. 1386-1421

Fasan, M., Magrin, A., Amadio, C., Romanelli, F., Vaccari, F., and Panza, G. F., 2016. A seismological and engineering perspective on the 2016 Central Italy earthquakes. *International Journal of Earthquake and Impact Engineering*, **1**(4), 395–420. DOI: 10.1504/IJEIE.2016.10004076

Fasan, M., 2017. *Advanced seismological and engineering analysis for structural seismic design*. Italy: University of Trieste.

Hassan, H. M., Fasan, M., Sayed, M. A., Romanelli, F., ElGabry, M. N., Vaccari, F., and Hamed, A., 2020. Site-specific ground motion modeling for a historical Cairo site as a step towards computation of seismic input at cultural heritage sites. *Engineering Geology*, **268**(April 2019), 105524. Elsevier. DOI: 10.1016/j.enggeo.2020.105524

IAEA (2011). Earthquake Preparedness and Response for Nuclear Power Plant. TECDOC-1905 https://www.iaea.org/publications/8473/earthquake-preparedness-and-response-for-nuclear-power-plants

IAEA (2020). Seismic Isolation Systems for Nuclear Installations. Safety Report Series nº66 https://www.iaea.org/publications/13646/seismic-isolation-systems-for-nuclear-installations

Irikura K., Miyake H. (2011) Recipe for predicting strong ground motion from crustal earthquake scenarios, *Pure Appl. Geophys*, DOI: 10.1007/s00024-010-0150-9.

Magrin, A., 2012. *Multi-scale seismic hazard scenarios*. Italy: University of Trieste.

Magrin, A., Gusev, A. A., Romanelli, F., Vaccari, F., and Panza, G. F., 2016. Broadband NDSHA computations and earthquake ground motion observations for the Italian territory. *International Journal of Earthquake and Impact Engineering*, **1**(1/2), 28. DOI: 10.1504/IJEIE.2016.10000979

Mordret, A., Brenguier, F., Causse, M., Boué, P., Voisin, C., Dumont, I., ... & Ampuero, J. P. (2020). Seismic stereometry reveals preparatory behavior and source kinematics of intermediate-size earthquakes. *Geophysical research letters*, *47*(17), e2020GL088563.

Mazzieri, I, Stupazzini M, Guidotti R, Smerzini C (2013) SPEED: SPectral Elements in Elastodynamics with Discontinuous Galerkin: a non-conforming approach for 3D multi-scale problems. Int J Numer Meth Eng 95(12):991–1010.

Paolucci, R., I. Mazzieri, G. Piunno, C. Smerzini, M. Vanini, and A. G. Özcebe (2021a). Earthquake ground motion modelling of induced seismicity in the Groningen gas field, Earthq. Eng. Struct. Dynam. 50, 135–154, doi: 10.1002/eqe.3367.

Paolucci, R., C. Smerzini, and M. Vanini (2021b). BB-SPEEDset: A Validated Dataset of Broadband Near-Source Earthquake Ground Motions from 3D Physics-Based Numerical Simulations, Bull. Seismol. Soc. Am. XX, 1–19, doi: 10.1785/0120210089

Panza, G. F., Mura, C. La, Peresan, A., Romanelli, F., and Vaccari, F., 2012. Seismic Hazard Scenarios as Preventive Tools for a Disaster Resilient Society (pp. 93–165). DOI: 10.1016/B978-0-12-380938-4.00003-3

RESIF (1995a). RESIF-RAP French Accelerometric Network, doi: 10.15778/RESIF.RA.

RESIF (1995b) RESIF-RLBP French Broad-band network, RESIF-RAP strong motion network and other seismic stations in metropolitan France, doi: 10.15778/RESIF.FR.

Ritz, J. F., Baize, S., Ferry, M., Larroque, C., Audin, L., Delouis, B., & Mathot, E. (2020). Surface rupture and shallow fault reactivation during the 2019 Mw 4.9 Le Teil earthquake, France. *Communications Earth & Environment*, *1*(1), 1-11.

SFEN (2020). Resilience of nuclear power plants to seismic risk: case study of the Le Teil earthquake https://www.sfen.org/avis/la-resilience-des-centrales-nucleaires-au-risque-sismique-cas-du-seisme-du-teil/

Sira, C., Schlupp, A., Maufroy, E., Provost, L., Dretzen, R., Bertrand, E., ... & Schaming, M. (2020). *Rapport macrosismique n 4, Séisme du Teil (Ardèche) 11 novembre 2019 à 11 h 52 locale, Magnitude 5, 2 ML (RENASS), Intensité communale max VII-VIII (EMS98)*. BCSF-RENASS-2020-R2. https://doi. org/10.13140/RG. 2.2. 27570.84166.

Transactions, SMiRT-26
Berlin/Potsdam, Germany, July 10-15, 2022
Division V

DYNAMIC CHARACTERISTICS TESTS OF FULL-SCALE LEAD RUBBER BEARING (LRB)

Kentaro Mori[1], Gentaro Nagashima[2], Takahiro Mori[3], Akitsugu Muramatsu[4] and Takanori Ogata[5]

[1] Senior Engineer, Mitsubishi Heavy Industries, Ltd., Hyogo, Japan (kentaro.mori.ea@nu.mhi.com)
[2] Principal Engineer, Mitsubishi Heavy Industries, Ltd., Hyogo, Japan
[3] Technology Specialist, Bridgestone Corporation, Kanagawa, Japan
[4] Chief Manager, Taisei Corporation, Tokyo, Japan
[5] Senior Engineer, Obayashi Corporation, Tokyo, Japan

ABSTRACT

Several types of dynamic tests were performed using a full-scale lead rubber bearing (LRB) that has a lead plug embedded at the centre of laminated natural rubber. The horizontal and vertical characteristics of the LRB due to various shear strains, frequencies, cyclic effect and compressive stresses were obtained by the experiments. It was confirmed that the variations of the obtained horizontal and vertical characteristics satisfied allowable variations defined in European standard for Anti-seismic devices (EN15129-2009, See References 1).

INTRODUCTION

In order to improve safety of nuclear power plants (NPPs) against high seismic condition, it had been studied to apply seismic isolation devices to reactor building in NPPs in a past project. A large size of lead rubber bearing (LRB) that has a lead plug embedded at the centre of laminated natural rubber had been developed by Bridgestone Corporation (Figure 1). In addition, static and quasi-static tests using full-scale of the LRB had been conducted to confirm its failure capacity in the project (See Reference 2). Dynamic tests using small size LRBs for typical industries had been conducted to confirm dynamic characteristics, but there was no data of dynamic characteristics of the LRB. In this experiments, dynamic tests were performed to confirm dynamic characteristics of the LRB. Taking into consideration the size and weight of the LRB, dynamic tests were performed using Seismic Response Modification Device (SRMD) at University of California San Diego.

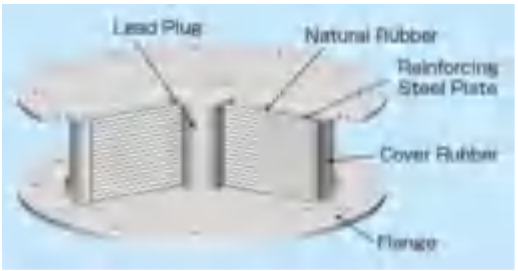

Diameter of isolator D_r	1600	mm
Total thickness of rubber h_r	260	mm
Thickness of rubber sheet t_s	10.0	mm
Number of rubber layers n_r	26	-
Thickness of inner steel plate t_p	6.8	mm
Number of steel plate layers n_s	25	-
Diameter of lead plug D_p	392	mm

Figure 1. Specifications of Full-Scale LRB

OUTLINES OF TESTS

Several types of dynamic tests are performed using full-scale LRBs in this study. Table 2 shows a test series of the dynamic tests. Dependence of horizontal and vertical characteristics due to various shear strains, frequencies, cyclic effect and compressive stresses (ID 2 through 5) were confirmed in accordance with European standard for Anti-seismic devices (EN15129-2009) followed by basic characteristics tests (ID 1). As basic characteristics of the LRB, a horizontal stiffness (post yield stiffness) K_2, a yield strength Q_d and a vertical compressive stiffness K_v are confirmed in this test series. Total three (3) specimens are used for the tests.

Table 2: A Series of Full-Scale Tests

ID	Test Objectives
1	Basic characteristics (K_2, Q_d and K_v)
2	Dependence of horizontal characteristics on rubber shear strain
3	Dependence of horizontal characteristics on frequency
4	Dependence of horizontal characteristics on repeated cycling
5	Dependence of vertical stiffness on compressive stresses

TEST RESULTS

Basic characteristics test (ID1)

The purpose of this test is to confirm the basic characteristics (K_2, Q_d and K_v) of the LRB. The test condition is as follows.

- Shear strain of LRB: ±100% (horizontal displacement is 260mm)
- Compressive stress: 5 MPa const.
- Shaking frequency: Horizontal 0.33Hz (sinusoidal wave)
- Number of test specimen: 2 specimens

Figure 2 shows horizontal load-displacement curve in 3rd cycle. Test results match well to the target of basic characteristics of the LRB. It is also confirmed that there are little differences between the specimens.

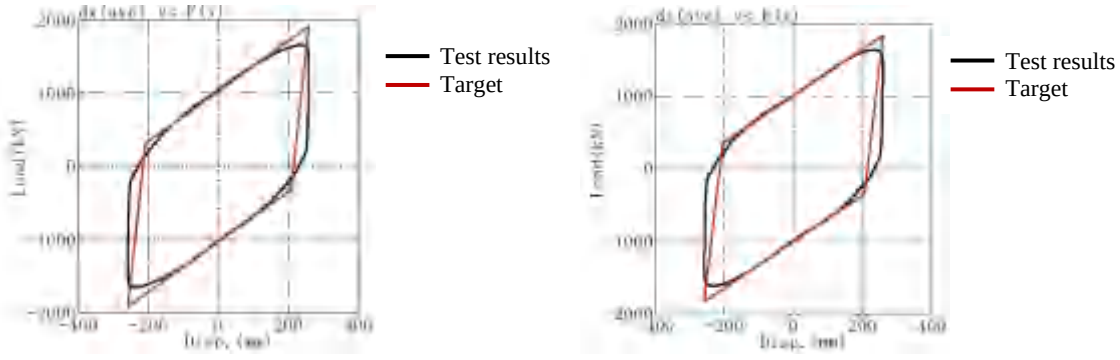

<Specimen No.2> <Specimen No.3>

Figrue 2 Horizontal Load-Displacement Curve in 3rd cycle

Table 3 shows the basic characteristics test results. The test results (K_2, Q_d and K_v) are averaged by the results of two (2) specimens. The allowable variations to the basic specifications are specifically set for NPPs considering the seismic design. It is confirmed that the basic characteristics obtained by the test satisfy the allowable variations, except yield strength Q_d. It is considered that the variation of Q_d of the

LRB is caused by an increasing of a diameter of lead plug comparing to LRBs for typical buildings. It is confirmed that a dependence of Q_d on frequency based upon the test data should be incorporated into a basic specification of the LRB which is calculated in delivery inspection (static test). In the following dynamic tests (ID 2 through 5), the basic specification of K_2 and Q_d are set based upon the test results. The basic specification of K_v is set as same as original spec., since K_v is NOT sensitive depend on frequency and it is based upon a lot of delivery inspection data in the past tests (See References 2).

Table 3 Basic Characteristics Test Results

Characteristics	Test Results (Average)	Original Spec.	Ratio	Allowable Variations
K_2 (kN/mm)	3.34	3.17	1.04	0.9~1.1 (±10%)
Q_d (kN)	1058	890	1.19	0.9~1.1 (±10%)
K_v (kN/mm)	6122	7480	0.82	0.8~1.2 (±20%)

Dependence of horizontal characteristics on rubber shear strain (ID2)

The purpose of this test is to confirm the dependence of horizontal characteristics (K_2 and Q_d) on rubber shear strain of the LRB. The test condition is as follows.

- Shear strain of LRB: ±50%, ±75%, ±100%, ±150%, ±200%, ±250%
- Compressive stress: 5 MPa const.
- Shaking frequency: Horizontal 0.33Hz (sinusoidal wave)
- Number of test specimen: 2 specimens

Table 4 shows the minimum and maximum variations of K_2 and Q_d. The variations is calculated by "Test result at 3rd cycle in ID2/basic spec. in ID1" and the allowable variations is set as ±20% in accordance with EN15129. Both K_2 and Q_d satisfy the allowable variation in case that the shear strain is greater than ±75%. It is confirmed that K_2 decreases slightly with the increasing shear strain and Q_d is constant with shear strains.

Table 4 Variations of horizontal characteristics (K_2 and Q_d)

Contents	Test results		Allowable variation
	Min.	Max.	
K_2	-20%	+17%	±20%
Q_d	-8%	+2%	±20%

Dependence of horizontal characteristics on frequency (ID3)

The purpose of this test is to confirm the dependence of horizontal characteristics (K_2 and Q_d) on frequency of shaking. The test condition is as follows.

- Shear strain of LRB: ±100%
- Compressive stress: 5 MPa const.
- Shaking frequency: Horizontal 0.05Hz, 0.25Hz, 1.0Hz (sinusoidal wave)
- Number of test specimen: 3 specimens

Table 5 shows the minimum and maximum variations of the K_2 and Q_d. Figure 3 shows the ratio of K_2 and Q_d on various shaking frequencies. Both K_2 and Q_d satisfy the allowable variation in accordance with EN 15129. According to the test results, it is confirmed that the dependence of horizontal characteristics (K_2 and Q_d) on frequency is greater than past experimental tests for LRBs for typical buildings whose size is smaller than the LRB (test specimens).

Table 5 Variations of horizontal characteristics (K_2 and Q_d)

Contents	Test results		Allowable variation
	Min.	Max.	
K_2	-7%	+15%	±20%
Q_d	-13%	+19%	±20%

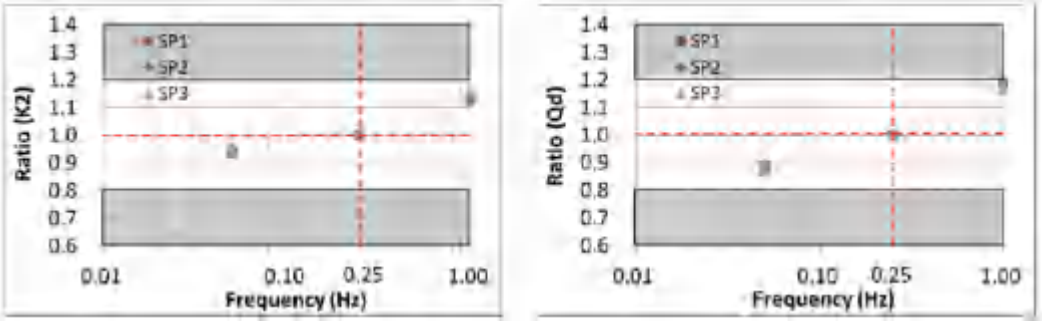

<Ratio of horizontal stiffness K_2> < Ratio of yield strength Q_d >

Figure 3 Horizontal characteristics on various shaking frequencies

Dependence of horizontal characteristics on repeated cycling (ID4)

The purpose of this test is to confirm the dependence of horizontal characteristics (K_2 and Q_d) on repeated cycling. The test condition is as follows.

- Shear strain of LRB: ±100%
- Compressive stress: 5 MPa const.
- Shaking frequency: Horizontal 0.1Hz (sinusoidal wave)
- Number of cycle: 10 cycles
- Number of test specimen: 2 specimens

Table 6 shows the variations of the horizontal characteristics (K_2 and Q_d) at 10th cycle comparing to the one at 2nd cycle and 1st cycle. Figure 4 shows the ratio of K_2 and Q_d on repeated cycling. K_2 satisfy the allowable variations in accordance with EN 15129. It is confirmed that the dependence of Q_d on repeated cycling is greater than past experiences of LRBs for typical buildings whose size is smaller than the LRB. It is necessary to conduct a confirmatory analysis to confirm the LRB's behaviour using the test results in next phase study. It would also be necessary to accumulate an additional data of the full-scale LRBs on repeated cycling.

Table 6 Variations of horizontal characteristics (K_2 and Q_d)

Contents	Test results	Allowable variation
K_2 (Ratio of 10th cycle/ 1st cycle)	-8%	±40%
K_2 (Ratio of 10th cycle/ 2nd cycle)	+2%	±30%
Q_d (Ratio of 10th cycle/ 2nd cycle)	-38%	±30%

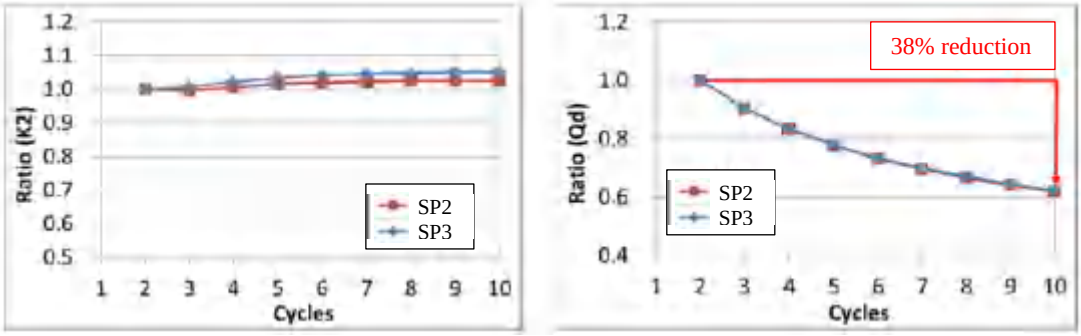

<Ratio of horizontal stiffness K_2> < Ratio of yield strength Q_d >

Figure 4 Horizontal characteristics on repeated cycling

Dependence of vertical stiffness on compressive stresses (ID5)

The purpose of this test is to confirm the dependence of vertical stiffness (K_v) on compressive stresses. The test condition is as follows.

- Shear strain of LRB:0% (const.)
- Compressive stress: 5 MPa ± 2.5MPa
- Shaking frequency: Vertical 0.0125Hz, 0.33Hz (sinusoidal wave)
- Number of test specimen: 2 specimens

Figure 5 shows the variations of the vertical stiffness (K_v) on compressive stresses. The ratio of K_v is calculated by "test results at 3rd cycle in ID 5/basic spec. in ID1". The maximum variation of K_v is -18% comparing to the basic specification of the LRB. It is confirmed that the variation obtained by the test is within the allowable variations in accordance with EN 15129 (±30%).

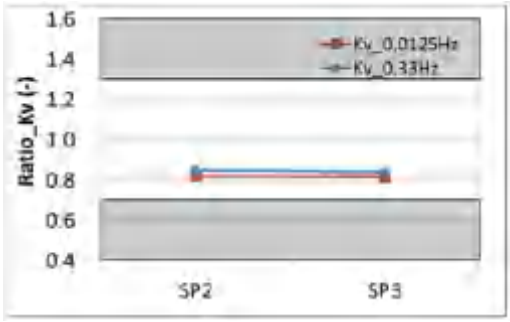

Figure 5 Vertical stiffness on compressive stresses

Summary of Test Series (ID 2 through 5)

Table 7 shows the summary of the results. The horizontal and vertical characteristics of the LRB obtained by the experiments satisfy the allowable variations in accordance with EN 15129. It is confirmed that further investigations are necessary regarding a reduction of Q_d of the LRB on repeated cycling to confirm an impact on seismic design of base isolated reactor building in an NPP.

Table 7 Summary of the Results (ID 2 through 5)

ID	Test Objectives	Allowable Variations	Test Results
2	Dependence of horizontal characteristics on rubber shear strain	K_2 : ±20% Q_d : ±20%	K_2 :-20%~+17% Q_d :-8%~+2%
3	Dependence of horizontal characteristics on frequency	K_2 : ±20% Q_d : ±20%	K_2 :-7%~+15% Q_d :-13%~+19%
4	Dependence of horizontal characteristics on repeated cycling	K_2 : ±30% ($2^{nd}/10^{th}$ cycle) ±40% ($1^{st}/10^{th}$ cycle) Q_d : ±30% ($2^{nd}/10^{th}$ cycle)	K_2 :+2%($2^{nd}/10^{th}$) -8%($1^{st}/10^{th}$) Q_d : -38% ($2^{nd}/10^{th}$)
5	Dependence of vertical stiffness on compressive stresses	K_V : ±30%	K_V : -18%

CONCLUSIONS

Several types of dynamic tests were performed using full-scale lead rubber bearings (LRBs) that have a lead plug embedded at the centre of laminated natural rubber. The horizontal and vertical characteristics of the LRB due to various shear strains, frequencies, cyclic effect and compressive stresses were obtained by the experiments. It was confirmed that the variations of the obtained horizontal and vertical characteristics satisfied allowable variations defined in European standard for Anti-seismic devices (EN15129-2009).

REFERENCES

European Committee for Standardization (CEN) (2009), Anti-seismic device, EN15129.

T. Imaoka et al (2015), *DEVELOPMENT OF EVALUATION METHOD FOR SEISMIC ISOLATION SYSTEMS OF NUCLEAR POWER FACILITIES -BREAK TEST OF FULL SCALE LEAD RUBBER BEARINGS FOR NUCLEAR FACILITIES, PART 1 OUTLINE OF BREAK TEST OF LRB OF 1.6M IN DIAMETER-*, SMiRT23, Manchester, United Kingdom

Transactions, SMiRT-26
Berlin/Potsdam, Germany, July 10-15, 2022
Division V

GENERATING MOTION FOR SEISMIC QUALIFICATION OF COMPONENTS ON SEMI-RIGID SUPPORTS. APPLICATION TO THE ITER LEAK DETECTION SYSTEM

Didier Combescure[1], Simone Kaldas[2], and Joseba Mugica[3]

[1] Dr Ing., Technical Officer, ITER Delivery, Fusion for Energy, Barcelona (didier.combescure@f4e.europa.eu)
[2] M., Trainee, ITER Delivery, Fusion for Energy, Barcelona (currently Ing., SRS, Italy)
[3] Dr Ing., IDOM, Madrid

INTRODUCTION

The determination and the control of the seismic motion transferred to the mechanical components and their supporting structures represent a major issue for the seismic design of non-structural elements, the anchoring and the seismic qualification of active components. Structures that can not be considered as completely rigid are very commonly used in the industry. This type of support may amplify the input seismic motion imposed by the building structure. It is interesting to use simplified analytical formulae to generate the FRS transferred by these support from the input FRS provided in the building structure.

This paper presents an adaptation of the approach promoted in several (French) working groups within the Association Française du génie Parasismique (AFPS) in charge of drafting guideline for critical industrial facilities and for critical facilities (hospital, school, emergency facilities). The methodology has been applied to a component of the ITER Fusion facility under construction in Cadarache (France).

SIMPLIFIED METHOD TO GENERATE SEISMIC SPECTRA

The approach promoted in several (French) working groups within the Association Française du génie Parasismique (AFPS) in charge of drafting guidelines for critical industrial facilities and for critical facilities (hospital, school, emergency facilities) has been applied and improved. The AFPS guidelines for the supporting structures of critical industrial facilities propose a simplified formula based on the work developed inside the French Association for Earthquake Engineering (AFPS, 2011 and 2013) and the German standard for nuclear facilities (KTA, 2012).
The seismic floor response spectrum is given by the following formula:

$$a_H = S_a\left(T_i, q_p, D_1\right) \times K_T(T_E, D_1, D_2) \quad (1)$$

where:

- $S_a\left(T_i, q_p, D_1\right)$: absolute acceleration at period T_i of the building, for the reduction factor q_p and damping factor D_1 of the building structure;
- q_p: reduction factor taking into account the nonlinear behaviour of the building structure, the support of the equipment and the equipment itself;
- D_1: damping factor for the building structure;
- $K_T(T_E, D_1, D_2)$: amplification factor taking into account the interaction between the building structure and the equipment;
- T_E: period of the equipment;
- D_2: damping factor for the equipment.

The zero period acceleration (ZPA) of the floor response spectrum, with a reduction factor $q_p = 1$, is given by:

$$S_a = \sqrt{\bar{\gamma}^2\left(1 - \sum_{i=1,N} \Gamma_i \varphi_i\right)^2 + \sum_{i=1,N} (\Gamma_i \varphi_i S_a(T_i))^2} \quad (2)$$

- $\bar{\gamma}$: ground acceleration for T = 0;
- S_a : spectral acceleration of the design spectrum at period T_i. If S_a is known for 5% damping (for EC8) and the modal damping is different from 5%, a correction factor (n_1) has to be applied to S_a;
- φ_i: i^{th} mode shape value;
- Γ_i : modal participation factor for mode i;
- N: number of dynamic modes considered;
- The amplification function for a damping value of 5% for the building structure and 5% for the equipment is given by the formulas:

$$K_T = 1 \quad \text{if: } f_{limit} < f_E \quad (3a)$$

$$K_T = 5n - \left[(5n-1)(log(1.2\frac{f_n}{f_E})/log\frac{1.2f_n}{f_{limit}}\right] \quad \text{if: } 1.2f_n \le f_E \le f_{limit} \quad (3b)$$

$$K_T = 5n \quad \text{if: } 0.8f_1 \le f_E \le 1.2f_n \quad (3c)$$

$$K_T = 5n/\left(0.8\frac{f_1}{f_E}\right)^2 \quad \text{if: } f_E \le f_1 \quad (3d)$$

- f_1 to f_n – main eigenmodes of the building in the considered direction ;
- f_{limit} – limit frequency equal to 16.7 Hz [7] ;

For different values of damping for the building structure and for the equipment:

$$n = n_1 \times n_2 \text{ with } n_1 = \sqrt{\frac{10}{5+D_1}}, \quad n_2 = \sqrt{\frac{5}{D_2}} \quad (4)$$

For 5% damping in the system, in case of resonance between the building structure and the equipment, the amplification factor is equal to $K_T = 5$.
Details of these formula and example of applications are given in Combescure *et al*. (2021).

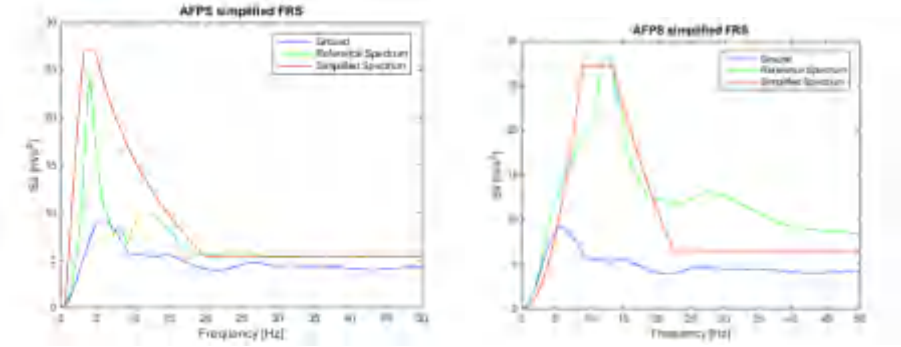

a: Flexible structure (f_1=4.0Hz, f_2= 10.5Hz) b: Stiff structure (f_1=11.2Hz, f_2=29.4Hz)

Figure 1. Comparison between time-history (green) and the original AFPS simplified method (red) with different input motion (blue)

The approach has been adapted to the case of semi-rigid supports with input FRSs with potential complex shape. The results obtained from the original simplified method have been compared to results of time-history analysis on two simplified models of structure/support with 2 dofs (Figure 1). In the case of a flexible structure (Figure 1a), we can observe that the original formula is envelop of the FRS determined with a time-history analysis. In the case of a stiff structure (Figure 1b), we can observe that the original simplified formula is not enveloping the FRS and the ground response spectrum at low frequency.

The original simplified formula has been modified by taking a weighted average between the ground spectrum and the peak value predicted by the standard simplified formulas.

$$S_a(f, D_1) = \alpha \cdot S_{a,\ ground} + (1-\alpha) \cdot S_a(f_{peak}) \qquad 0 \le f \le f_{peak} \tag{5}$$

The weight α is defined:

$$\alpha = \begin{cases} 1 & for\ 0 \le f \le k \cdot f_{peak,ground} \\ 1 - \frac{f - k \cdot f_{peak,ground}}{f_{peak} - k \cdot f_{peak,ground}} & for\ f_{peak,ground} \le f \le k \cdot f_{peak} \end{cases} \tag{6}$$

- $S_{a,\ ground}$: elastic response spectrum at the ground level;
- $f_{peak,\ ground}$: frequency at which the ground spectrum assumes its maximum values;
- f_{peak} : frequency at which the maximum value of the structure is predicted by the three previous formulas e.g. $0.8f_1$;
- k: is a factor that represents the fraction of $f_{peak,ground}$ from which the weighted average starts. It depends on the rigidity of the system.

A second modification has been made to better reproduce the response of stiff system. Rigid systems with The amplification factor K_T has been modified to get K_T=1 for extremely rigid systems and intermediate values for not highly rigid ones:

$$\begin{cases} 5 & if\ f_1 < 1.5\boldsymbol{f_c} \\ 1 & if\ f_1 > 3\boldsymbol{f_c} \\ 5 + \frac{1-5}{3\boldsymbol{f_c} - 1.5\boldsymbol{f_c}}(f_1 - 1.5\boldsymbol{f_c}) & if\ 1.5\boldsymbol{f_c} \le f_1 \le 3\boldsymbol{f_c} \end{cases} \tag{7}$$

The modified simplified formula has been applied to the 2 dofs stiff structure submitted to a large band motion representative of a ground motion (Figure 2a) and to a narrow band motion representative of a transferred seismic input (Figure 2b). The results of the simplified formula has been compared with the results of time history analysis (green curves).

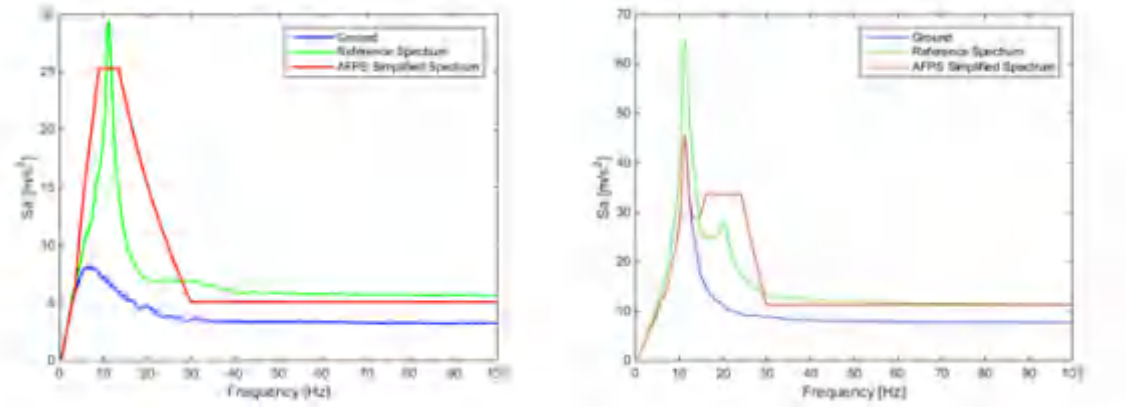

a: 2 dofs model excited by a large band motion b: 2 dofs system excited by a narrow band motion

Figure 2. Comparison between time-history (green) and the improved simplified method (red) with different input motion (blue)

APPLICATION TO THE ITER LEAK DETECTION SYSTEM (LDS)

The methodology has been applied to the ITER Leak Detection System (LDS) that aims to provide the leak detection capabilities for the primary vacuum systems comprising Torus vacuum vessel, Neutral Beam vacuum systems and the Cryostat vacuum system of the ITER machine (Figure 3). The structures, systems and components (SSC) used on the design of the Leak Detection Systems shall meet the requirements under the specified load cases including the seismic action. A part of the systems will be qualified by test or using existing tests. An independent FEA model has been developed with ANSYS using pipe and beam elements with lumped masses for the main components that should be qualified on shaking table (Figure 4). This model has been developed in order to control the work performed by the consortium in charge of the design and the qualification of the system.
The system has been studied performing static analysis, response spectrum analysis and applying the simplified formulae above-mentioned to transfer the seismic FRSs (Kaldas, 2021). The FRS available at the location of the components inside the ITER Tokamak complex has been used as input response spectrum. The FEA model shows 12 natural frequencies below 35 Hz starting from 11.25Hz. They are mainly local eigenmodes. The results of the application of the simplified formulae to generate the FRS together with the values of the main eigenfrequencies (vertical green lines) are given in Figure 5. From these results, we can conclude that the supports are not fully rigid but are amplifying the seismic motion only at high frequencies.

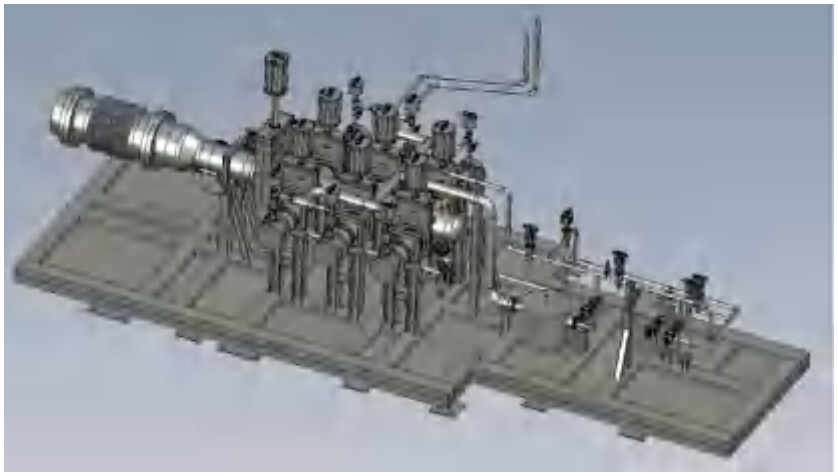

Figure 3. View of one of the system of the ITER Leak Detection System (LDS)

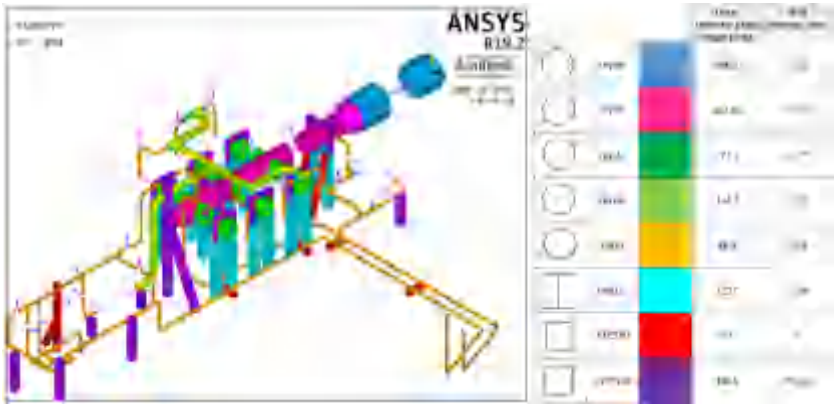

Figure 4: View of the ANSYS model including supports, pipes and components.

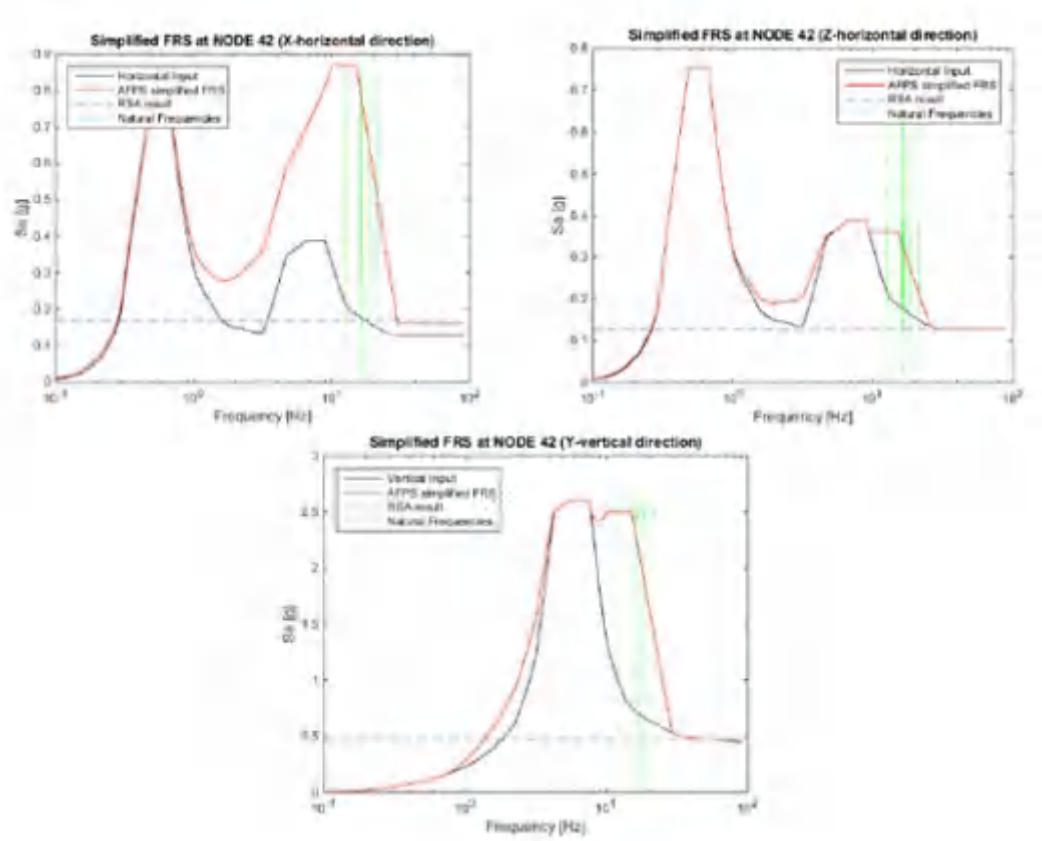

Figure 5. Example of transferred FRS using the simplified method (in red) compared to the input FRS (in black).

DEVELOPMENT OF RRS FOR THE SEISMIC QUALIFICATION OF ACTIVE COMPONENTS

The experimental seismic qualification of Safety Important active Components requires the determination of the RRS (Required Response Spectrum). The propagation of this input data for the qualification should be properly controlled and the information well stored in the qualification database. The seismic FRSs determined with transient calculations, frequency-based direct calculations or simplified method are curves. It is important to characterize the seismic input for the seismic qualification through, if possible, few physical parameters. The idea is to simplify the RRS curves into a set of parameters in order to ease their propagation to the experimental facilities in charge of the seismic qualification. For example, in standards such as RCC-E, the RRS is defined by a limited number of parameters (Figure 6). At low frequency, the RRS is defined by a value of spectral displacement compatible with the limitation of the shaking tables used for the qualification. It is completed by the values of ZPA and the spectral acceleration on the RRS plateau with lower and upper corners frequencies.

In the Tokamak building of ITER facility, the seismic FRSs are given at more than 1000 locations. The potential amplification through the local support should also be considered for the definition of the RRSs. A method has been proposed to identify the main physical parameters of the FRSs and calculate easily envelops (Mugica, 2021). Because of the seismic isolation, the horizontal FRSs have a specific shapes with two peaks and low values of ZPA but high values of spectral displacement. The automatic generation of the simplified RRS is based on the determination of local maximum values of spectral quantities. In addition to the spectral acceleration S_a, spectral velocity S_v and spectral displacement S_d, we have introduced the derivative of the acceleration named as S_c and the integral of the displacement named S_f:

$$Sc = \omega Sa \quad (8a)$$

$$Sf = \omega^{-1} Sd \quad (8b)$$

The local maximum values are determined in two intervals:

- From 0 to 2 Hz: it corresponds to the first peak for the horizontal FRSs and to the non-amplified part of the vertical FRSs;
- From 2Hz to 35 Hz: it corresponds to the second peak for the horizontal FRSs and to the part of the vertical motion amplified by the vertical eigenmodes of the building.

Once the local maximum known, the values of frequency determining the transition between two constant spectral quantities (constant Sa, constant Sv, constant Sd, etc…) can be defined with the following formulae:

$$f_{Sa-Sv} = \frac{S_a}{2\pi S_v} \tag{9a}$$

$$f_{Sv-Sd} = \frac{S_v}{2\pi S_d} \tag{9b}$$

$$f_{Sd-Sf} = \frac{S_d}{2\pi S_f} \tag{9c}$$

$$f_{Sc-Sa} = \frac{S_c}{2\pi S_a} \tag{9d}$$

The RRS plateau (constant spectral acceleration) is defined by the 2 frequencies $f_{Sa\text{-}Sv}$ (lower corner) and $f_{Sc\text{-}Sa}$ (upper corner). In addition, the zero-period-acceleration is the magnitude of the spectral acceleration at which all curves converge regardless of damping. ZPA starts at the so-called cut-off frequency.

For the horizontal RRSs, the valley between the two peaks deserves a special treatment for the determination of the constant acceleration segment that is independent of the damping values similarly to the ZPA.

Once all points defined, the RRS is defined piecewise linear (Figure 7).

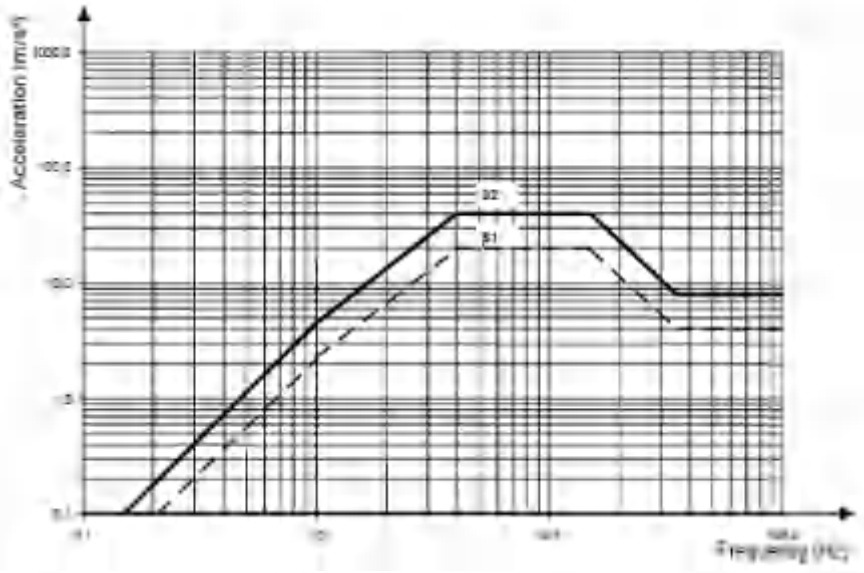

Singular point/ Seismic level	Below 1 Hz (constant movement)	1 Hz (movement)	4 Hz	15 Hz	35 Hz	Above 35 Hz
S2	0.114 m	0.114 m	40 m/s²	40 m/s²	8 m/s²	8 m/s²
S1	0.057 m	0.057 m	20 m/s²	20 m/s²	4 m/s²	4 m/s²

Figure 6. Example of RRS from RCC-E (RCC-E 2019)

Additional margins may be added only on a part of the RRS through an increase of the spectral acceleration or a broadening of the RRS (Figure 8). It is also common that the initial RRS cannot be used due to the capacity of the testing tables. The capacity of the shaking table is given by its maximum values of displacement, velocity and acceleration. When the values of spectral displacement and spectral velocities exceed the maximum permissible for the shaking table in question, the need arises to filter the RRS. Because of the seismic isolation, it is the case of the horizontal RRS in ITER. Table 2 shows an example of such a filtering for a shaking table with maximum values of spectral displacement and pseudo velocity of 0.25 m and 2.5 m/s respectively (shaking table with maximum displacement of 0.10 m and maximum velocity of 1m/s).
Statistics can also be elaborated in order to define a limited number of RRS for qualification.

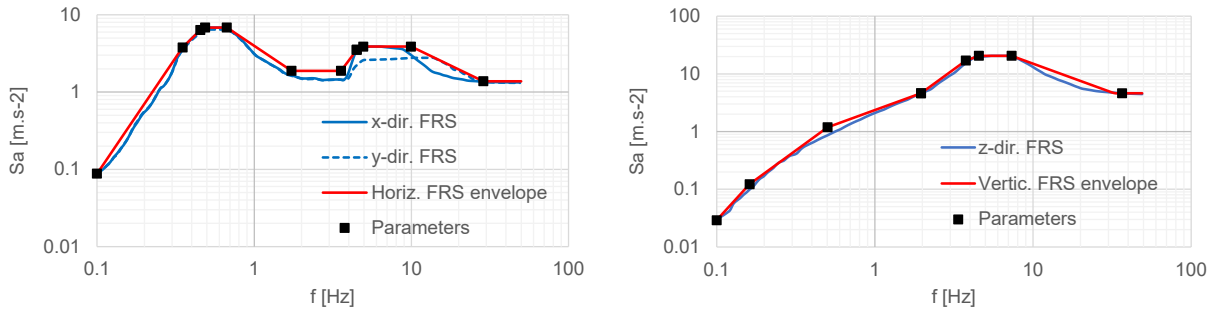

a: Horizontal RRS b: Vertical RRS

Figure 7. Example of RRSs

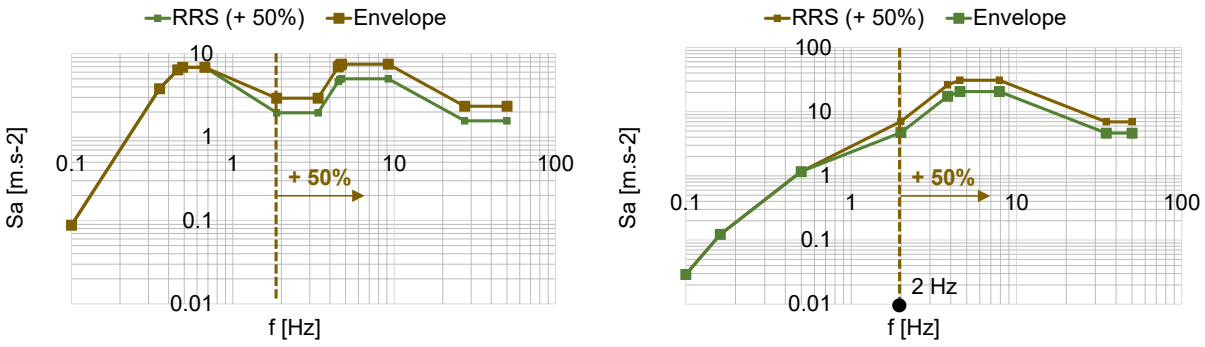

a: Horizontal RRS b: Vertical RRS

Figure 8. Example of margin application

CONCLUSION

This paper has presented an adaptation of the AFPS simplified formula to transfer the seismic floor response spectrum. The basis of this formula and the main assumptions have been summarized. An application to several 2 dofs stiff and flexible structures and to a real system have been presented. The approach has been adapted to the case of semi-rigid supports with input FRSs with potential complex shape (with two peaks). The results obtained from the simplified method have been compared to results of time-history analysis on simplified model of structure/support. In the last part, an automatic procedure is proposed to simplify the FRS and obtain the Required Response Spectrum (RRS) for the experimental qualification of components. With the proposed format, the propagation and the storage of the seismic input used for the qualification are easier.

Table 1: Example of horizontal RRS (see Figure 8a).

Id.	f [Hz]	S_c [m.s^{-3}]	S_a [m.s^{-2}]	S_v [m.s^{-1}]	S_d [m]	S_f [m.s]
#1	0.10	5.54E-2	8.82E-2	1.40E-1	2.23E-1	3.55E-1
#2	0.351	8.38	3.80	1.73	7.83E-1	3.55E-1
#3	0.455	1.83E+1	6.41	2.24	7.83E-1	2.74E-1
#4	0.488	2.11E+1	6.87	2.24	7.31E-1	2.38E-1
#5	0.671	2.90E+1	6.87	1.63	3.87E-1	9.19E-2
#6	1.87	3.44E+1	2.93	2.50E-1	2.13E-2	1.81E-3
#7	3.37	6.21E+1	2.93	1.39E-1	6.55E-3	3.09E-4
#8	4.49	1.97E+2	6.97	2.47E-1	8.73E-3	3.09E-4
#9	4.61	2.13E+2	7.33	2.53E-1	8.73E-3	3.01E-4
#10	4.72	2.23E+2	7.50	2.53E-1	8.53E-3	2.88E-4
#11	9.19	4.33E+2	7.50	1.30E-1	2.25E-3	3.90E-5
#12	27.3	4.04E+2	2.35	1.37E-2	7.97E-5	4.64E-7
#13	50.0	7.38E+2	2.35	7.48E-3	2.38E-5	7.58E-8

Table 2: Example of filtered RRS.

Filtered RRS				
Id.	f [Hz]	S_a [m.s^{-2}]	S_v [m.s^{-1}]	S_d [m]
#1	0.100	9.87E-2	1.57E-1	2.50E-1
#2	0.796	6.25	1.25	2.50E-1
#3	4.72	7.50	2.53E-1	8.53E-3
#4	9.19	7.50	1.30E-1	2.25E-3
#5	27.3	2.35	1.37E-2	7.97E-5
#6	50.0	2.35	7.48E-3	2.38E-5

REFERENCES

AFPS (2011). Cahier technique CT 30: Guide méthodologique pour la conception, l'installation et le diagnostic des équipements en zone sismique , French Association for Earthquake Engineering (in French).

AFPS (2013). Guide AFPS, Guidelines for the seismic design of the supporting structure, ICPE-AFPS/UIC Working Group, French Association for Earthquake Engineering (in French).

Combescure D., Naze P-A, Dujarric C., Potin G. (2021), Transfer of the seismic motion for the design and assessment of components. A simplified approach. 2nd International Conference on Seismic Design of Industrial Facilities, Aachen.

Kaldas (2021). Generation of simplified Floor Response Spectra and application to simple models of buildings, F4E_D_2RQ7VD, F4E Report.

KTA (2012). KTA 2201.4 Design of Nuclear Power Plants against Seismic Events; Part 4: Components, KTA, Germany.

Mugica (2021). User's guide to FRS processing using in-house Python code, F4E_D_2VN3F7, IDOM Report.

RCC-E (2019). Règles de Conception et de Construction des Systèmes et Matériels Electriques et de Contrôle Commande.

DISCLAIMER

The work leading to this publication has been partially funded by Fusion for Energy under the contract OMF-0825-02-01. This publication reflects the views only of the author. Fusion for Energy and IO-CT cannot be held responsible for any use which may be made of the information contained therein.

Transactions, **SMiRT-26**
Berlin/Potsdam, Germany, July 10-15, 2022
Division VIII

Radiation resistance of 3D viscoelastic fluid dampers applied for the reduction of operational vibrations and seismic upgrading of piping systems in NPPs

Frank Barutzki[1], Victor Kostarev[2], Vladimir Lomasov[3], Dmitry Pavlov[2]

[1] GERB Schwingungsisolierungen GmbH & Co. KG, Berlin, Germany
[2] CKTI-Vibroseism, Saint Petersburg, Russia,
[3] Polytechnic University, Saint Petersburg, Russia

ABSTRACT

This paper describes the effects of ionizing radiation on the dynamic behavior of viscous fluid dampers by comparing stiffness and damping values before and after irradiation. Three different types damping fluids have been investigated.

INTRODUCTION

GERB Vibration Control Systems in Berlin and CKTI-Vibroseism in St. Petersburg have long lasting experience with viscoelastic fluid dampers in the fields of vibration control of heavy industrial machinery and seismic protection of equipment and large structures. Dampers for the protection of piping systems in conventional and nuclear power plants have been developed and are used worldwide. These dampers act as dynamic restraints and reduce the effects of operational vibrations as well as vibrations due to disturbances or seismic excitations.

These dampers work with different highly viscous fluids depending on the specific requirements of each application. In case of nuclear applications, the question of irradiation resistance is very important. GERB and CKTI have agreed on the testing of viscoelastic dampers by exposing them to different irradiation levels (γ-ray, Co-60) and measuring the impact on stiffness and damping characteristics. These tests have been performed with a standard damper design for piping applications.

VISCODAMPER - GENERAL DESIGN AND APPLICATIONS

Viscodampers are viscoelastic fluid dampers used to limit the motions of elastically supported systems in case of resonances or when subjected to shock-type, transient or random excitation. They add damping to a dynamic system and reduce occurring vibrations by dissipating mechanical energy.

In principle a viscoelastic fluid damper consists of three main components: damper housing, damper piston and damping fluid, see figure 1. The damper housing is filled with a highly viscous fluid and the damper piston is immersed in the damping fluid and can move in all directions, its motion only limited by the damper housing. Therefore, these dampers react and dampen motions in all directions. The damping force results from shearing and displacing the damping fluid. The force is approximately proportional to

the relative velocity between damper piston and damper housing. Thus, viscoelastic fluid dampers do not support any static loads.

The actual damper response to dynamic loads consists of elastic and viscous components due to the viscoelastic behavior of the fluid and the elasticity of the steel parts. Thus, a damper is not only adding damping to a structure but also additional dynamic stiffness.

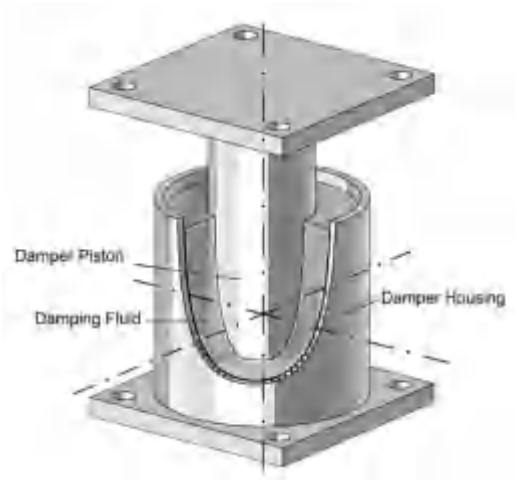

Figure 1: Principle Design of Viscodamper®

Viscodampers are used for:

- Vibration isolation of machinery and equipment
- Seismic protection of machinery and structures
- Damping and seismic protection of piping systems
- Damping of TMDs

VISCOELASTIC BEHAVIOR

Viscoelastic fluid dampers show distinct frequency dependent viscoelastic behaviour that can be described by means of the complex stiffness that combines elastic and viscous components in one quantity. The complex stiffness $\underline{K}$ is the quotient of the force and displacement amplitudes, see Equation 1 below:

$$\underline{K} = \frac{\hat{F}}{\hat{\underline{s}}} = K_{el} + j \cdot K_{vis} = K \cdot (\cos\delta + j \sin\delta) \qquad (1)$$

The real part K_{el} is the elastic stiffness and is a measure for the elastic deformation resistant. The imaginary part K_{vis} is the damping stiffness and is a measure for the damping ability of the viscous elastic element, as shown in Equation 2:

$$K_{el} = K \cdot \cos\delta \quad and \quad K_{vis} = K \cdot \sin\delta \qquad (2)$$

The absolute amount K of the complex stiffness is also called equivalent stiffness K_{eq}. The damping resistance d can be derived from the damping stiffness K_{vis} as shown in Equation 3

$$d = \frac{K_{vis}}{\omega} = \frac{\hat{F}}{\hat{s} \cdot 2\pi \cdot f} \cdot sin\,\delta = \frac{\hat{F}}{\hat{v}} \cdot sin\,\delta \qquad (3)$$

The dynamic characteristics are determined by force-displacement tests. These can be harmonic or random type motion tests. To describe the viscoelastic behaviour over a larger frequency range, measurements at several frequencies are taken by random noise excitation.

VISCOUS DAMPING FLUIDS

Today several different highly viscous fluids are used in dampers to provide specific damper characteristics and to meet application requirements. In this study the following damping fluids have been investigated:

- Bituminous damping fluids with high temperature dependency (VM20/0.6)
- Polybutene based damping fluids with medium temperature dependency (VM20-MTA/5)
- Silicone oil-based damping fluids with low temperature dependency (VM20/114)

These fluids have different base viscosities and temperature dependencies.

TEST PROGRAMS

Prior to the actual radiation exposure, the stiffness and damping behavior of all test dampers were determined in vertical and horizontal directions. All dampers are identical in design and dimensions, only dampers type VRD-10-40.x had 50% thicker walls.

During the irradiation test program, the dampers were exposed to 4 irradiation levels. Table 1 shows the scheduled and achieved levels. The relative error of the radiation exposure measurement of the test facility is +/- 12% with a confidence of 95%.

Table 1: Irradiation dosage

Damper Designation	Damping Fluid	Irradiation Power [kGy/h]	Duration [h]	Radiation Dosage [kGy]	
				scheduled	final
VRD-10-10.3	VM20/114 (silicone)	0,79	63	50	49,8
VRD-10-10.1	VM20/114 (silicone)	0,8	125	100	100
VRD-10-10.4	VM20/114 (silicone)	0,8	188	150	150,4
VRD-10-10.2	VM20/114 (silicone)	0,8	250	200	200
VRD-10-20.2	VM20-MTA/5 (polybutene)	0,79	63	50	49,8
VRD-10-20.1	VM20-MTA/5 (polybutene)	0,8	125	100	100
VRD-10-20.4	VM20-MTA/5 (polybutene)	0,8	188	150	150,4
VRD-10-20.3	VM20-MTA/5 (polybutene)	0,8	250	200	200
VRD-10-30.3	VM20/0.6 (bitumen)	0,79	63	50	49,8
VRD-10-30.4	VM20/0.6 (bitumen)	0,8	125	100	100
VRD-10-30.2	VM20/0.6 (bitumen)	0,8	188	150	150,4
VRD-10-30.1	VM20/0.6 (bitumen)	0,8	250	200	200
VRD-10-40.3	VM20/114 (silicone)	0,79	63	50	49,8
VRD-10-40.1	VM20/114 (silicone)	0,8	125	100	100
VRD-10-40.4	VM20/114 (silicone)	0,8	188	150	150,4
VRD-10-40.2	VM20/114 (silicone)	0,8	250	200	200

The properties of the fluids were checked visually and by tactile comparison (“screwdriver pinch test”). The color of the fluids had not changed, however with increasing irradiation level the silicone oil-based fluid got jelly-like as shown in table 2.

Table 2 Status of damping fluid

Damper Designation	Radiation dose [kGy]	Status of viscous fluid
VRD-10-10.3	50,0	Viscosity increased
VRD-10-10.1	100,0	Viscosity significantly increased
VRD-10-10.4	150,0	Gel
VRD-10-10.2	200,0	Gel
VRD-10-20.2	50,0	Viscosity unchanged
VRD-10-20.1	100,0	Viscosity unchanged
VRD-10-20.4	150,0	Viscosity decreased slightly
VRD-10-20.3	200,0	Viscosity decreased slightly
VRD-10-30.3	50,0	Viscosity unchanged
VRD-10-30.4	100,0	Viscosity unchanged
VRD-10-30.2	150,0	Viscosity unchanged
VRD-10-30.1	200,0	Viscosity unchanged
VRD-10-40.3	50,0	Viscosity increased
VRD-10-40.1	100,0	Viscosity significantly increased
VRD-10-40.4	150,0	Gel
VRD-10-40.2	200,0	Gel

DYNAMIC TEST RESULTS

Dynamic Tests before Irradiation

For comparison the following diagrams show the equivalent stiffness and the damping resistance of all dampers in vertical directions. The tests were performed at 20°C. The shown curves are averaged for each damper-damping fluid combination.

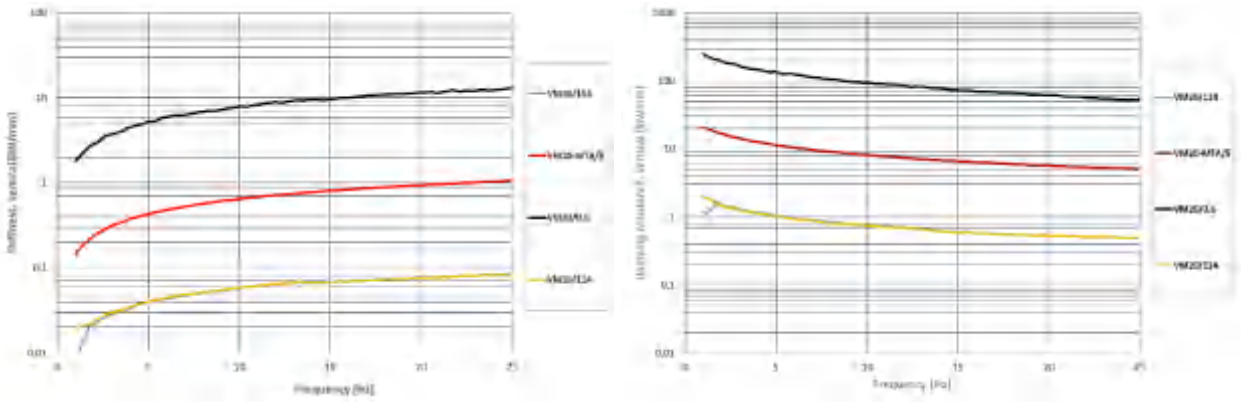

Figure 2: Equivalent stiffness and damping resistance before irradiation, vertical

Both curves show the impact of the different base viscosities of the fluids. In this test series the bituminous fluid has the highest viscosity followed by polybutene and silicone oil.

Dynamic Tests after Irradiation

The following diagrams show the measured vertical stiffness and damping curves of the different damper-fluid combinations for 50, 100, 150, and 200 kGy. For comparison the curves of a corresponding unirradiated damper is also shown.

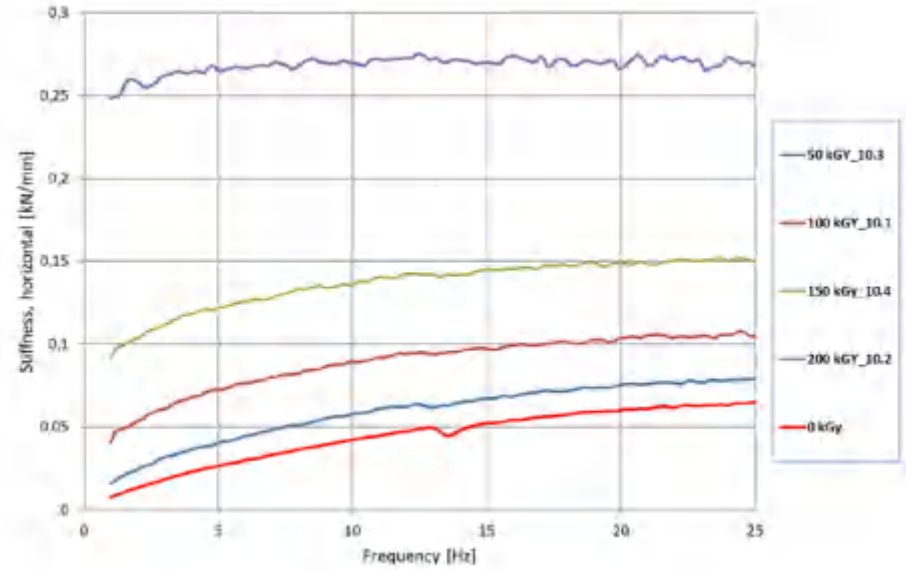

Figure 3: Comparison of horizontal stiffness VRD-10.10.1-4 (silicone)

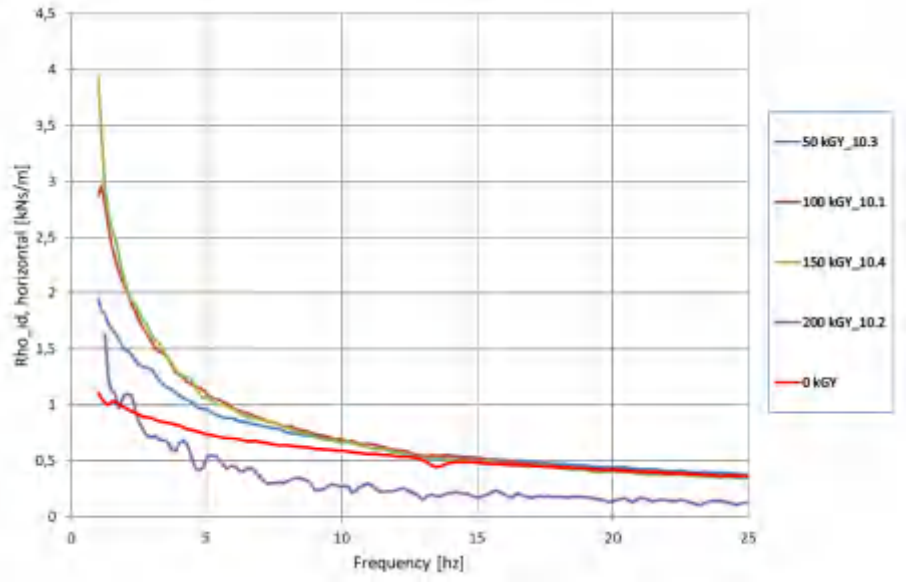

Figure 4: Comparison of horizontal damping resistance VRD-10.10.1-4 (silicone)

With increasing irradiation dosage, the reaction force and the equivalent stiffness of the dampers with silicone oil went up significantly. However, the damping resistance changes to a much smaller extend as the phase angle between force and displacement also gets smaller with increasing elasticity.

The silicone oil filled dampers type VRD-10-40.1-4 with 50% thicker walls show very similar results. With these high levels of irradiation, the increase of the wall thickness has no apparent effect on the radiation resistance.

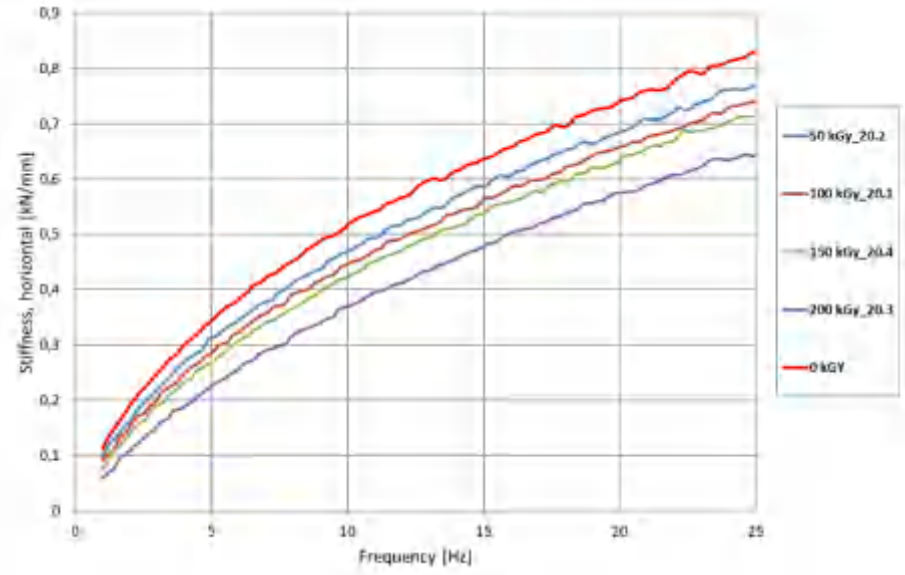

Figure 5: Comparison of horizontal stiffness VRD-10.20.1-4 (polybutene)

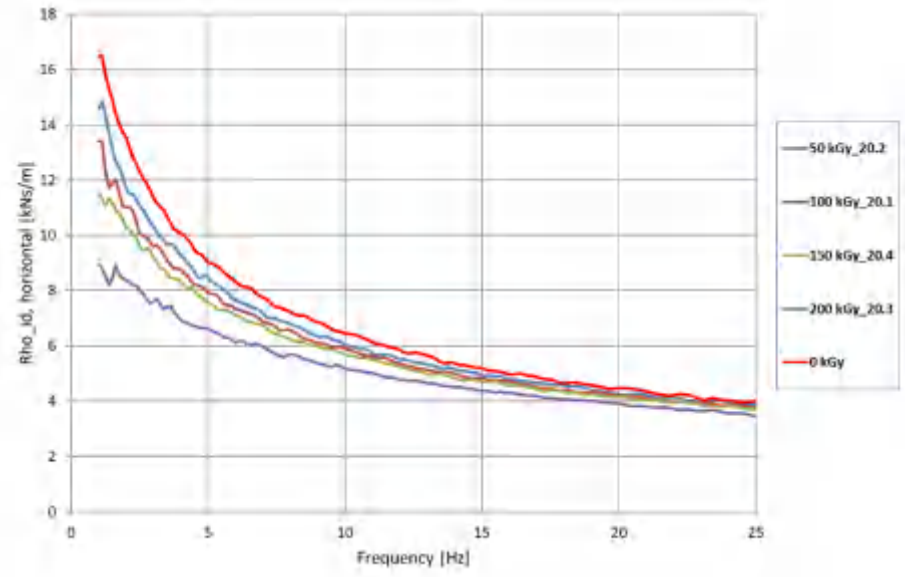

Figure 6: Comparison of horizontal damping resistance VRD-10.20.1-4 (polybutene)

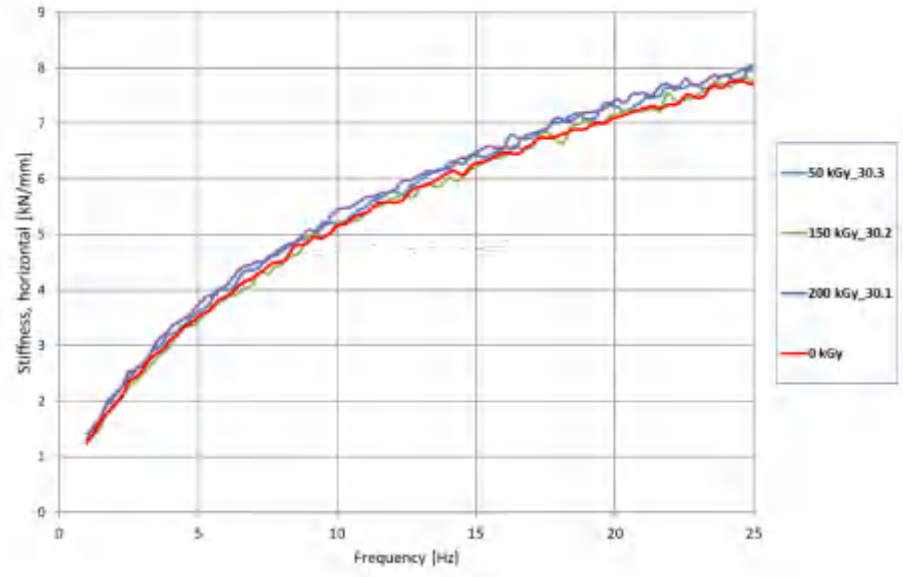

Figure 7: Comparison of horizontal stiffness VRD-10.30.1-3 (bitumen)

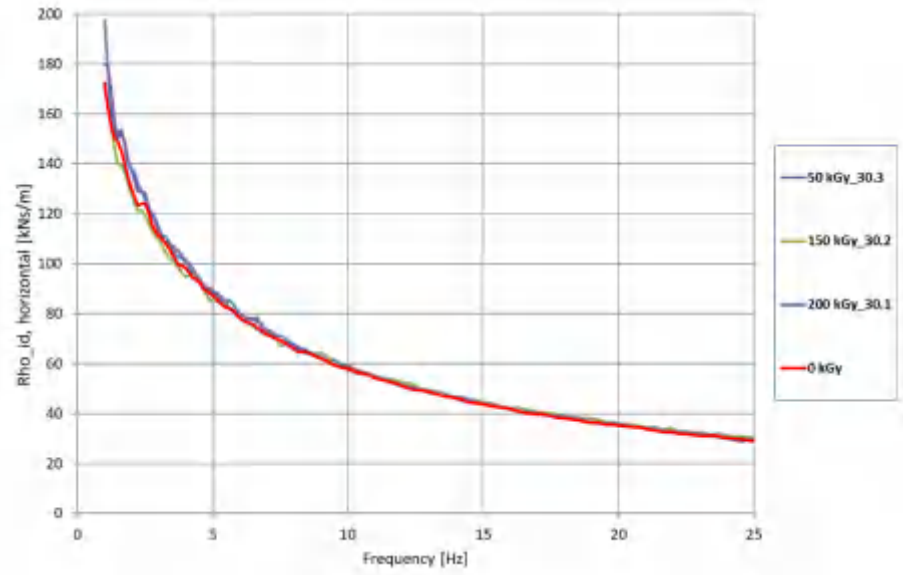

Figure 8: Comparison of horizontal damping resistance VRD-10.30.1-3 (bitumen)

The stiffness and damping curves show comparatively the resistance of the different damping fluid against ionizing radiation. Bitumen shows the highest resistance followed by polybutene and silicone oil. However, the small changes at lower irradiation levels allow for the use of silicone oils in radioactive environments for longer periods of time. Depending on the acceptable change of dynamic properties and the occurring irradiation a service life can be predicted and maintenance measures defined.

The following diagrams show resulting hysteresis loops of harmonic tests in vertical direction. The area is measure of the dissipated energy and damping. The inclination of the loop shows the elastic stiffness of the damper for the given frequency and amplitude. The viscosity of silicone oil increases with the absorbed radiation dosage. At some point the silicone fluid changes to gel and becomes more and more elastic losing its damping capabilities.

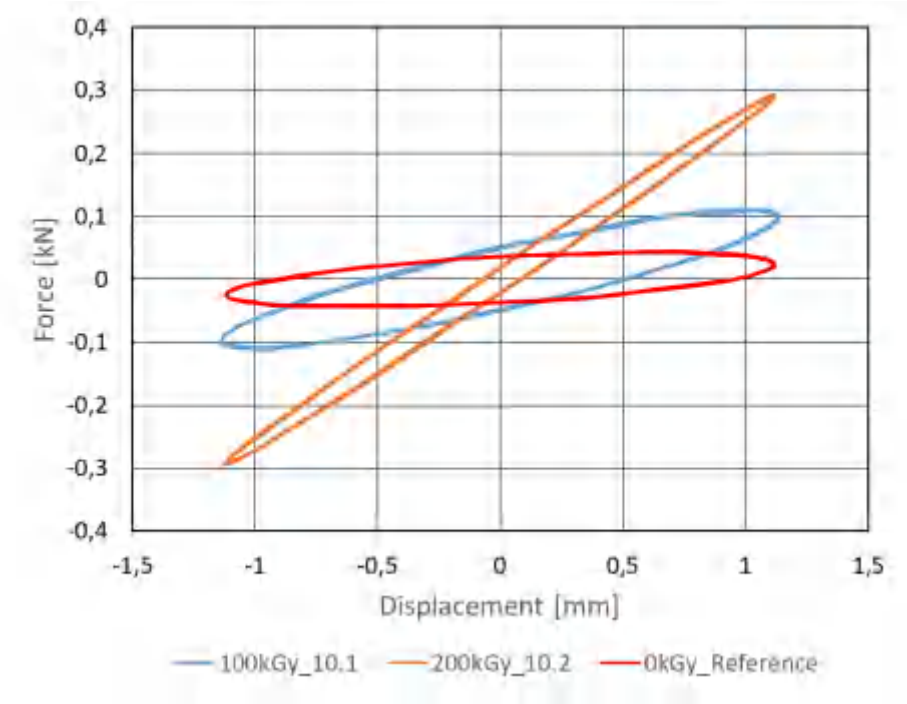

Figure 9: Vertical hysteresis loops, VRD-10.10 (silicone) (5 Hz, +/-1 mm)

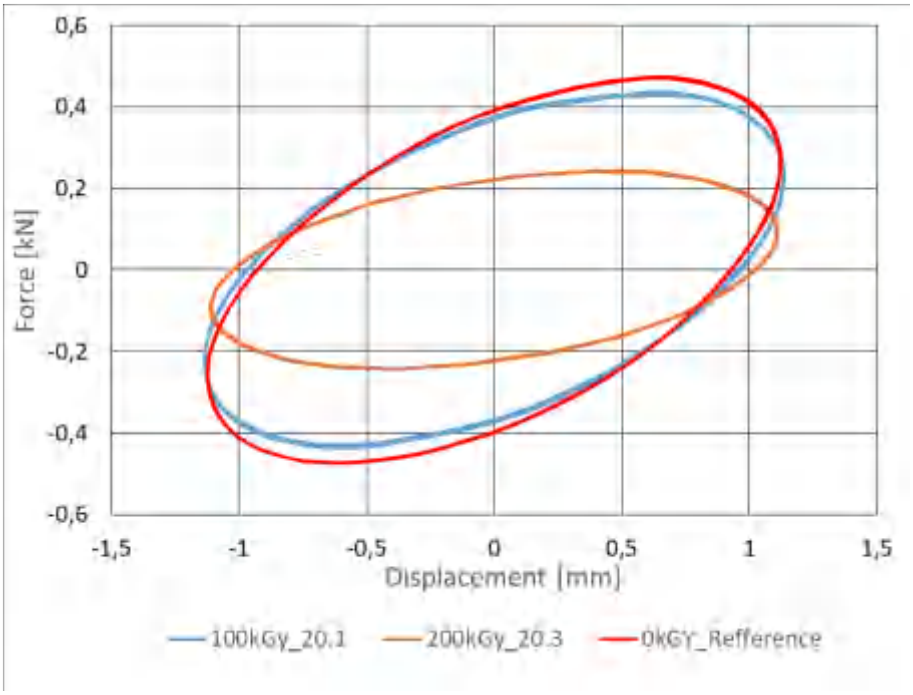

Figure 10: Vertical hysteresis loops, VRD-10.20 (polybutene) (5 Hz, +/-1 mm)

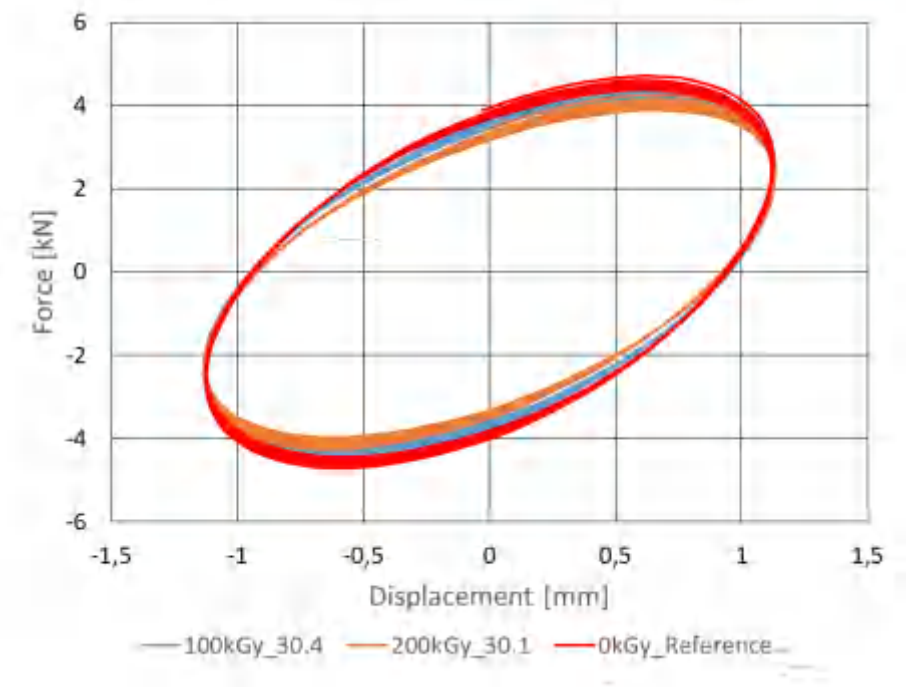

Figure 11: Vertical hysteresis loops, VRD-10.30 (bitumen) (5 Hz, +/-1 mm)

Bitumen didn't alter its viscosity despite the absorbed radiation dosage. Its molecule structure is very stable and radiation resistant. Stiffness and damping capabilities are not affected. This is one reason why bituminous dampers are often used in nuclear facilities with high radiation levels despite their high temperature dependent characteristics.

SLOW MOTION BEHAVIOR

In case viscoelastic fluid dampers are used for the protection of hot piping systems they might see slow thermal movement of the pipe when heating up and cooling down. In general, the resistance to these slow motions is very small due to the approximately velocity proportional behavior. Bitumen and polybutene don't change their resistance against thermal movement even after high irradiation dosage, whereas silicone oil shows an increasing resistance with higher irradiation levels. Table 3 shows force measurements of the different damping fluids for two velocities in vertical and horizontal direction. The resistances against slow motions of bitumen and polybutene is not affected by radiation whereas silicone oil shows an increasing resistance with higher irradiation levels especially when the fluid gels.

Table 3 Status of damping fluid

Damper	Irradiation level [kGy]	Fluid	Vertical Velocity		Horizontal Velocity	
			0.3 mm/s	0.033 mm/s	0.3 mm/s	0.033 mm/s
			max force [kN]		max force [kN]	
10.3	50	silicone	0,05	0,06	0,02	0,01
10.1	100	silicone	0,22	0,21	0,19	0,13
10.2	200	silicone	3,9	2,9	2,6	2,6
10.3	50	polybutene	0,04	0,04	0,02	0,01
20.1	100	polybutene	0,04	0,05	0,02	0,02
20.3	200	polybutene	0,05	0,05	0,04	0,04
30.3	50	bitumen	0,7	0,2	0,6	0,2
30.4	100	bitumen	---	0,2	0,7	0,2
30.1	200	bitumen	0,7	0,2	0,7	0,2
40.3	50	silicone	0,04	0,03	0,02	0,01
40.1	100	silicone	0,14	0,1	0,11	0,07
40.2	200	silicone	3,6	3,1	2,5	2,3

CONCLUSIONS

Random noise, harmonic and slow motion tests show all the impact of irradiation on the dynamic properties of viscoelastic fluid dampers.

- The bituminous fluid is most stable and hardly changes its characteristics within the tested irradiation range up to 200 kGy. This is true for all bituminous damping fluids used for pipework applications.
- The polybutene based fluid softens slightly when irradiated but stays fully functional within the tested irradiation range.
- The silicone oil-based damping fluid shows increasing stiffness and decreasing damping values with increasing irradiation levels. At high irradiation levels they gel and lose their liquid properties.

However, the tests prove that all three types of fluid can be used in areas of low and high irradiation. Depending on the occurring irradiation levels, inspection intervals for each fluid type can be defined. Exchange of fluid or replacement of devices can be scheduled in advance at those times.

REFERENCES

Walter Noll “Chemistry and Technology if Silicones”, 1968.